

**Development of “Core-Suction” Technique for Fabrication of  
Highly Doped Fibers for Optical Amplification  
and Characterization of Optical Fibers for Raman Amplification**

Nitin Kumar Goel

Dissertation submitted to the faculty of the Virginia Polytechnic Institute and State  
University in partial fulfillment of the requirements for the degree of

Doctor of Philosophy  
in  
Electrical Engineering

Dr. Roger H. Stolen Chair  
Dr. Gary Pickrell Co-Chair  
Dr. Ira Jacobs  
Dr. Ahmad Safaai-Jazi  
Dr. Anbo Wang  
Dr. Randy Heflin

October 11<sup>th</sup>, 2005  
Blacksburg, Virginia

Keywords: “Core-Suction” Technique, Highly Nonlinear Fibers, Raman Amplifier,  
Erbium Doped Fiber Amplifier

Copyright © 2005 Nitin Kumar Goel

# **Development of “Core-Suction” Technique for Fabrication of Highly Doped Fibers for Optical Amplification and Characterization of Optical Fibers for Raman Amplification**

Nitin Kumar Goel

## **Abstract**

This dissertation presents a novel technique named “Core Suction” for fabricating optical fiber preforms for manufacturing highly doped fibers (HDFs) for optical amplification (Raman effect based or Erbium fiber based). The technique involves drawing the molten non-conventional core glass material into the silica cladding tube to form the preform. The developed technique is simple, inexpensive and shows great potential for fabricating preforms of highly nonlinear non-conventional multi-component glasses as the core material. Preforms were made with various core glasses such as Schott SF6, Lead-Tellurium-Germanate, Lead-Tellurium-Germanate- Neodymium -Erbium and MM2 in silica cladding tubes and then pulled into fibers.

The fabricated fibers were measured for refractive index profile, loss spectrum and spontaneous Raman spectra. Elemental analysis of the fiber samples was also performed using an electron microprobe. Erbium doped fiber amplifiers (EDFAs) were setup using 30 cm, 5cm and 1 cm lengths of fabricated erbium doped fibers and their gain spectra measured. The distributed gain spectrum for an EDFA was also measured using an optical frequency domain reflectometry (OFDR) technique. Commercial dispersion compensated fiber (DCF) with very high  $\text{GeO}_2$  doping was used to setup a Raman amplifier and the gain spectrum measured.

One of the needs of Raman amplification in optical fibers is to predict an accurate Raman gain based on the fiber’s refractive index profile. A method of predicting Raman gain in  $\text{GeO}_2$  doped fibers is presented and the predicted Raman gain values are compared with the measured ones in the same fibers. Raman gain issues like the dependence of the Raman gain on the  $\text{GeO}_2$  concentration, polarization dependence were taken into account for the gain calculations. An experimental setup for Raman gain measurements was made and measurement issues addressed. Polarization dependence of the Raman gain in one kilometer of polarization maintaining fiber was also measured.

## Acknowledgements

I have always admired this statement from Albert Einstein: *"A hundred times every day I remind myself that my inner and outer life are based on the labors of other men and women, living and dead, and that I must exert myself in order to give in the same measure as I have received and am still receiving"*. This research work is also the result of the support and encouragement from many whom I would like to acknowledge.

First of all I am greatly indebted to my advisor Dr. Roger Stolen who has always been a constant source of inspiration for me. He not only encouraged me to be a better researcher but also inspired me to be a better human being. He was too patient in dealing with me in my hard times and without him I would have never been able to continue my research. I heartily appreciate the emotional support, concerns and advice from Dr. Lucy Stolen along with Dr. Roger Stolen during the time of my personal hardship.

I express my deep gratitude to my mentor Dr. Mansoor Saifi and Dr. Ira Jacobs, without their help and support I could never be at this place where I am today. I am thankful to Dr. Gary Pickrell for his advice, help and support in my research work. I also thank Dr. Ira Jacobs, Dr. Ahmad Safaai-Jazi, Dr. Anbo Wang, and Dr. Randy Heflin for being my advisory committee members.

I am grateful to my parents and my family members who supported all of my decisions. Without their love, support and encouragement I could have never reached this point.

Thanks to my ex-employer, my friend, Jon Greene, President Lambda Instruments Inc., for the many times he helped in my PhD. Also many thanks to my friends Sameer Arabasi and Harsha Rajasimha who were my angels in my difficult times and who made my stay in Blacksburg memorable.

I would also like to acknowledge the assistance and financial support from Tycom Ltd (previously AT&T Submarine Systems), NSF, NASA, COMSET Clemson University, Fibertek Inc. and Kigre Inc.

Finally, I also must thank all those who helped me over the years in my research work; Carvel Holton, Clayton Loehn, Robert Tracy, Jong-Kook Kim, Yuhong Kong, Dan Kominsky, Harsh Sanghvi, Ismael Torres from Virginia Tech, Dr. Idan Mandelbaum from JDS Uniphase, Dr. David DiGiovanni and Dr. Andrew Yablon from OFS Labs, Mark Froggatt and Brian Soller from Luna Technologies, Robert Stegeman from CREOL, University of Central Florida and Dr. Steven Morgan from Fisk University.

# Table of Contents

<b>Abstract</b> .....	ii
<b>Acknowledgements</b> .....	iii
<b>Table of Contents</b> .....	iv
<b>List of Figures</b> .....	vii
<b>List of Tables</b> .....	xii
<b>Overview of the Work</b> .....	1
<b>I. Highly Doped Fibers (HDF's) for Optical Amplification</b> .....	4
1.1 Optical Amplification: Basics.....	4
1.1.1 Erbium Doped Fiber Amplifier (EDFA).....	5
1.1.2 Raman Amplifier.....	6
1.2 Highly Doped Fibers.....	9
1.2.1 GeO <sub>2</sub> based HDFs (HNLFs) .....	9
1.2.2 TeO <sub>2</sub> based HDFs (HNLFs) .....	10
1.3 Multi-Component Glasses.....	11
1.4 Summary.....	15
1.5 References.....	16
<b>II. Fabrication of Highly Doped Fibers: “Core-Suction” Technique</b> .....	18
2.1 Conventional Methods for Fabrication of HDFs.....	18
2.1.1 Modified Chemical Vapor Deposition (MCVD).....	18
2.1.2 Vapor Axial Deposition (VAD).....	20
2.1.3 Rod in Tube Technique.....	20
2.1.4 Crucible Technique.....	21
2.2 Core Suction Technique.....	22
2.2.1 Use of Muffle Furnace for Core Suction Technique.....	23
2.2.2 Use of Tube Furnace for Core Suction Technique .....	26
2.2.2.1 Fabrication of SF <sub>6</sub> Glass Fiber.....	28
2.2.2.2 Fabrication of Lead-Germanate-Tellurite-Neodymium .....	30
Glass Fibers	
2.2.2.3 Fabrication of Lead-Germanate-Tellurite Glass Fibers.....	31

2.2.2.4 Fabrication of Lead-Germanate-Tellurite-Erbium Glass Fiber.....	33
2.2.2.5 Fabrication of MM2 (Phosphate-Erbium) Glass Fibers.....	34
2.2.3 Advantages of Core-Suction Technique.....	36
2.3 Summary.....	36
2.4 References.....	36
<b>III. Characterization of Highly Doped Fibers.....</b>	<b>39</b>
3.1 Loss Measurement by Cut-Back Method.....	39
3.2 Refractive Index Profile Measurement.....	43
3.3 Electron Micro Probe Analysis (EMPA) for Dopant Concentrations.....	46
3.4 Spontaneous Scattering Spectrum Measurements.....	62
3.5 Summary.....	68
3.6 Reference.....	68
<b>IV. Application of Highly Doped Fibers for Optical Amplification.....</b>	<b>69</b>
4.1 Setup of an optical Amplifier using 30 cm of Sample S1 fiber.....	69
4.2 Distributed Gain Measurement.....	71
4.2.1 Optical Frequency Domain Reflectometer (OFDR): Principle.....	72
4.2.2 Distributed Gain Measurement of Sample S1 Fiber using OBR.....	73
4.3 EDFA using 5 cm length of Kigre MM2 Fiber.....	75
4.4 EDFA using 1 cm length of Kigre MM2Fiber.....	76
4.5 Setup of a Raman Amplifier using commercial (OFS Labs) Dispersion Compensated Fiber (DCF).....	78
4.6 Summary.....	80
4.7 References.....	81
<b>V: Calculation of Raman Gain in GeO<sub>2</sub> doped Fibers.....</b>	<b>82</b>
5.1 Raman Amplification.....	82
5.2 Effect of GeO <sub>2</sub> doping on Raman gain coefficient.....	83
5.3 Calculation of effective Raman gain for GeO <sub>2</sub> doped fibers.....	85
5.4 Summary.....	89
5.5 References.....	89

<b>VI. Measurement of Raman gain in GeO<sub>2</sub> doped fibers</b> .....	90
6.1 Basic Setup of a Raman Amplifier.....	90
6.2 Characterization of Fiber Components of the Raman Amplifier Setup.....	91
6.3 Issues in Raman Gain Measurement .....	96
6.4 Characterization of Optical Fibers for Raman Amplifiers.....	99
6.5 Measurement of the Peak Raman Gain in Different Fiber Types.....	107
6.6 Measurement of the Polarization Dependence of Raman Gain.....	110
6.7 Summary.....	113
6.8 References.....	113
<b>VII. Conclusions and Recommendations for Future Work</b> .....	114
7.1 Conclusions Related to “Core-Suction” Technique.....	114
7.2 Future Work Directions in “Core-Suction” Technique.....	115
7.3 Conclusions Related to the Application of Highly Doped Fibers for .....	116
Optical Amplification	
7.4 Future Work Directions Related to the Application of Highly Doped.....	116
Fibers for Optical Amplification	
7.5 Conclusions Related to the Calculation and Measurement of Raman.....	117
Gain in GeO <sub>2</sub> Doped Fibers	
7.6 Future Work Directions Related to the Calculation and Measurement.....	117
of Raman Gain in GeO <sub>2</sub> Doped Fibers	
<b>VITA</b> .....	118

## List of Figures

Figure 1.1	Schematic diagram of the EDFA.....	5
Figure 1.2	Typical Gain Spectrum of an EDFA.....	6
Figure 1.3	Spontaneous Raman Scattering.....	7
Figure 1.4	Parallel and Perpendicular Raman Gain Spectrum of fused Silica.....	7
Figure 1.5	Schematic diagram of a Raman Amplifier.....	8
Figure 1.6	Raman Spectrum of Fused GeO <sub>2</sub> Glass.....	10
Figure 1.7	Raman Spectra of (67-x) GeO <sub>2</sub> . xTeO <sub>2</sub> . 27PbO. 10CaO glasses.....	11
Figure 1.8	Raman spectrums for 85TeO <sub>2</sub> 15WO <sub>3</sub> glass. .... Superimposed is the Raman gain spectrum of fused silica with its gain coefficient multiplied by a factor of 10.	12
Figure 1.9	Raman gain curve of 59.5TeO <sub>2</sub> – 25.5TiO <sub>2</sub> – 15PbO.....	13
Figure 1.10	Reduced Raman spectra of a glass system xZnO.(100-x)TeO <sub>2</sub> .....	14
Figure 1.11	Reduced Raman spectra of Sb <sub>2</sub> O <sub>3</sub> –TeO <sub>2</sub> , P <sub>2</sub> O <sub>5</sub> –TeO <sub>2</sub> , GeO <sub>2</sub> –TeO <sub>2</sub> , ..... and TiO <sub>2</sub> –TeO <sub>2</sub> glasses.	14
Figure 2.1	Crucible Method of Making HDF.....	21
Figure 2.2	Crucible Preforms Showing Blow-Out, Cracking and Stresses..... on the Interfaces	22
Figure 2.3	Schematic Diagram of Core Suction Technique for Making HDF.....	23
Figure 2.4	Use of Muffle Furnace for Core Suction Technique.....	24
Figure 2.5	Photograph of Glass Preform made by “Core-Suction” technique,.....	24
Figure 2.6	Micrographs of Fibers made by “Core-Suction” technique.....	25
Figure 2.7	Micrograph of Fiber with Conventional Core made by ..... “Core-Suction” technique using Muffle Furnace	25
Figure 2.8	Use of a Tube Furnace for Core Suction Technique .....	27
Figure 2.9	Preforms Made By Core Suction Technique Using a Tube Furnace ..... (Before Cool Down)	28
Figure 2.10	Preforms Made By Core Suction Technique Using a Tube Furnace ..... (After Cool Down)	28
Figure 2.11	Cross Sections of the Fiber Fabricated By “Core-Suction” ..... Technique Using SF <sub>6</sub> as the Core Glass in Silica Cladding Tube	29

Figure 2.12	Output Multimode Pattern of the SF6-Core in Silica Cladding Fiber with Red He-Ne Light Launched at the Input .....	29
Figure 2.13	Fiber Cross Section of the Fiber Fabricated By “Core-Suction” Technique Using Sample 3 (26PbO. 33GeO <sub>2</sub> . 30TeO <sub>2</sub> . 5CaO. 1Nd <sub>2</sub> O <sub>3</sub> . 5Na <sub>2</sub> CO <sub>3</sub> ) As the Core Material .....	31
Figure 2.14	Vertical Lathe Shrinking the Cladding Tube.....	31
Figure 2.15	Fiber Cross Sections of the Fiber Fabricated By “Core-Suction” Technique Using Sample 3 (26PbO. 33GeO <sub>2</sub> . 30TeO <sub>2</sub> . 5CaO .1Nd <sub>2</sub> O <sub>3</sub> . 5Na <sub>2</sub> CO <sub>3</sub> ) as the Core Material .....	32
Figure 2.16	Fiber Cross Sections of the Fiber Fabricated By “Core Suction” Technique” Using Sample 5 (27PbO. 33GeO <sub>2</sub> . 30TeO <sub>2</sub> . 10CaCO <sub>3</sub> ) as the Core Material .....	33
Figure 2.17	Fiber Cross Section of the Fiber Fabricated By “Core Suction” Technique Using Sample 1 (27PbO. 43GeO <sub>2</sub> . 20TeO <sub>2</sub> . 10CaCO <sub>3</sub> . 0.2 Er <sub>2</sub> O <sub>3</sub> ) as the Core Material .....	33
Figure 2.18	Blown Out Preforms.....	34
Figure 2.19	MM2 Glass Sample.....	34
Figure 2.20	Horizontal Lathe Shrinking the Cladding Tube.....	35
Figure 2.21	Cross Sections of the Fiber Fabricated by the “Core-Suction” Technique Using MM2 Core Glass in Silica Cladding Tube .....	35
Figure 3.1	Loss Spectrum of Sample 1 Fiber.....	40
Figure 3.2	Loss Spectrum of Sample 3 Fiber.....	41
Figure 3.3	Loss Spectrum of Sample 5 Fiber.....	42
Figure 3.4	Loss Spectrum of MM2 Glass Fiber (Measured On 5 Cms Length).....	43
Figure 3.5	Refractive Index Profile of the Fiber Fabricated by “Core-Suction” Technique Using Sample 1 as the Core Material .....	43
Figure 3.6	Refractive Index Profile of the Fiber with Sample 3 Core Glass in Silica Cladding Tube .....	44
Figure 3.7	Cross Section of the Bell Labs Fiber.....	45
Figure 3.8	Refractive Index Profile of the Bell Labs Fiber.....	45
Figure 3.9	Photographs of the Electron Microprobe Samples (With 5 Fiber.....	46



Samples in the Middle)

Figure 3.10	Schematic Diagram of the Cross-Sections of the Electron.....	47
	Microprobe Samples (with 5 fibers labeled A,B,C,D and E in the Middle)	
Figure 3.11	SEM Images of Fiber Samples Labeled ‘A’s in EMPA#1 and EMPA#2.	48
Figure 3.12	SEM Images of Fiber Samples Labeled ‘B’s in EMPA#1 and EMPA#2.	48
Figure 3.13	SEM Images of Fiber Samples Labeled ‘C’s in EMPA#1 and EMPA#2.	49
Figure 3.14	SEM Images of Fiber Samples Labeled ‘D’s in EMPA#1 and EMPA#2.	49
Figure 3.15	SEM Images of Fiber Samples Labeled ‘E’s in EMPA#1 and EMPA#2.	50
Figure 3.16	Horizontal Axis Profile of Fiber “A” in Sample EMPA#1.....	51
Figure 3.17	Vertical Axis Profile of Fiber “A” in Sample EMPA#1.....	51
Figure 3.18	Horizontal Axis Profile of Fiber “A” in Sample EMPA#2.....	52
Figure 3.19	Vertical Axis Profile of Fiber “A” in Sample EMPA#2.....	52
Figure 3.20	Horizontal Axis Profile of Fiber “B” in Sample EMPA#1.....	53
Figure 3.21	Vertical Axis Profile of Fiber “B” in Sample EMPA#1.....	53
Figure 3.22	Horizontal Axis Profile of Fiber “B” in Sample EMPA#2.....	54
Figure 3.23	Vertical Axis Profile of Fiber “B” in Sample EMPA#2.....	54
Figure 3.24	Horizontal Axis Profile of Fiber “C” in Sample EMPA#1.....	55
Figure 3.25	Vertical Axis Profile of Fiber “C” in Sample EMPA#1.....	55
Figure 3.26	Horizontal Axis Profile of Fiber “C” in Sample EMPA#2.....	56
Figure 3.27	Vertical Axis Profile of Fiber “C” in Sample EMPA#2.....	56
Figure 3.28	Horizontal Axis Profile of Fiber “D” in Sample EMPA#1.....	57
Figure 3.29	Vertical Axis Profile of Fiber “D” in Sample EMPA#1.....	57
Figure 3.30	Horizontal Axis Profile of Fiber “D” in Sample EMPA#2.....	58
Figure 3.31	Vertical Axis Profile of Fiber “D” in Sample EMPA#2.....	58
Figure 3.32	Horizontal Axis Profile of Fiber “E” in Sample EMPA#1.....	59
Figure 3.33	Vertical Axis Profile of Fiber “E” in Sample EMPA#1.....	59
Figure 3.34	Horizontal Axis Profile of Fiber “E” in Sample EMPA#2.....	60
Figure 3.35	Vertical Axis Profile of Fiber “E” in Sample EMPA#2.....	60
Figure 3.36	Geo2 Concentration (Weight %) Profile of Bell Labs Geo2 Core Fiber...	61
Figure 3.37	Schematic Diagram for Spontaneous Scattering Measurement Setup.....	63
Figure 3.38	Spontaneous Scattering Spectrum of 30 Cm Length of Sample S1 Fiber.	63

Figure 3.39	Spontaneous Scattering Spectrum of Sample S3 Fiber.....	64
Figure 3.40	Raman Gain Spectrum of 1.5 Meter Length of Sample S3 Fiber.....	65
Figure 3.41	Raman Gain Spectrum of 2 Meters Length of Sample S5 Fiber.....	66
Figure 3.42	Spontaneous Spectrum of 5 Cms Length of MM2 Fiber.....	67
Figure 3.43	Spontaneous Raman Spectrum of Bell Labs Geo2 Core Fiber, Measured Using the 514.5 nm Line of an Argon Ion Laser	67
Figure 4.1	Schematic Diagram of the EDFA Setup Comprising Erbium Based Fiber	70
Figure 4.2	Gain Spectrum of the Erbium Based Sample S1 Fiber.....	71
Figure 4.3	Schematic Diagram of an OFDR.....	72
Figure.4.4	Schematic of OBR use for Distributed Gain Measurement in Er. Fiber..	73
Figure 4.5	Distributed Gain of Fabricated Sample S1 Fiber Measured Using OBR..	74
Figure 4.6	Photograph of the 5 cm MM2 Glass Fiber Spliced to ..... Standard Fiber Pigtails	75
Figure 4.7	Gain Spectrum of 5 cm Length of Erbium Based MM2 Glass Fiber.....	76
Figure 4.8	Photograph of 1 cm MM2 Glass Fiber Spliced to Standard ..... Fiber Pigtails	77
Figure 4.9	Gain Spectrum of 1 Cm Length of Erbium Based MM2 Glass Fiber.....	77
Figure 4.10	Schematic Diagram of Raman Amplifier Comprising OFS DCF.....	78
Figure 4.11	Amplification Spectrum of the Raman Amplifier Setup by OFS DCF....	79
Figure 4.12	Gain Spectrum of the Raman Amplifier Setup by OFS DCF.....	80
Figure 5.1	Peak Raman Intensity Normalized to Silica with Mol % GeO <sub>2</sub> .....	84
Figure 5.2	Refractive Index Profile of Sumitomo Z-Plus Fiber.....	85
Figure 5.3	Refractive Index Profile of Spectran Standard Fiber.....	86
Figure 5.4	Refractive Index Profile of Lucent Truewave Fiber.....	86
Figure 5.5	Variation of Mol % GeO <sub>2</sub> with Refractive Index.....	87
Figure 5.6	Flowchart for the Effective Raman Gain Calculation.....	88
Figure 6.1	Basic Setup of Raman Amplifier.....	90
Figure 6.2	Schematic Diagram of a Coupler.....	91
Figure 6.3	Output Spectra of a 3-dB 1480 nm Coupler.....	92
Figure 6.4	Output Spectra of a 10-dB Tap Coupler.....	92

Figure 6.5	Output Spectra of a 1480/1550 nm WDM Coupler.....	93
Figure 6.6	Schematic Diagram of an Optical Circulator.....	94
Figure 6.7	Output Spectra of an Optical Circulator.....	94
Figure 6.8	Schematic Diagram of an Optical Isolator.....	95
Figure 6.9	Spectra of an Optical Isolator in Forward and Backward Directions.....	95
Figure 6.10	Attenuation Spectrum of an Optical Attenuator.....	96
Figure 6.11	Raman Spectra of A Z-PLUS Fiber Obtained Using A 3-dB Coupler, A WDM Coupler and an Optical Circulator (Pumped at 1487 nm Wavelength)	97
Figure 6.12	Signal Spectra With and Without Isolator.....	98
Figure 6.13	Schematic Diagram of the Setup for Measuring the Power Stability .....	98
Figure 6.14	Power Stability Curves for the Pump and the Signal.....	99
Figure 6.15	Attenuation Spectra of Sumitomo Z-PLUS Fiber.....	100
Figure 6.16	Attenuation Spectra of Spectran Standard Fiber.....	100
Figure 6.17	Attenuation Spectra of Lucent Truwave Dispersion Shifted Fiber.....	101
Figure 6.18	Attenuation Spectra of OFS Labs Dispersion Shifted Fiber.....	101
Figure 6.19	Attenuation Spectra of OFS Labs Dispersion Compensated Fiber.....	102
Figure 6.20	Schematic Diagrams for Spontaneous Scattering Measurement Setup...	103
Figure 6.21	Spontaneous and Raman Gain Spectra of Z-Plus Fiber.....	104
Figure 6.22	Raman Gain Spectrum of Spectran Standard Fiber.....	104
Figure 6.23	Raman Gain Spectrum of Lucent Truwave Fiber.....	105
Figure 6.24	Raman Gain Spectrum of OFS Truwave Fiber.....	105
Figure 6.25	Raman Gain Spectrum of OFS Dispersion Compensated Fiber.....	106
Figure 6.26	Raman Gain Spectra of Different Fiber Types.....	106
Figure 6.27	Schematic Diagram of the Raman Gain Measurement Setup.....	107
Figure 6.28	Spectrum of the Pump Laser Used for Raman Gain Measurement.....	108
Figure 6.29	Schematic Diagram of the Setup for the Measurement of Polarization Dependence of the Raman Gain	111
Figure 6.30	Spectrum of the Pump.....	111
Figure 6.31	Polarized Components of the Raman Gain in a PM Fiber.....	112
Figure 6.32	Depolarization Ratio of Raman Scattering at Lower Frequency Shifts...	112

## List of Tables

Table 3.1	List of the Fibers Measured.....	39
Table 3.2	List of the Fibers Analyzed by Electron Microprobe.....	47
Table 3.3	Elemental Make up of Fiber “A” In Sample EMPA#1.....	51
Table 3.4	Elemental Make up of Fiber “A” In Sample EMPA#2.....	52
Table 3.5	Elemental Make up of Fiber “B” In Sample EMPA#1.....	53
Table 3.6	Elemental Make up of Fiber “B” In Sample EMPA#2.....	54
Table 3.7	Elemental Make up of Fiber “C” In Sample EMPA#1.....	55
Table 3.8	Elemental Make up of Fiber “C” In Sample EMPA#2.....	56
Table 3.9	Elemental Make up of Fiber “D” In Sample EMPA#1.....	57
Table 3.10	Elemental Make up of Fiber “D” In Sample EMPA#2.....	58
Table 3.11	Elemental Make up of Fiber “E” In Sample EMPA#1.....	59
Table 3.12	Elemental Make up of Fiber “E” In Sample EMPA#2.....	60
Table 3.13	Mole Fraction Analysis for Core of Bell Labs Fiber.....	62
Table 4.1	List of the Fibers Used for Optical Amplifiers.....	69
Table 5.1	Calculated Effective Raman Gain Values for Z-PLUS, STF and Truwave Fibers.....	88
Table 6.1	Attenuation of Different Fiber Types at 1450.4 nm.....	102
Table 6.2	Effective Lengths for Different Fiber Types.....	102
Table 6.3	Raman Gain Peak of Different Fiber Types (Pumped at ~1450 nm).....	107
Table 6.4	Raman Amplification Values Measured for Different Fiber Types.....	108
Table 6.5	Raman Gain Values Calculated for Different Fiber Types.....	109
Table 6.6	Comparison of Calculated and Measured Raman Gain.....	109

## **Overview of the Work**

There has been an increasing interest in optical amplifiers and lasers based on highly doped specialty optical fibers. These fibers are normally doped with elements which either enhance the nonlinear effects or provide meta-stable states for stimulated emission. These highly doped fibers can have a high doping of elements like Erbium, Germanium ( $\text{GeO}_2$ ) and/or Tellurite ( $\text{TeO}_2$ ) for optical amplification. Most of the optical amplifiers previously employed are based on fibers doped with erbium, a rare earth element that has the appropriate energy levels for amplifying light. Although erbium doped fiber amplifiers (EDFAs) are deployed extensively in optical networks they have a limited gain bandwidth centered around a wavelength of 1550nm. As the demand for telephony and internet increases so does the demand for ultra-wide band optical amplification in this bandwidth hungry world. Raman amplification in optical fibers satisfies the demand for bandwidth and non dependency on a particular wavelength band. Because of the availability of high power pump lasers and their significant advantages over the EDFA, interest in distributed and discrete Raman amplifiers is growing for applications in optical fiber communication systems and fiber lasers. Optical amplifiers and fiber lasers based on Raman amplification are called Raman amplifiers and Raman fiber lasers, respectively.

The fundamental advantages of Raman amplification are that the transmission fiber itself acts as an amplifying medium and one can have amplification at any wavelength provided the appropriate pump sources are available. Pump sources can also be combined together to obtain Raman amplification over an ultra-wide band. Unfortunately, Raman gain is quite small in standard germanium-doped silica-core fibers. Attempts are continuing to highly dope the fibers with elements which will increase the Raman gain. For example a very high doping of Germanium can provide a Raman gain up to  $\sim 10$  times that of pure silica. Fibers doped with Tellurite, Bismite etc. show much higher Raman gain values. Thus it is highly desirable to dope the fibers with these Raman gain enhancing dopants. These dopants not only provide higher Raman gain but also increase the Raman gain spectral bandwidth. These highly doped fibers can be used in optical amplifiers and fiber lasers as well.

This interest in highly doped fibers for optical amplifiers and lasers has stimulated a new look at the fiber fabrication methods. Efforts for making highly doped fibers with  $\text{GeO}_2$ ,  $\text{TeO}_2$  and/or non-conventional multi-component glass are still in progress. In the first part (chapter 2) of this thesis, our efforts for making such fibers are presented. Conventional techniques of making fibers with non-conventional glasses in the core are discussed and the development of a novel technique named “Core-Suction” presented. The technique involves drawing the molten non-conventional core glass material into the silica cladding tube to form the preform. The developed technique is simple, inexpensive and shows great potential for fabricating preforms of highly nonlinear non-conventional multi-component glasses as the core material. Preforms are made with various core glasses like Schott SF6, Lead-Tellurium-Germanate, Lead-Tellurium-Germanate-Neodymium-Erbium and Kigre MM2 in silica cladding tubes and then pulled into fibers.

In the second part (chapter 3) of the thesis, characterization of fibers fabricated by the “Core-Suction” technique is presented. The fabricated fibers are measured for their refractive index profiles, loss spectra and spontaneous Raman scattering spectra. The spontaneous Raman spectrum for a very highly  $\text{GeO}_2$  doped experimental fiber from Bell Labs is also measured. To check if the glass composition in the core remains the same after the drawing, elemental analysis using an electron microprobe is done on the fabricated fibers and highly  $\text{GeO}_2$  doped Bell Labs experimental fiber. It is shown that silica from the cladding tube diffuses into the core and the majority of the glass in the core is silica. No matter what core glasses one starts with, the core ends up being a silicate glass doped with highly doped materials like  $\text{GeO}_2$  and  $\text{PbO}$  etc.

In the third part (chapter 4) of the thesis, experimental realization of practical amplifiers using fabricated fibers is presented. Three different amplifiers having 30 cm, 5 cm and 1 cm lengths of active (erbium) fibers are implemented and their gain spectrum measured with varying pump powers. Luna Technologies’s optical backscatter reflectometer (OBR), which is based on optical frequency domain reflectometry, is used to measure the distributed gain of the active fibers. A Raman amplifier using commercial dispersion

compensated fiber is also implemented and gain spectrum is measured using an erbium ASE source as the signal.

One of the main advantages of Raman amplification is that the transmission fiber itself acts as an amplifying medium. The transmission fiber can be a conventional step index fiber with a low GeO<sub>2</sub> doping or triangular index dispersion shifted fiber with relatively high GeO<sub>2</sub> doping. The transmission fibers vary in GeO<sub>2</sub> doping and have different effective areas. So it is necessary to know the Raman gain characteristics of different fiber types with different GeO<sub>2</sub> doping levels. However in a fiber, the calculation of the actual Raman gain coefficient is complicated because the gain coefficient depends on GeO<sub>2</sub> concentration and the GeO<sub>2</sub> concentration varies across the index profile.

In the fourth part (chapter 5) of this thesis, Raman gain for a pure silica core Sumitomo Z-PLUS with no GeO<sub>2</sub> doping, Spectran standard step-index fiber with very small GeO<sub>2</sub> doping and Lucent Truwave triangular index dispersion shifted fiber with high GeO<sub>2</sub> doping are calculated. To calculate the Raman gain, the index profile of the fiber under investigation is measured first and then mode fields at pump and signal wavelengths are calculated. The Raman gain is then calculated by taking the Raman gain coefficient  $g$ , which is a function of GeO<sub>2</sub> doping, into the overlap integral between the pump and the signal mode fields. The polarization dependence of the Raman gain is also taken into account.

In the fifth part (chapter 6) of the thesis the Raman gain for optical fibers is measured and compared with the calculated Raman gain. An experimental setup is made to measure the accurate value of Raman gain. Measurement issues and their solutions are addressed. The measured Raman gain is produced by measuring the Raman amplification in the fiber with the pump on and off technique. From the measured Raman amplification, pump power and the fiber length values, Raman gain is calculated. Measurements and calculations showed good agreement for Sumitomo ZPlus and Lucent Truwave fibers but not for Spectran standard fiber. The polarization dependence of Raman gain in one kilometer of a polarization maintaining fiber was also measured.

# **I. Highly Doped Fibers (HDFs) for Optical Amplification**

With the demand for longer transmission lengths and ultra-wide bandwidth, optical amplifiers have become an essential component in long-haul fiber optic systems. An optical amplifier is a device that amplifies an optical signal directly, without the need to first convert it to an electrical signal, then amplify it electrically, and finally reconvert it to an optical signal. Optical fiber amplifiers are optical amplifiers which use a doped optical fiber carrying the communication signal, and is optically pumped with a laser having a high-powered continuous output at an optical frequency slightly higher than that of the communication signal. For EDFAs the pump lasers operate either at a wavelength of around 980 nm or at a wavelength of around 1480 nm.

## **1.1 Optical Amplification: Basics**

Optical amplifiers amplify an incident weak light signal through the process of stimulated emission<sup>1</sup>. The main ingredient of any optical amplifier is the optical gain realized when the amplifier is optically pumped to achieve population inversion. The optical gain, in general, depends mainly on the doping material, on the frequency (or wavelength) of the incident signal, and also on the local beam intensity at any point inside the amplifier. So by a proper choice of the doping materials, the amplifier characteristics such as the operating wavelength and the gain bandwidth can be modified. Many different dopants such as erbium, holmium, neodymium, samarium, thulium, ytterbium, germanium, tellurium, bismuth and thallium can be used to realize fiber amplifiers operating at different wavelengths covering a wide region extending over 0.5 -3.5  $\mu\text{m}$ .

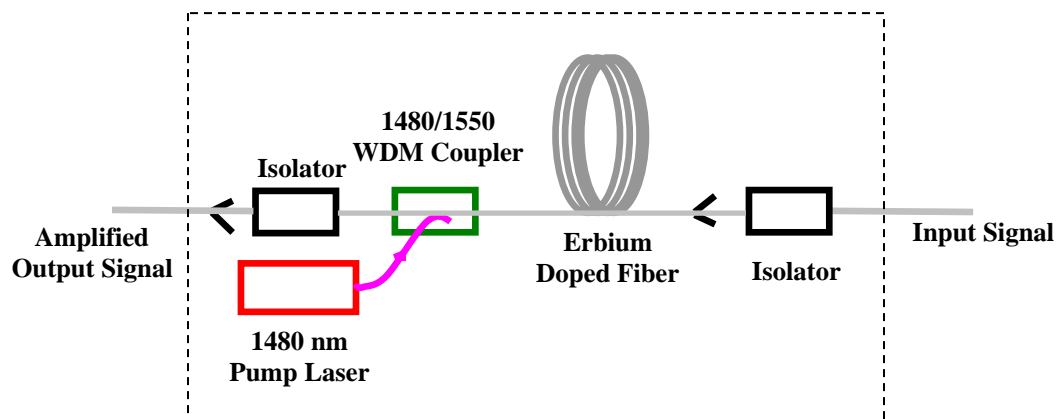
At standard telecommunication wavelengths ( $\sim 1.55 \mu\text{m}$ ) optical amplification in silica based fibers is achieved mainly either by doping silica with a rare earth element erbium or by the process of stimulated Raman scattering. The amplifiers based on erbium doped fibers are called erbium doped fiber amplifiers (EDFAs) and are the most commonly deployed in long haul networks. The amplifiers based on stimulated Raman scattering are termed Raman amplifiers and are gaining wide interest in optical networks because of



their significant advantages over EDFAs. The newest trend in optical networks is to use a combination of Raman amplifiers and EDFAs.

### 1.1.1 Erbium Doped Fiber Amplifier (EDFA)

In an erbium doped fiber amplifier<sup>2</sup>, the fiber is doped with erbium, a rare earth element that has the appropriate energy levels in their atomic structures for amplifying light. EDFAs are designed to amplify light at ~1550 nm. The device utilizes a 980 nm or 1480nm pump laser to inject energy into the doped fiber. When a weak signal at ~1550 nm enters the fiber, the light stimulates the rare earth atoms to release their stored energy as additional optical power at 1550 nm. This process continues as the signal travels down the fiber, growing stronger and stronger as it goes. The schematic diagram of an EDFA is shown in figure 1.1.



Erbium Doped Fiber Amplifier (EDFA)

*Figure 1.1- Schematic diagram of the EDFA*

An EDFA is comprised of an erbium doped fiber, a wavelength division multiplexer (WDM) coupler, isolators and a 1480 nm pump laser. This EDFA is setup in a counter-propagating configuration, in which the pump energy travels in the direction opposite to the signal. A WDM coupler is used to combine the input signal and the pump laser. The isolator blocks the pump power from going into the signal laser. A weak signal in the 1550 nm band gets amplified at the cost of the high power pump laser at 1480 nm (980

nm pump can also be used). The measured typical gain spectrum of an EDFA is shown in figure 1.2

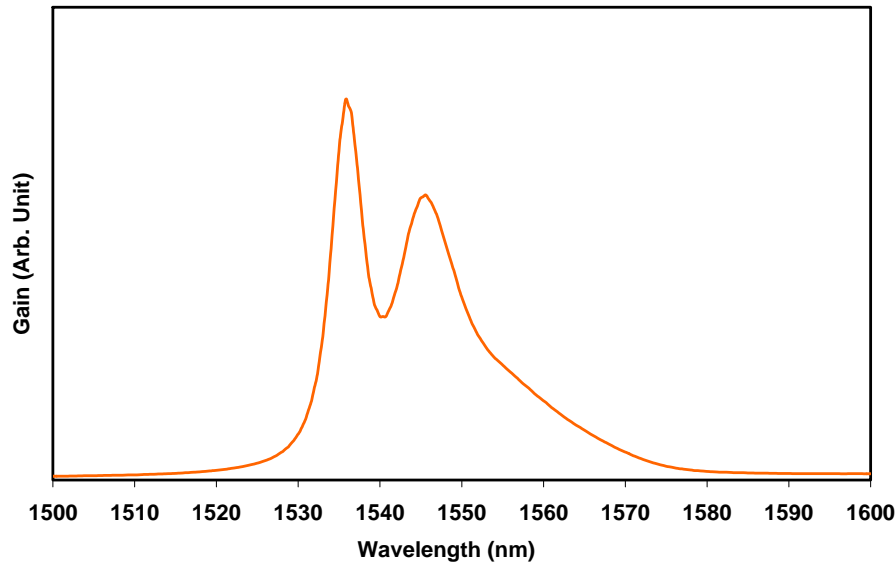


*Figure 1.2- Typical Gain Spectrum of an EDFA*

It can be seen from the gain spectrum that an EDFA has a gain peak at a wavelength of 1535 nm with another peak at around 1545 nm. Signals in the wavelength band from 1530 to 1565 nm can be amplified.

### **1.1.2 Raman Amplifier**

Raman amplification in optical fibers is based on Raman scattering (named after C.V. Raman). Raman scattering is divided into two categories called spontaneous Raman scattering and stimulated Raman scattering. Spontaneous Raman scattering is an interaction between light and a material (like the glass in a glass fiber) that causes some of the incident light to be shifted to different frequencies spontaneously. Light down-shifted in frequency from the incident frequency is called a Stokes shift and up-shifted frequency is called an Anti-Stokes shift. The amount of the frequency shift depends on the vibrational modes of the material. This effect is shown in figure 1.3, where  $\nu$  is the incident frequency and  $\nu_R$  being the frequency of the vibrational mode of the material.

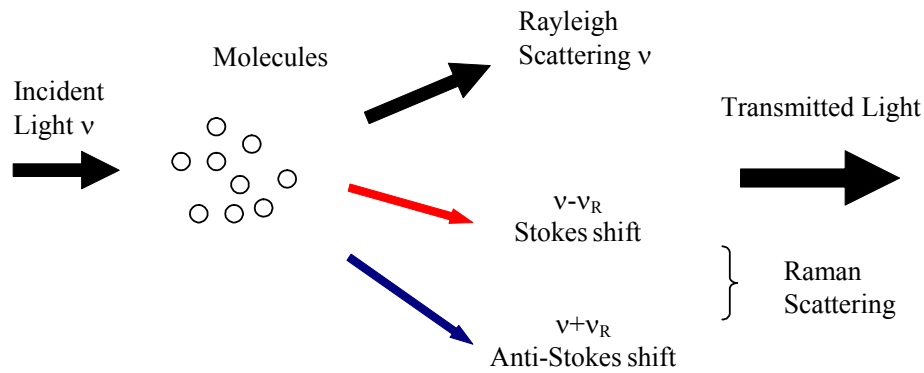


**Figure 1.3- Spontaneous Raman Scattering**

Now on the same material, if we send a weaker signal at a Stokes frequency along with the stronger incident beam, called a pump, it stimulates the Raman scattering. This is called stimulated Raman scattering and leads to the Raman amplification of the weaker signal at the cost of the stronger incident pump. As stated earlier, the magnitude of the frequency shift (Stokes shift) depends on the vibrational modes supported by the material. The gain spectrum of fused silica<sup>3</sup> is shown in figure 1.4.

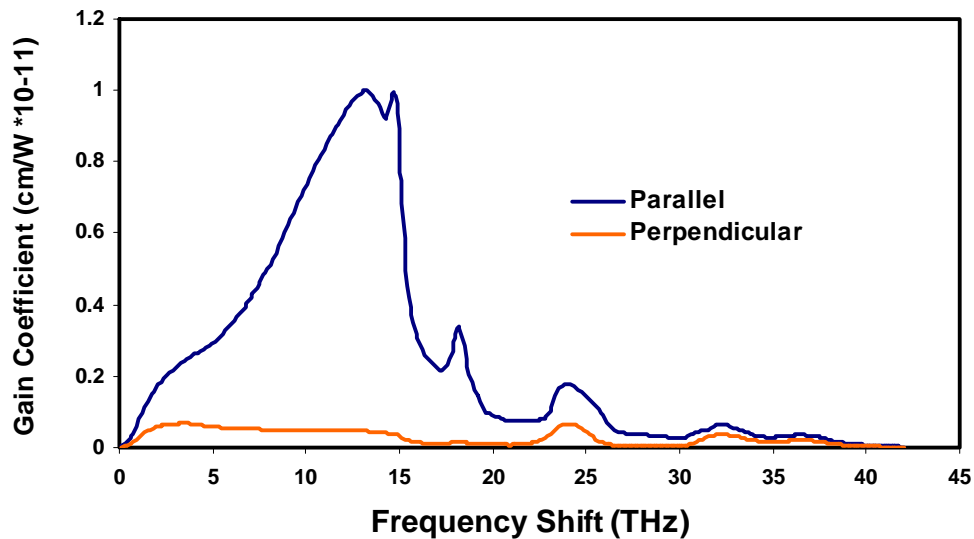


**Figure 1.4 - Parallel and Perpendicular Raman Gain Spectrum of fused Silica**

Fused silica, due to its amorphous nature, shows a broad (over 20 THz) gain spectrum. The larger gain coefficient curve in figure 1.4 is for the case when the polarization states of the scattered light and the incident light are parallel and the smaller gain curve is when

the polarizations are perpendicular. When silica is pumped by a  $\sim 1450$  nm wavelength pump, the Raman gain peak is at about a 100 nm shift ( $\sim 1550$  nm). So a simple Raman amplifier can be built by choosing the signal at Stokes shift ( $\sim 1550$  nm) and pumping the silica fiber with a 1450 nm wavelength pump.

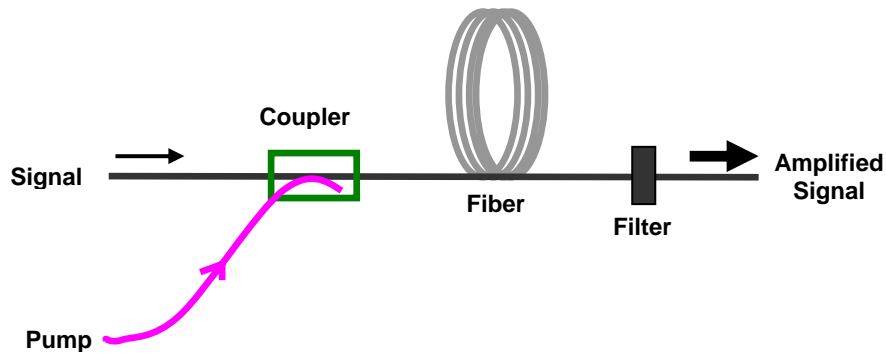


*Figure 1.5- Schematic diagram of a Raman Amplifier*

The schematic diagram of a Raman amplifier is shown in figure 1.5, which is comprised of an optical fiber, a coupler to couple the pump and the signal into the fiber and an optical filter which is used to block the high power pump. This configuration shown in figure 1.5 is known as forward pumping (or co-pumping) where the signal and the pump travel in the same direction. Raman amplifiers can also be setup in a backward pumping (counter-pumping) configuration, in which the pump travels in a direction opposite to the signal. The backward scheme has an advantage over the forward scheme in that the amplified signal does not see most of the pump variations.

Unlike an EDFA, Raman amplification is based on a nonlinear-optical interaction between an optical signal and the high power pump light. This nonlinear optical interaction in optical fibers can be enhanced by doping the fibers highly with materials showing high optical nonlinearity and by decreasing the core diameter to increase the optical intensity. These highly doped fibers (HDFs) with small core size, specially designed for enhancement of nonlinear interactions, are known as highly nonlinear fibers (HNLFs).

## 1.2 Highly Doped Fibers

As the name suggests, highly doped fibers (HDFs) are specialty fibers with a high concentration of dopants. Most of the highly doped fibers discussed in this thesis are HNLFs which are primarily used to generate high Raman gain efficiently at various Raman frequency shifts. These fibers are also known as Raman fibers<sup>4</sup>. Although pure silica core and standard silica fiber with small GeO<sub>2</sub> doping do show Raman gain<sup>5</sup> they require longer lengths and higher pump powers.

Highly nonlinear fibers allow us to shorten the fiber length and to reduce the required pump power. The nonlinear coefficient  $\gamma$  of the fiber is defined as  $\gamma = 2\pi n_2/\lambda A_{\text{eff}}$ , where  $n_2$  is the nonlinear refractive index,  $\lambda$  is the wavelength, and  $A_{\text{eff}}$  is the effective area of the fiber<sup>6</sup>. Thus the fiber nonlinearity  $\gamma$  can be enhanced by reducing the effective area  $A_{\text{eff}}$  and (or) by using a glass material with high nonlinear index  $n_2$ . Highly nonlinear glasses usually have a high refractive index, so there is also a reduction in the fiber's effective area  $A_{\text{eff}}$ , to keep the fiber single mode.

There are a large number of glass materials which have been studied so far, among them single component glasses, doped silica glasses, and various multi-component glasses, including heavy-metal oxide doped glasses<sup>7-8</sup>. The purpose of the study was to find glasses with high Raman gain and possible wide gain spectra, which could be used as the core material in HNLFs. It was found that the Germania (GeO<sub>2</sub>) glass Raman cross-section is nine times that of silica<sup>7</sup>. Recently Tellurite (TeO<sub>2</sub>) based glasses with Raman gain coefficients as much as 30 times larger than that of fused silica and more than twice its gain spectrum are reported<sup>9</sup>. In the next section the properties of the GeO<sub>2</sub> and TeO<sub>2</sub> based glasses are presented.

### 1.2.1 GeO<sub>2</sub> based HDFs (HNLFs)

The Raman gain spectrum of fused GeO<sub>2</sub> is shown in reference 7. This spectrum has a peak gain at a frequency shift of around 420 cm<sup>-1</sup>. The gain spectrum has two components for the scattering of light polarized parallel (HH) and perpendicular (HV) to

the polarization of the exciting light. The perpendicular gain coefficient is much lower than the parallel one.

Doping GeO<sub>2</sub> into SiO<sub>2</sub> glass has been proved to significantly increase the Raman gain coefficient for silica-based fibers. However, it turned out that the optical loss of the doped fibers also increases with the dopant content. Great efforts using different fiber making techniques and different glass compositions were directed to the development of low-loss GeO<sub>2</sub>-based fibers.

So far the lowest loss was reported at 2.0 μm<sup>10</sup> in a VAD made fiber and amounts to 4.0 dB/km. This fiber had a 70 μm core made of GeO<sub>2</sub>+Sb<sub>2</sub>O<sub>3</sub> glass with a 150 μm GeO<sub>2</sub> glass cladding. In the similar fiber, the first observation of single-pass Raman generation was made in 28 meter of fiber lengths<sup>11</sup>. The core and the cladding diameters of the fibers were 93 and 185 μm respectively. This and other similar observations<sup>12</sup> confirmed a high Raman gain efficiency of GeO<sub>2</sub> based fibers. Another report had an intermediate germanosilicate cladding and P<sub>2</sub>O<sub>5</sub>- and F- doped silica cladding matched with a silica substrate tube<sup>13-14</sup>. This approach generated MCVD fibers composed of a core with a GeO<sub>2</sub> concentration of up to 97-mol%.

Germania-glass-core silica-glass-cladding single-mode fibers with a minimum loss of 20 dB/km at 1.85 μm were fabricated by modified chemical-vapor deposition. A Raman gain of 300 dB/(km-W) was determined at 1.12 μm.<sup>13-14</sup>

### **1.2.2 TeO<sub>2</sub> based HDFs (HNLFs)**

Tellurite-based glasses have been studied extensively over the past few decades<sup>15-18</sup>, mainly because of their high nonlinearity, high transparency at visible and infra-red wavelengths, and good mechanical characteristics. Tellurite-based glasses have very high Raman gain coefficients and show large gain bandwidth. Although the first tellurite-based optical fiber<sup>4</sup>, with 1 dB/m and 20 dB/m losses at 2 and 4 μm respectively, was reported in 1980, not much progress was seen in tellurite based fibers until very recently.

Recently an ultra-wideband Raman fiber amplifier based on tellurite-based fiber, was presented<sup>19-20</sup>. The tellurite based fiber had a refractive index difference ( $\Delta n$ ) of 2.2% and loss of 20 dB/km at 1560 nm; however the manufacturing technique and the composition of this fiber were not disclosed. The maximum Raman gain coefficient of the tellurite-based fiber was 16 times larger than that of silica based high GeO<sub>2</sub> doped fiber (DCF) and about 30 times larger than that of pure silica. The main gain peak Stokes shift (170 nm) of tellurite fiber is 1.7 times larger than that of silica based fiber (100 nm). Another major difference is that a tellurite based fiber gain is twin-peaked; while the silica based fiber gain is single-peaked.

### 1.3 Multi-Component Glasses

The wide gain spectrum accompanied by the large Raman gain coefficient makes tellurite based fibers suitable for ultra-wideband Raman fiber amplifiers.

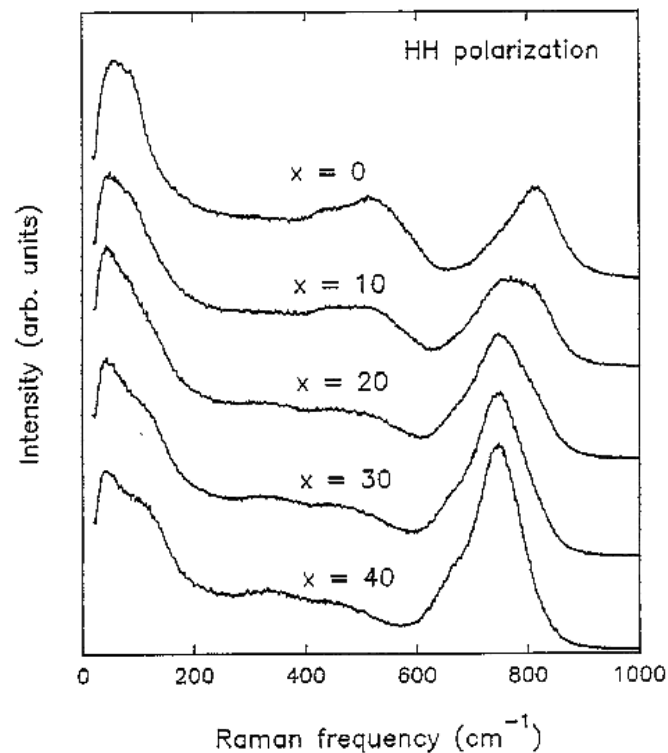


**Figure 1.7**–Raman Spectra of  $(63-x) \text{GeO}_2 \cdot x\text{TeO}_2 \cdot 27\text{PbO} \cdot 10\text{CaO}$  glasses [22]

(Reprinted from J. Non-Crystalline Solids, 210, Z. Pan, S.H. Morgan, “Raman spectra and thermal analysis of a new lead-tellurium-germanate glass system,” 130-135, Copyright (1997), with permission from Elsevier)

Tellurite is not able to form a glass by itself, but it forms glasses with modifying oxides. Lead-tellurite-germanate glass system has been studied and shown to have a wider spectrum<sup>21-22</sup>. The Raman gain spectra for such a glass system with varying tellurite composition are presented in figure 1.7. It can be seen from figure 1.7 that with increasing TeO<sub>2</sub> content and decreasing GeO<sub>2</sub> content, the high frequency Raman band decreases in frequency (820 cm<sup>-1</sup> to 750 cm<sup>-1</sup>) and increases in intensity.

Efforts of making highly stable tellurite based glasses are continuing and a Raman spectrum of such a glass<sup>9</sup> containing heavy metal- oxides (85TeO<sub>2</sub>.15WO<sub>3</sub>) is shown in figure 1.8. The Raman gain coefficient of this glass was shown to be as much as 30 times larger than that of fused silica with more than twice its spectral coverage.

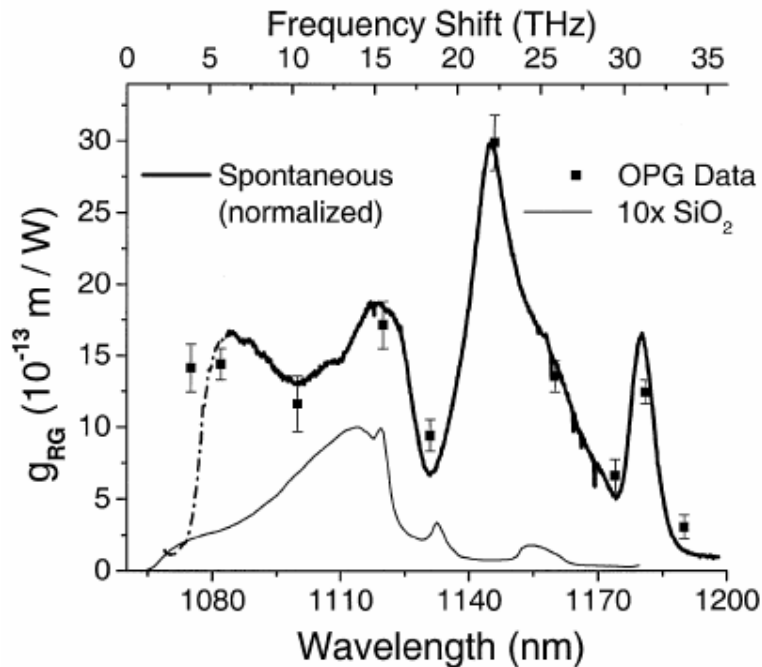


**Figure 1.8- Raman spectrum for 85TeO<sub>2</sub>.15WO<sub>3</sub> glass. Superimposed is the Raman gain spectrum of fused silica with its gain coefficient multiplied by a factor of 10 .[9]**

(Reprinted from Optics Letters, Vol. 28 Issue 13, Robert Stegeman, Ladislav Jankovic, Hongki Kim, Clara Rivero, George Stegeman, Kathleen Richardson, Peter Delfyett, Yu Guo, Alfons Schulte, Thierry Cardinal, "Tellurite glasses with peak absolute Raman gain coefficients up to 30 times that of fused silica", Page 1126 Copyright (2003), with permission from OSA)



Several different compositions of tellurium-thallium oxide glasses are also reported to have been tested for their Raman gain performance<sup>23</sup>. The Raman gain spectrum of such a glass is shown in figure 1.9. The reported maximum material Raman gain coefficient experimentally obtained was  $(58 \pm 3)$  times higher than the peak Raman gain of a 3.18 mm thick Corning 7980-2F fused silica sample ( $\Delta\nu = 13.2$  THz).

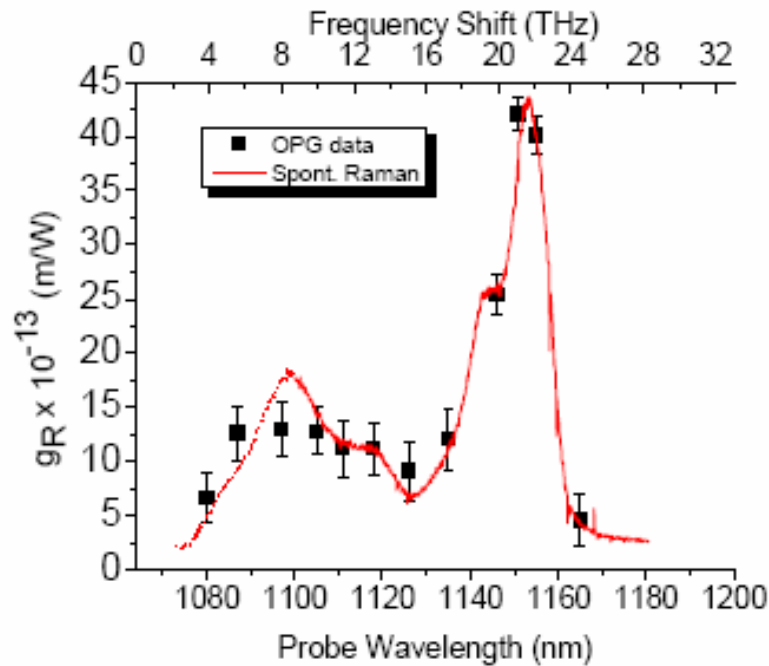


**Figure 1.9 - Raman gain curve of 59.5TeO<sub>2</sub> – 25.5TlO<sub>0.5</sub> – 15PbO [23]**

(Reprinted from Optics Express, Vol. 13 Issue 4, Robert Stegeman, Clara Rivero, Kathleen Richardson, George Stegeman, Peter Delfyett, Jr., Yu Guo, April Pope, Alfons Schulte, Thierry Cardinal, Philippe Thomas, Jean-Claude Champarnaud-Mesjard “Raman gain measurements of thallium-tellurium oxide glasses”, Page 1144 Copyright (2005), with permission from OSA)

Measurement of the Raman spectra of TeO<sub>2</sub>-based glasses doped with ZnO, GeO<sub>2</sub>, TiO<sub>2</sub>, P<sub>2</sub>O<sub>5</sub> and Sb<sub>2</sub>O<sub>3</sub> is also reported<sup>24</sup>. These spectra are shown in figure 1.10 and figure 1.11.

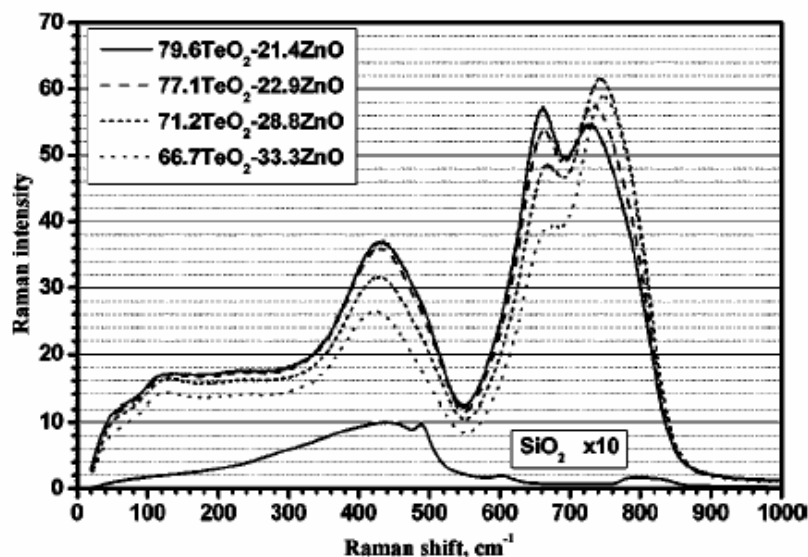


**Figure 1.10 - Reduced Raman spectra of a glass system  $x\text{ZnO} \cdot (100-x)\text{TeO}_2$ . [24]**

(Reprinted from Optics Letters, Vol. 30 Issue 10, V. G. Plotnichenko, V. O. Sokolov, V. V. Koltashev, E. M. Dianov, I. A. Grishin, M. F. Churbanov, “Raman band intensities of tellurite glasses”, Page 1156-1158 Copyright (2005), with permission from OSA)

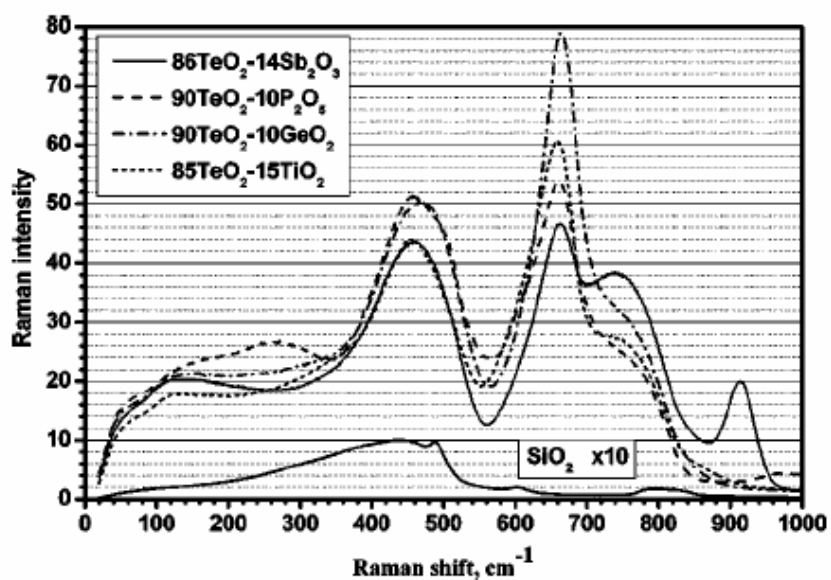


**Figure 1.11- Reduced Raman spectra of  $\text{Sb}_2\text{O}_3\text{-TeO}_2$ ,  $\text{P}_2\text{O}_5\text{-TeO}_2$ ,  $\text{GeO}_2\text{-TeO}_2$ , and  $\text{TiO}_2\text{-TeO}_2$  glasses. [24]**

(Reprinted from Optics Letters, Vol. 30 Issue 10, V. G. Plotnichenko, V. O. Sokolov, V. V. Koltashev, E. M. Dianov, I. A. Grishin, M. F. Churbanov, “Raman band intensities of tellurite glasses”, Page 1156-1158 Copyright (2005), with permission from OSA)

The intensity of bands in the Raman spectra in these glasses is seen to be much higher than that for silica glass. It is shown that these glasses can be considered as one of the most promising materials for Raman fiber amplifiers.

#### 1.4 Summary

It is clear from the previous section on multi-component glasses that these non-conventional multi-component glasses show a great potential for tellurite-based fibers as Raman amplifiers. Optical fibers highly doped with these glasses will provide a much higher Raman gain and much wider gain spectrum than that of silica. Ideally one would want to have highly doped fibers (HDFs) with these glasses as the core and silica as the cladding, to make it compatible with the standard optical fiber communication systems. However there are serious problems in manufacturing that kind of fiber because of different softening temperatures and different thermal expansion coefficients. Efforts of making such fibers are still continuing, which are presented in the next chapter. A new technique called “Core-Suction” will be presented which seems promising for fabricating HDFs.

#### 1.5 References

1. Agarwal G P, “*Nonlinear Fiber Optics*”, Academic Press, Boston 1989
2. Ajoy Ghatak and K. Thyagrajan, “*Introduction to Fiber Optics*”, Cambridge University Press, USA 1998
3. R.H. Stolen, C. Lee, and R.K. Jain, “*Development of the stimulated Raman spectrum in single-mode fibers*,” J. Opt. Soc. Am., 652 (1984)
4. Evgeny M. Dianov, “*New Raman fibers*”, chap. 7, pp. 191-211 “*Raman amplifiers for Telecommunications I, Physical principles*” ed. Mohd. Islam, Springer 2004.
5. G. E. Walrafen and J. Stone, “*Raman spectral characterization of pure and doped fused silica optical fibers*,” Appl. Spectrosc., vol. 29, pp.337–338, 1975.
6. G. P. Agrawal, *Nonlinear fiber optics*, San Diego: Academic Press, 1995
7. F. L. Galeener, J. C. Mikkelsen, R. H. Geils, and W. J. Mosby, “The relative Raman cross sections of vitreous SiO<sub>2</sub>, GeO<sub>2</sub>, B<sub>2</sub>O<sub>3</sub> and P<sub>2</sub>O<sub>5</sub>,” *Appl. Phys. Lett.*, vol. 32, pp. 34–36, 1978.

8. M. E. Lines, "Raman-gain estimates for high-gain optical fibers," *J. Appl. Phys.*, vol. 62, pp. 4363–4370, 1987.
9. Robert Stegeman, Ladislav Jankovic, Hongki Kim, Clara Rivero, George Stegeman, Kathleen Richardson, Peter Delfyett, Yu Guo, Alfons Schulte, Thierry Cardinal, "Tellurite glasses with peak absolute Raman gain coefficients up to 30 times that of fused silica", *Optics Letters*, Vol. 28 Issue 13 Page 1126 (July 2003)
10. Hiroshi Takahashi and Iwane Sugimoto, "A germanium-oxide glass optical fiber prepared by a VAD method", *IEEE JLT*, Vol. LT-2, No.5, Oct.1984, pp 613-615.
11. H. Takahashi, J. Chang, K. Nakamura, I. Sugimoto, T. Kababayashi, A. Oyobe and Y. Fujii, "Efficient single-pass Raman generation in a  $GeO_2$  optical fiber and its application to measurement of chromatic dispersion", *Optics letters*, Vol. 11, No. 6, June 1986, pp. 383-385.
12. Nakashima, T., Seikai, S., and Nakazawa, A, "Dependence of Raman gain on the relative index difference for  $GeO_2$  doped single mode fibers", *Optics Letters*, 1985,10, pp.420-423
13. V. M. Mashinsky, V. B. Neustruev, V. V. Dvoyrin, S. A. Vasiliev, O. I. Medvedkov, I. A. Bufetov, A. V. Shubin, E. M. Dianov, A. N. Guryanov, V. F. Khopin, M. Yu. Salgansky, "Germania-glass-core silica-glass-cladding modified chemical-vapor deposition optical fibers: optical losses, photorefractivity, and Raman amplification", *Optics Letters*, Vol. 29 Issue 22 Page 2596 (November 2004)
14. Yu. P. Yatsenko, A. D. Pryamikov, V. M. Mashinsky, M. E. Likhachev, A. O. Mavritsky, E. M. Dianov, A. N. Guryanov, V. F. Khopin, M. Yu. Salgansky, "Four-wave mixing with large Stokes shifts in heavily Ge-doped silica fibers" *Optics Letters*, Vol. 30 Issue 15 Page 1932 (August 2005),
15. Chun Jiang, Peizhen Deng, Junzhou Zhang, Fuxi Gan, "Emission properties of ytterbium-doped  $GeO_2$ - $TeO_2$  glasses" *Physics Letters A*, 324 (2004) 91–94.
16. P. Beneventi, D. Bersani, P.P. Lottici, L. Kovfics, F. Cordioli, A. Montenero, G. Gnappi, "Raman study of  $Bi_2O_3$ - $GeO_2$ - $SiO_2$  glasses", *Journal of Non-Crystalline Solids*, 192& 193 (1995), 258-262.
17. S. Q. Man, E.Y.B. Pun, P.S. Chung, "Tellurite glasses for 1.3  $\mu m$  optical amplifiers", *Optics Communications* 168, 1999, pp. 369–373.

18. G.Dai, F. Tassone, A.Li Bassi, V. Russo, C.E. Bottani, and F.D' Amore, "*TeO<sub>2</sub> based glasses containing NB<sub>2</sub>O<sub>5</sub>, TiO<sub>2</sub>, and WO<sub>3</sub> for discrete Raman fiber amplification*", IEEE Phot. Tech. lett., Vol.16, No. 4, April 2004, pp. 1011-1013.
19. A. Mori, H. Masuda, K. Shikano, K. Oikawa, K. Kato and M. Shimizu, "*Ultra-wideband Tellurite-Based Fibre Raman Amplifier*", Electronics Letters, Vol.37, No. 24, November 2001, pp 1442-1443.
20. A. Mori, H. Masuda, K. Shikano, and M. Shimizu, "Ultra-Wide-Band Tellurite-Based Fiber Raman Amplifier", JLT, Vol. 21, No. 5, May 2003, pp 1300-1306.
21. Z. Pan, S.H. Morgan, "*Optical transitions of Er<sup>3+</sup> in lead-tellurium-germanate glasses,*" J.Lum.75, 301-308 (1997)
22. Z. Pan, S.H. Morgan, "*Raman spectra and thermal analysis of a new lead-tellurium-germanate glass system,*" ,130-135 (1997).
23. Robert Stegeman, Clara Rivero, Kathleen Richardson, George Stegeman, Peter Delfyett, Jr., Yu Guo, April Pope, Alfons Schulte, Thierry Cardinal, Philippe Thomas, Jean-Claude Champarnaud-Mesjard "*Raman gain measurements of thallium-tellurium oxide glasses*", Optics Express, Vol. 13 Issue 4 Page 1144 (February 2005)
24. V. G. Plotnichenko, V. O. Sokolov, V. V. Koltashev, E. M. Dianov, I. A. Grishin, M. F. Churbanov, "*Raman band intensities of tellurite glasses*", Optics Letters, Volume 30, Issue 10, 1156-1158, May 2005

## II. Fabrication of Highly Doped Fibers: “Core-Suction” Technique

Recently there has been a significant interest in optical amplifiers and lasers based on highly doped fibers (HDFs). These fibers have either a high concentration of  $\text{GeO}_2$ ,  $\text{TeO}_2$ ,  $\text{PbO}$  and/or rare earth elements like erbium or use multi component glasses having a high concentration of highly nonlinear compound glasses. Highly doped fibers are termed as highly nonlinear fibers (HNLFs) if the multi-component glasses used in the core are to enhance the nonlinear effects e.g. stimulated Raman scattering for Raman amplifier purposes. This interest in highly doped multi-component core glass fiber amplifiers and lasers has stimulated a new look at the fiber fabrication methods. In this section conventional methods of making highly doped fibers are discussed followed by the development of a novel technique named “core-suction”. Efforts of making highly doped fibers using conventional techniques are presented and the successful use of the “Core-Suction” technique for making highly doped fibers is demonstrated.

### 2.1 Conventional Methods for making HDF

HNLFs could have a highly doped single-component glass like pure  $\text{GeO}_2$  or multi-component glasses like  $\text{GeO}_2$ - $\text{TeO}_2$ - $\text{PbO}$  in the core. Attempts to fabricate these highly doped fibers fall into four general categories. These can be classified as, MCVD techniques, “VAD” methods, Rod-in-Tube (RIT) methods, and Crucible methods.

#### *2.1.1 Modified Chemical Vapor Deposition (MCVD) technique*

Most of the preforms (and so the fiber) in the world have been made using MCVD technology, developed by MacChesney and his Bell Labs colleague P.B. O'Connor in the early 1970s<sup>1,2</sup>. In MCVD, the highly controlled mixture of desired chemicals is carried to the inside of a rotating glass tube made of pure synthetic  $\text{SiO}_2$ . The pure silica tube is mounted on a lathe equipped with a special heat torch. As the gasses flow inside the tube, they react to the heat by forming solid submicron particles, called "soot," in the vicinity of the heat zone. Once the soot is formed, it is deposited on the inner wall of the tube. As the burner traverses over the deposited soot, the heat transforms these solid white particles into pure, transparent glass. The deposited material forms the core region of the

optical fiber (sometimes some part of the cladding is also deposited by MCVD). The process is repeated for many hours as each subsequent core layer is formed. This gives us the ability to manufacture a wide range of ultra-pure optical fiber types. After the desired amount of core material is deposited the chemical flow is eliminated, the speed of the torch is decreased and the temperature of the flame is increased so that the tube collapses into a solid rod called a preform. This preform can then be drawn on the drawing tower to give the desired fiber.

Attempts to use the basic MCVD process to fabricate a pure GeO<sub>2</sub> core in a silica cladding have failed because of the difference in softening temperatures between silica and germania glasses and the mismatch in their thermal expansion coefficients. Also there appear problems during the preform collapse step and seem to involve both vaporization of the germania and penetration of the Ge into the silica cladding. An early report deposited GeO<sub>2</sub> inside a small-bore silica tube and avoided the usual collapse step by collapsing the tube during the actual drawing of the fiber<sup>3</sup>. In that work the core appeared to be a mixture of Germania and Silica suggesting that Silica still diffused into the core. This method gave multimode fibers having ~ 50-mol % GeO<sub>2</sub> doping in the core. Another approach had an intermediate germanosilicate cladding and P<sub>2</sub>O<sub>5</sub>- and F-doped silica cladding matched with a silica substrate tube<sup>4-5</sup>. This approach generated MCVD fibers composed of a core with a GeO<sub>2</sub> concentration of up to 97-mol%.

An alternative fabrication technique is to use a lower melting temperature glass such as Pyrex™ as the MCVD substrate tube for the cladding. This was done successfully at Bell Labs in the 1980's. This fiber was measured as a part of this thesis work and the fiber was found to have only 30-mol % GeO<sub>2</sub> in the core showing a diffusion of silica into the core. Measurements on this fiber will be discussed in the next chapter.

The MCVD technique can be modified to fabricate fibers with multi-component glasses in the core but it will be very difficult, time consuming and expensive. An extension of MCVD technique is known as the solution-doping<sup>6-7</sup> technique. It is mainly used for the fabrication of rare-earth-doped fibers and provides a way of introducing additional co-

dopant like erbium along with other index modifying materials like germanium. The solution doping technique involves combining rare-earth-containing compounds with the soot before the consolidation of preform. This technique offers the greatest potential for high purity and tight optical confinement, but the process is very slow and somewhat complicated.

### ***2.1.2 Vapor Axial Deposition (VAD) technique***

The VAD process, developed by NTT, Japan, permits a continuous length endless silica fiber preform to be produced unlike MCVD<sup>8-9</sup>. The process consists of blowing dopant vapors with O<sub>2</sub> and H<sub>2</sub> into the lower end of a rotating silica glass rod which acts as a seed. A flame causes the hydrolysis reactions. A porous soot rod is formed, which is pulled up while being rotated. The porous rod is dehydrated and consolidated in a furnace. In addition to the possibility to have a continuous, endless length preform, this technique has several other advantages. The torch does not move, the gas flow rates are constant; a high deposition rate can be achieved. The disadvantage is that the flame control is difficult. This technique is reported to produce a Sb-GeO<sub>2</sub> doped, 93 microns diameter core, low loss fiber<sup>10-11</sup>. Smaller core single mode fibers are produced by first overcladding the VAD preform with a silica tube.

Other conventional methods of making HDF are Rod-in-tube approach and Crucible methods which usually involve processing bulk glass samples. Core glasses are processed separately and then combined with cladding material using the above mentioned techniques, as discussed below.

### ***2.1.3 Rod-in tube Method***

In this method, a thin rod of highly nonlinear glass is inserted into a small-bore silica tube. In a conventional rod-in-tube fiber drawing process, the outer tube is collapsed over the glass rod on a glass lathe prior to insertion in the draw tower furnace. This is how optical fibers were made prior to the invention of the MCVD process. It is particularly – suited to large-core fibers of lower melting temperature glasses although small-core single-mode fibers can be made by overcladding the preform before fiber drawing.



An alternative approach to the rod-in tube method is called ‘powder in tube’<sup>12</sup> which helps in reducing the crucible contamination. It involves inserting the core glass powder in the hollow core of a cladding tube. This cladding tube containing the core glass powder is then heated in the furnace on the draw tower. The powder then fuses during draw producing a fiber with a highly nonlinear glass core. This method allows for the potential application of  $\text{GeO}_2$  and alternate materials such as  $\text{TeO}_2$ .

#### **2.1.4 Crucible Technique**

In the crucible technique, the highly doped core glass sample (bulk or powder) is inserted in a thin hole in a thick-walled glass tube sealed at the bottom (crucible)<sup>13</sup>. Alternatively a glass sample can be inserted in a thin-walled tube sealed at the bottom (crucible) and then overlapped. The final assembly with a thick-walled glass tube is heated in a high temperature furnace and drawn into a fiber. This technique is illustrated in figure 2.1.

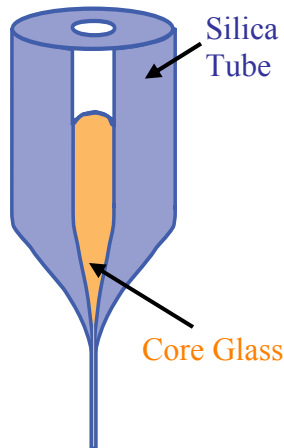


**Figure 2.1- Crucible Method of making HDF**

There is a little difference between rod-in-tube and crucible technique. In a conventional rod-in-tube fiber drawing process, the outer tube is collapsed over the glass rod on a glass lathe prior to insertion in the draw tower furnace. When adapted to a crucible method, all melting usually occurs directly in the draw tower furnace.

In our trials, crucibles were formed by sealing off the bottom ends of 6mm x 12 mm silica tubes. In two different trials, pure  $\text{GeO}_2$  and pure  $\text{TeO}_2$  powders were used as high

nonlinear core materials and inserted in the silica tube. This assembly was then heated on a Heathway vertical lathe to melt the powder and making the core preform. However this preform started cracking at the interface while cooling down (shown in figure-2.2). Stresses developed at the interface because of the different melting temperatures and thermal expansion coefficients of  $\text{SiO}_2$  and  $\text{GeO}_2$  or  $\text{TeO}_2$ ;<sup>14</sup> seem to be the possible cause of the crack down. Another failure mechanism was a blow-out of the side of the preform. This is probably a result of air trapped inside the preform during the over-cladding step.



*Figure 2.2- Crucible Preforms showing Blow-out, cracking and stresses on the interfaces*

A variant of the crucible technique named “Core-Suction” for fabricating the preforms with non-conventional multi-component glasses was developed later which is the key discussion topic of the current research work. This technique is discussed in the next section.

## **2.2 “Core-Suction” Technique**

This technique involves drawing the molten core glass material into a silica cladding tube. In the “core-suction” technique, the core glass is first melted in a conventional

alumina crucible inside a furnace and the molten glass is then drawn into a cladding tube to form the preform. After the preform is cooled, it can be drawn directly or overlapped to attain the desired core-cladding ratio.

This technique relies on the fact that the softening temperature of the multi-component core glass is much less than that of the cladding tube. The preform fabrication process includes three main steps; preparation of the cladding tube, preparation of the core glass sample and finally suction of the molten core glass into the cladding tube. A schematic diagram of this technique is illustrated in figure 2.3.

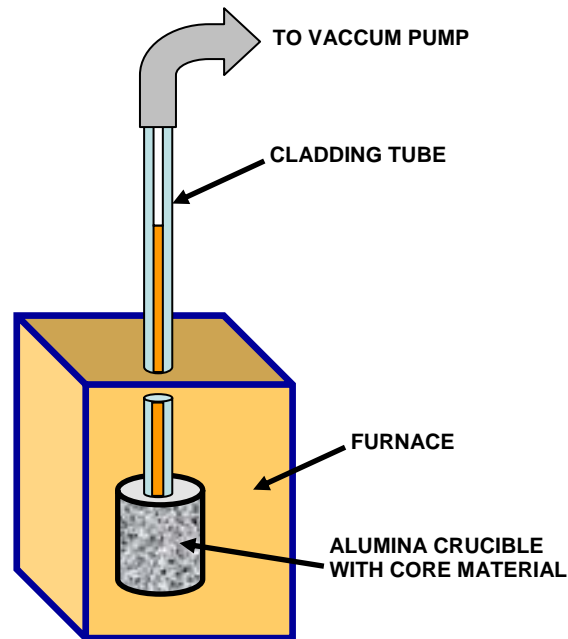


*Figure 2.3- Schematic Diagram of “Core-Suction” Technique for making HDF*

### **2.2.1 Use of Muffle Furnace for “Core-Suction” Technique**

Figure 2.4 shows a muffle furnace which has a hole in the top for the thermometer. The core glass sample is melted in a small alumina crucible and a silica tube is inserted into the crucible through the thermometer hole. A vacuum pump is used to draw the molten core glass into the cladding tube to form the preform. Drawn core material into the silica

cladding tube can be seen in the figure 2.4. Once the preform is cooled, the bottom is sealed and then pulled to give the desired fiber.



*Figure 2.4- Use of Muffle Furnace for “Core-Suction” Technique*

In the very first trial using a Muffle furnace, a mixture of pure  $\text{GeO}_2$  and pure  $\text{TeO}_2$  powders was used as the core material which was successfully drawn into a 1.0 mm x 6.0 mm silica tube. This mixture melted around  $1000^\circ\text{C}$ , unfortunately that is the upper limit of the muffle furnace, and so the heating element of the furnace was burned. Thus it was decided to experiment with lead based Schott SFL6 glass which has lower melting temperature. Another reason of doing so was to get expertise in this technique before using the expensive  $\text{GeO}_2$  and pure  $\text{TeO}_2$  powders. We successfully made many preforms by drawing the core glass into silica cladding tubes; figure 2.5 displays the photograph of one of the preforms made by this technique.

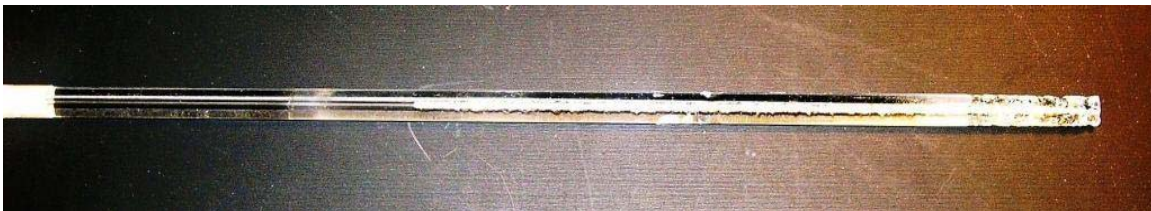


*Figure 2.5- Photograph of Glass Preform made by “Core-Suction” Technique*

The next step was to draw the fiber from these preforms. To check the stability of core material while drawing, preform was pulled into fiber first on the glass lathe. In most cases the core material moved away from the heating region, leaving an air hole behind in the pulled fiber core. Examples of such fibers are shown in the figure- 2.6(a) and 2.6(b); the SFL6 glass is the bright ring around the center hole. In some cases a conventional core (shown in figure-2.7) was observed, but in very small piece of the fiber.

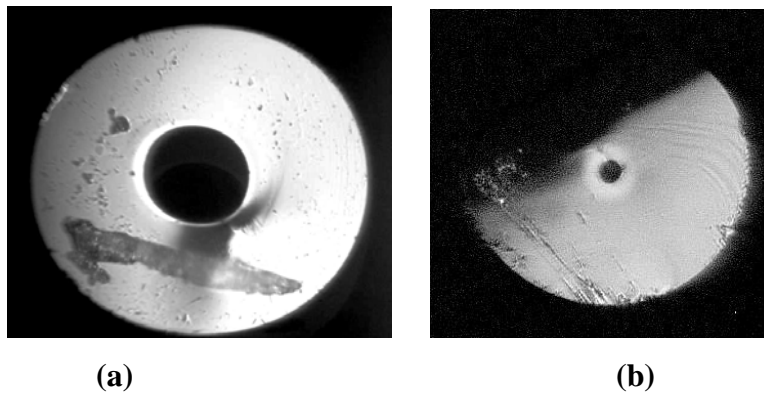


**Figure 2.6- Micrographs of fibers made by “Core-Suction” Technique**  
(SFL6 glass is the bright ring around the center hole)

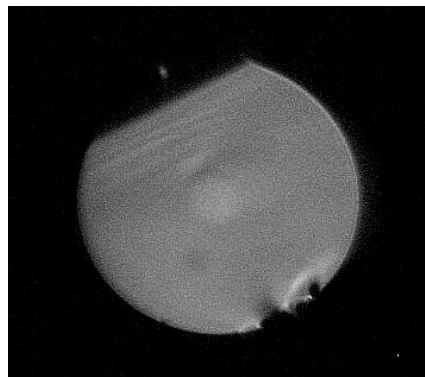


**Figure 2.7- Micrograph of the fiber with conventional core made by “Core-Suction”  
Technique using Muffle Furnace**

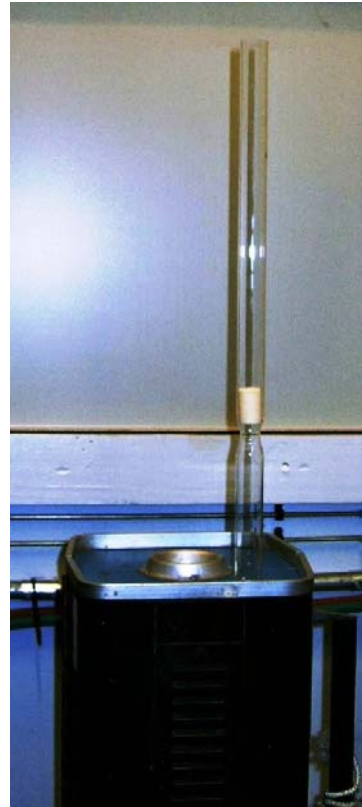
One of the major problems with the muffle furnace was its large heating zone (~ 6 inches x 6 inches) leading to high heat dissipation. Although the muffle temperature limit was around 1100<sup>0</sup>C, the temperature observed by the crucible was a maximum of around 1000<sup>0</sup>C making it impossible to melt glasses having a melting temperature around 1100<sup>0</sup>C. The heating element was destroyed trying to reach the limits of the furnace. Another problem with this furnace was its smaller depth of about 6 inches which resulted in very small length preforms. Also the crucible often tipped over while trying to draw the molten glass into the cladding tube.

### **2.2.2 Use of Tube Furnace for “Core-Suction” Technique**

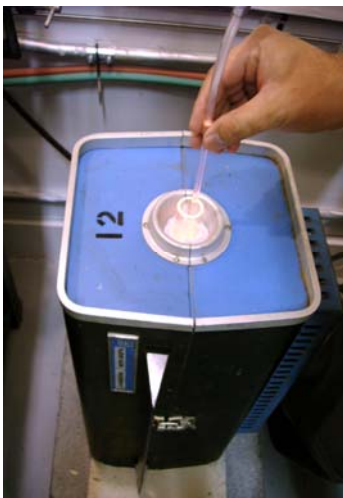
Most of the problems faced with the muffle furnace were solved by using a horizontal tube furnace vertically. This furnace is shown in figure 2.8 (a). This furnace was about 20 inches in height, having holes on the side of ~ 2 inches diameter. The heating element was ~ 13 inches long giving a preform length of about 12 inches. A crucible aligner was designed to avoid flipping over of the crucible. A glass tube was shrunk close to the bottom and the crucible sat tightly over the shrunken portion as shown in figure 2.8 (b). Figure 2.8(c) shows a silica cladding tube attached with a rubber tube for vacuum pump. This tube is dipped into the molten core material in the crucible. A cladding tube having molten core material just after the drawing up material can be seen in figure 2.8(d). Figure 2.8(e) shows the aligner tube having a crucible with molten core material after the suction. This furnace had a temperature limit of 1200<sup>0</sup>C but because of heat dissipation the maximum furnace temperature was measured to be ~ 1100<sup>0</sup>C.



*(a) Tube Furnace*



*(b) Tube Furnace with Crucible Aligner*



*(c) Suction of Core Material*



*(d) Cladding Tube just after  
Suction of Core Material*



*(e) Crucible inside the aligner  
with Molten Core Material*

*Figure 2.8- Use of a Tube Furnace for “Core-Suction” Technique*



***Figure 2.9- Preforms made by “Core-Suction” Technique using a tube Furnace  
(Before cool down)***

Preforms having a length of about 12 inches were made using this furnace. Two such preforms can be seen in figure 2.9; this figure shows the photographs of the preforms just after their fabrication before cooling down.



***Figure 2.10- Preforms made by “Core-Suction” Technique using a tube Furnace  
(After cool down)***

Figure 2.10 shows a preform after cool down. It is important to cool down the preform to check the uniformity of the core material and if there is any air trapped resulting in bubbles in the preform. While cooling down, bubbles often resulted in cracking the preform at the positions where bubbles were present.

#### **2.2.2.1 Fabrication of SF6 glass Fiber**

The first successful attempt, using the “core-suction” technique incorporated Schott SF6 glass, as the core glass. The cladding tube used was a silica capillary having a 1 mm inner diameter and 6 mm outer diameter. A small preform was made by the “core-suction” technique as described earlier. This SF6 core in silica cladding tube preform was



then pulled into fiber on the glass lathe. The fiber was about 2 inches in length and tapered having a core diameter ranging from 22 micron to 45 micron surrounded by a cladding having diameter varying from 172 micron to 352 micron. Figure 2.11 shows the cross sections of different ends of the pulled fiber.

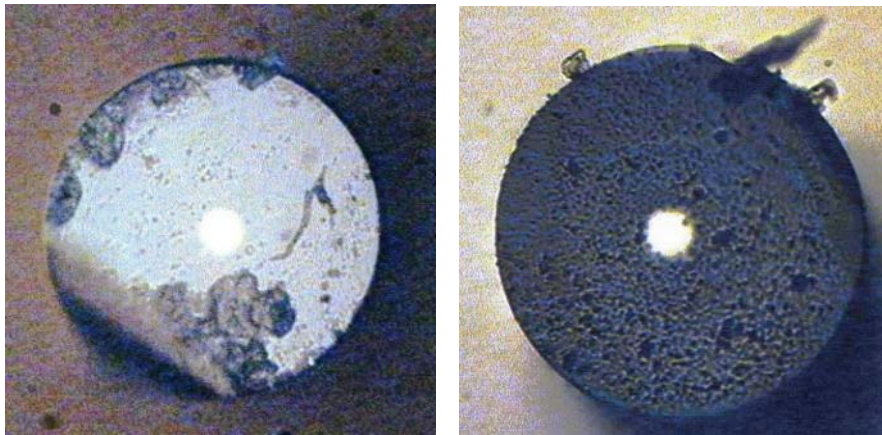


***Figure 2.11- Cross sections of the fiber fabricated by “Core-Suction” technique using SF<sub>6</sub> as the core glass in silica cladding tube***

This figure also shows the tight confinement of light inside the core because of the high index difference of the core and the cladding.

He-Ne light at 632.8 nm wavelength was launched in this fiber and the output multimode pattern of the fabricated fiber can be seen in figure 2.12.

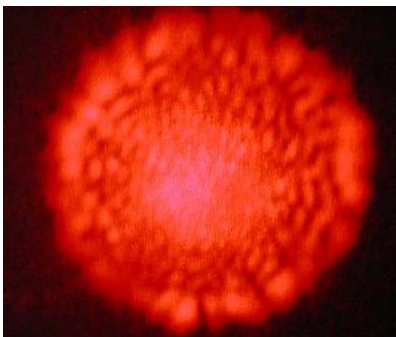


***Figure 2.12- Output multimode pattern of the SF<sub>6</sub>-core in silica cladding fiber with red He-Ne light launched at the input***

From the light acceptance cone angle, the numerical aperture (NA) was measured to be 0.46. From the refractive indices values of the SF6 core glass ( $n_1=1.7988$ ) and silica ( $n_2=1.4591$ ) cladding, the NA was calculated to be 1.052 using the formula  $NA = \sqrt{n_1^2 - n_2^2}$ . This difference in NA values indicates a possibility of silica diffusion into the SF6 core or vice versa. Since the fiber length was only about 4 cm, measurements such as the loss spectrum and index profile could not be performed on this fiber.

Other glass samples used as the core materials in silica cladding tubes were Lead-Germanate-Tellurite based<sup>15-16</sup>, obtained from Fisk University. They were labeled as Sample-1, Sample-3 and Sample-5 having the following compositions.

**Sample 1** - 27PbO.43GeO<sub>2</sub>.20TeO<sub>2</sub>.10CaO.0.2 Er<sub>2</sub>O<sub>3</sub>

**Sample 3** - 26PbO.33GeO<sub>2</sub>.30TeO<sub>2</sub>.5CaO.1Nd<sub>2</sub>O<sub>3</sub>.0.5Na<sub>2</sub>CO<sub>3</sub>

**Sample 5** - 27PbO.33GeO<sub>2</sub>.30TeO<sub>2</sub>.10CaCO<sub>3</sub>

Fabrication of optical fibers using these core glasses in the silica cladding tube is discussed in the following section.

#### 2.2.2.2 Fabrication of Lead-Germanate-Tellurite-Neodymium Glass Fiber

**Sample 3 glass fiber:** A second preform was made with a Lead-Tellurium-Germanate-Neodymium core glass sample labeled “sample-3”. A 1 mm inner diameter and 6 mm outside diameter silica capillary was used as the cladding tube. This preform was then pulled into fiber on a fiber drawing tower. A total length of about 10 meters was drawn but the longest sample length was about 2 meters because of the weak mechanical strength of the uncoated fiber. The cross section of the fiber drawn from this preform is shown in figure 2.13. This fiber had a core diameter of around 18 micron surrounded by a 120 micron diameter cladding.

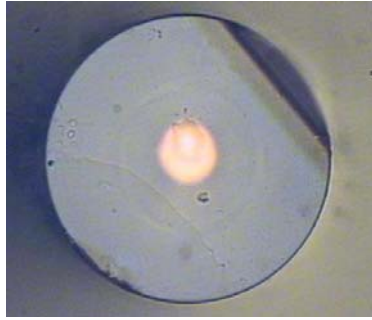


***Figure 2.13-Fiber Cross section of the fiber fabricated by “Core-Suction” Technique using Sample 3 (26PbO. 33GeO<sub>2</sub>. 30TeO<sub>2</sub>. 5CaO. 1Nd<sub>2</sub>O<sub>3</sub>. 5Na<sub>2</sub>CO<sub>3</sub>) as the core material***

An attempt was made to obtain a smaller core diameter by using a smaller hole cladding tube. A 1 x 6 mm silica cladding diameter tube was shrunk on a vertical glass lathe as shown in figure 2.14. The shrunken tube appeared to have an oval hole possibly because of misalignment of the chucks of the lathe. The molten “Sample-3” core glass was drawn into this tube by the “core-suction” technique as discussed above. A preform was fabricated and then drawn into a fiber on the drawing tower.

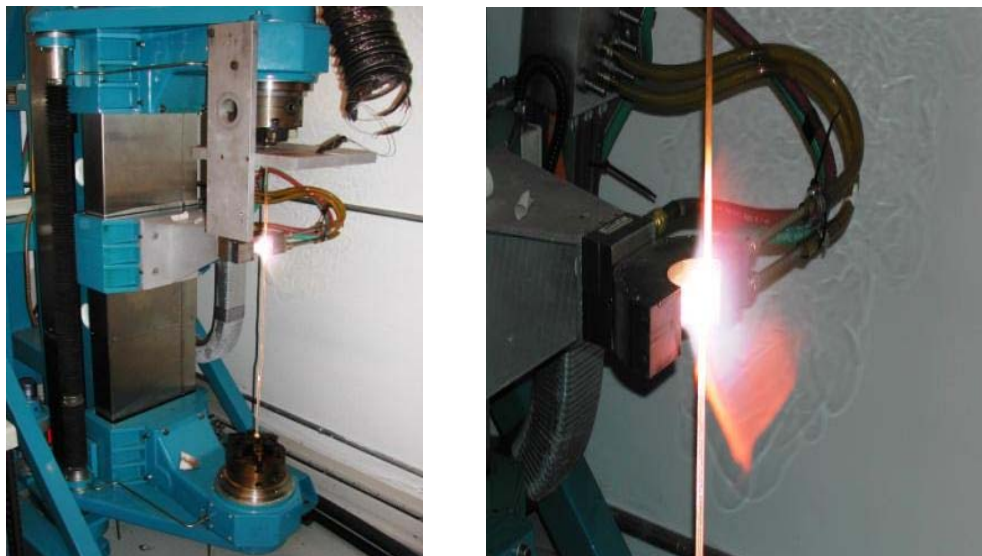


***Figure 2.14- Vertical Lathe Shrinking the Cladding Tube***

Figure 2.15 shows the cross-sections of two different fiber pieces drawn from the same preform. Core diameters in these fibers appeared to be smaller but the core was oval in shape.

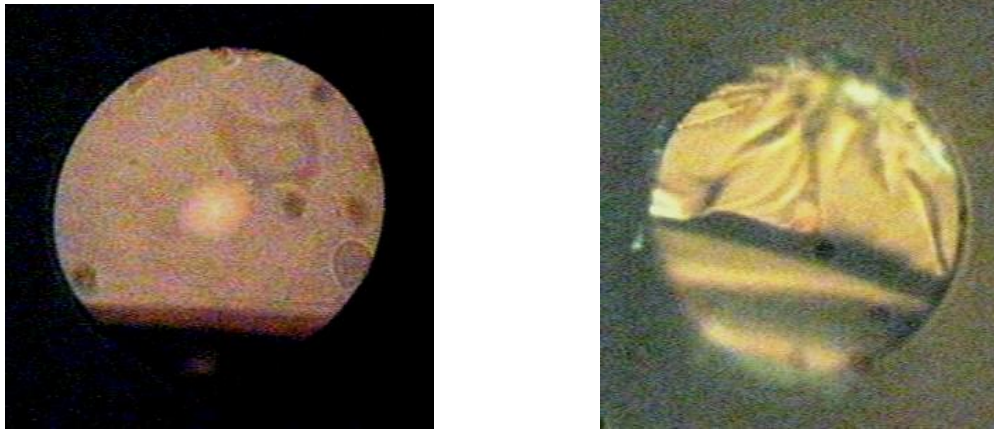


*Figure 2.15 - Fiber Cross sections of the fiber fabricated by “Core-Suction” Technique using Sample 3 ( $26\text{PbO}$ ,  $33\text{GeO}_2$ ,  $30\text{TeO}_2$ ,  $5\text{CaO}$ ,  $1\text{Nd}_2\text{O}_3$ ,  $5\text{Na}_2\text{CO}_3$ ) as the core material*

### **2.2.2.3 Fabrication of Lead-Germanate-Tellurite glass Fiber**

**Sample 5 glass fibers:** In another trial Lead-Tellurium-Germanate core glass sample labeled “sample-5” was used to fabricate the preform by “core-suction”. The starting silica cladding tube had a 1 mm inner diameter and 6 mm outside diameter. This tube was then shrunk to give a smaller holed tube. A preform was then fabricated by suction as before. This preform was pulled on a fiber drawing tower to give the desired fiber. The cross sections of some of the fiber pieces drawn from this preform are shown in figure 2.16. These fibers had core diameters of around 12 micron surrounded by 150 micron diameter claddings.

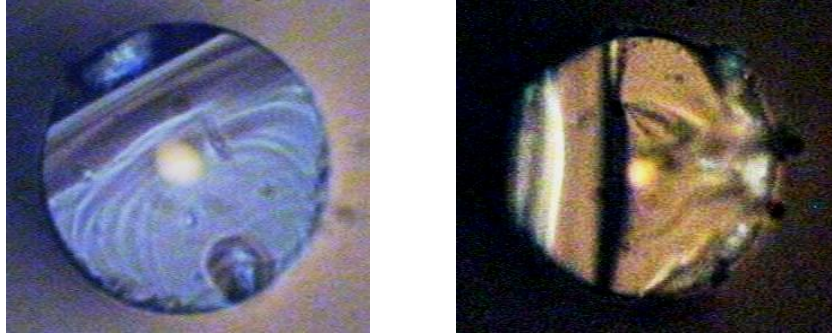


***Figure 2.16-Fiber Cross sections of the fiber fabricated by “Core-Suction” Technique using Sample 5 (27PbO. 33GeO<sub>2</sub>. 30TeO<sub>2</sub>. 10CaCO<sub>3</sub>) as the core material***

#### **2.2.2.4 Fabrication of Lead-Germanate-Tellurite-Erbium glass fiber**

A Lead-Germanate-Tellurite-Erbium glass fiber was drawn from a preform which had sample-1 as core glass. Sample 1 was a multi-component glass having the composition 27PbO.43GeO<sub>2</sub>.20TeO<sub>2</sub>.10CaCO<sub>3</sub>.0.2 Er<sub>2</sub>O<sub>3</sub>. In this case the 1 mm ID and 6 mm OD silica cladding tube was first shrunk using the vertical glass lathe to obtain a thicker wall cladding tube. By using core glass sample 1 and the silica cladding tube a small preform was then fabricated by “core-suction” as described earlier. Fiber from this preform was then drawn on the fiber drawing tower.

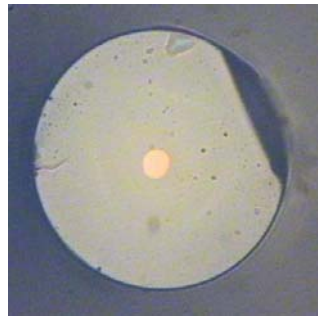


***Figure 2.17- Fiber Cross section of the fiber fabricated by “Core-Suction” Technique using Sample 1 (27PbO. 43GeO<sub>2</sub>. 20TeO<sub>2</sub>. 10CaCO<sub>3</sub>. 0.2 Er<sub>2</sub>O<sub>3</sub>) as the core material***

Figure 2.17 shows the cross section of the fiber drawn; this fiber had a 10 micron diameter core surrounded by a 102 micron diameter cladding.

One of the problems faced with all these preforms having TeO<sub>2</sub> in the core glass was the short lengths of the final fiber pieces during the drawing. The maximum length of fiber pieces was around 10 meters. The reason behind short lengths was that while drawing the

fiber became thinner at the top (inside the furnace) and finally separated from the preform. When the preforms were taken out of the furnace, blow-outs were found at the tip of the preforms as shown in figure 2.18.

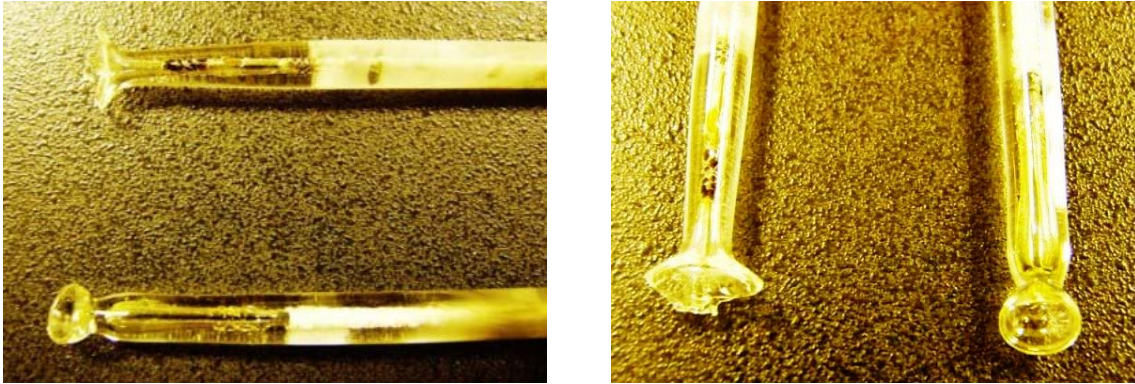


*Figure 2.18- Blow-Outs at the tips of the Preforms*

The possible cause of these blow-outs was the lower boiling temperature of  $\text{TeO}_2$  compared to silica and other glasses. As a result when the preform was drawn,  $\text{TeO}_2$  vaporized and pressurized the preform resulting in a blow out of the preform. This was later confirmed from the elemental analysis of the fibers which showed no  $\text{TeO}_2$  in the core. This analysis is described in the next chapter.

#### **2.2.2.5 Fabrication of MM2 (Phosphate-Erbium-Alumina) glass fibers**

The last sample tried using this technique was a very high gain glass called MM2 obtained from Kigre Incorporated<sup>17</sup>. Figure 2.19 displays the photographs of the MM2 glass sample.

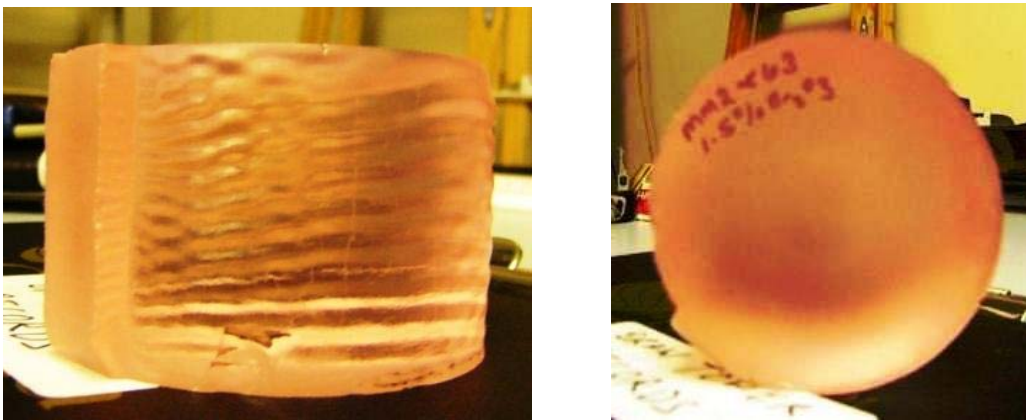


*Figure 2.19- MM2 Glass Sample*

The exact composition of this glass was unknown but it was composed of erbium, phosphate and alumina. This glass was melted in an alumina crucible inside a tube furnace as discussed before. The starting cladding tube had 2 mm inner diameter and 8 mm outside diameter. This tube was then shrunk on a horizontal glass lathe shown in figure 2.20.



***Figure 2.20- Horizontal Lathe Shrinking the Cladding Tube***

The molten MM2 glass was then drawn into the shrunken cladding tube by the “core-suction” technique, as discussed above. This preform was then pulled into fiber on the fiber drawing tower. A total length of about 10 meters was drawn but the longest sample length was about 2 meters because of the weak mechanical strength of the uncoated fiber. The cross sections of the fibers drawn from this preform are shown in figure 2.21.

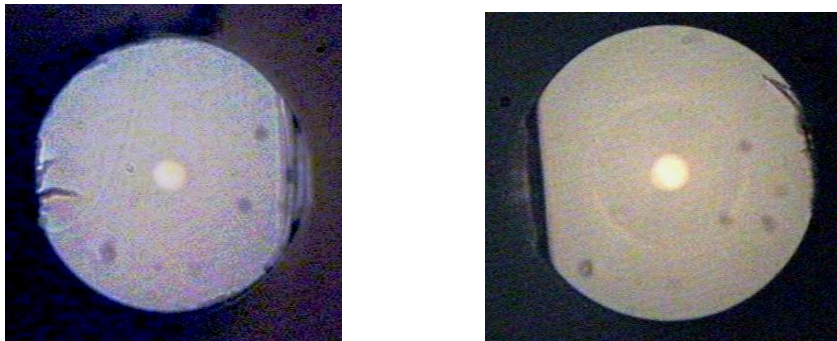


***Figure 2.21-Cross sections of the fiber fabricated by the “Core-Suction” technique using MM2 core glass in silica cladding tube***

This fiber had a core diameter ranging from 9 to 15 micron diameter and a cladding diameter varying from 130 to 150 micron.

### 2.3 Advantages of “Core-Suction” Technique

There are some significant potential advantages to the “core-suction” technique. Because of the extremely small quantities of molten glass, expensive high-purity materials can be used. The furnace can be designed with a high purity silica tube as an inner wall. A pure inert gas can flow through the inner tube as in conventional fiber draw furnaces. The use of a controlled atmosphere and extremely small quantities of starting material should make possible the safe use of toxic constituents. The additional processing steps involved in the earlier crucible techniques or in conventional rod-in-tube methods have been eliminated which will reduce contamination of the core glass in the final fiber. The suction process also avoids bubbles from trapped air which have appeared in earlier crucible techniques.

### 2.4 Summary

A new technique named “core-suction” for fabricating optical fiber preforms with non-conventional glasses in the core has been developed. Use of the developed technique for making fibers of SF<sub>6</sub>, Lead-Germanate-Tellurite based three different glass samples and one MM2 glass sample in the core and silica cladding has been successfully demonstrated. Measurements on the fabricated fibers will be presented in the next chapter.

### 2.5 References

1. J.B.; O'Connor, P.B.; Presby, H.M. MacChesney; “*A new technique for the preparation of low-loss and graded-index optical fibers*”, Proceedings of the IEEE Volume 62, Issue 9, Sept. 1974 Page(s):1280 – 1281
2. MacChesney, “*MCVD: Its origin and subsequent development*”, J.; Selected Topics in Quantum Electronics, IEEE Journal of Volume 6, Issue 6, Nov.-Dec. 2000 Page(s):1305 – 1306.
3. A.M. Peder-Gothi and M. Leppihalme, “*Germanium dioxide-core/ Silicon dioxide-cladding optical fibers made by MCVD for stimulated Raman applications,*” Appl.Phys.B, B42, 45-9 (1987).



4. V. M. Mashinsky, V. B. Neustruev, V. V. Dvoyrin, S. A. Vasiliev, O. I. Medvedkov, I. A. Bufetov, A. V. Shubin, E. M. Dianov, A. N. Guryanov, V. F. Khopin, M. Yu. Salgansky, “*Germania-glass-core silica-glass-cladding modified chemical-vapor deposition optical fibers: optical losses, photorefractivity, and Raman amplification*”, *Optics Letters*, Vol. 29 Issue 22 Page 2596 (November 2004).
5. Yu. P. Yatsenko, A. D. Pryamikov, V. M. Mashinsky, M. E. Likhachev, A. O. Mavritsky, E. M. Dianov, A. N. Guryanov, V. F. Khopin, M. Yu. Salgansky, “*Four-wave mixing with large Stokes shifts in heavily Ge-doped silica fibers*”, *Optics Letters*, Vol. 30 Issue 15 Page 1932 (August 2005).
6. J.Stone, C.A. Burrus, “*Neodymium-doped silica lasers in end-pumped fibers geometry*”. *Appl Phys Lett.*,3, pp.388-389, 1973.
7. J.E. Townsend, S.B. Poole, D.N. Payne, “*Solution-doping technique for the fabrication of rare-earth doped optical fibres*”. *Electron. Lett.*,23, pp.329-331, 1987.
8. Izawa, T.; Inagaki, N.; “*Materials and processes for fiber preform fabrication—Vapor-phase axial deposition*”, *Proceedings of the IEEE*, Volume 68, Issue 10, Oct. 1980 Page(s):1184 – 1187.
9. Takata, H.; Murata, H.; Kurauchi, N.; Inada, K.; “*Review of VAD fiber performance and processing*”, *Quantum Electronics, IEEE Journal of Volume* 17, Issue 12, Part 1, Dec 1981 Page(s):2368 – 2368.
10. Hiroshi Takahashi and Iwane Sugimoto , “*A germanium-oxide glass optical fiber prepared by a VAD method*”, *IEEE JLT*, Vol. LT-2, No.5, Oct.1984, pp 613-615.
11. H. Takahashi, J. Chang, K. Nakamura, I. Sugimoto, T. Kababayashi, A. Oyobe and Y.Fujii, “*Efficient single-pass Raman generation in a GeO<sub>2</sub> optical fiber and its application to measurement of chromatic dispersion*”, *Optics letters*, Vol. 11, No. 6, June 1986, pp. 383-385.

12. J. Ballato and E. Snitzer, "*Fabrication of Fibers with High Rare-Earth Concentrations for Faraday Isolator Applications*," Appl. Opt. 34, 6848 - 6854 (1995).
13. D. Kominsky and R. Stolen, "*Crucible technique for producing a Silica/Indium Phosphate hybrid fiber*", Optics in the Southeast, University of North Carolina at Charlotte, Charlotte, North Carolina, September 18, 2000.
14. Lide, D.R., *CRC Handbook of Chemistry and Physics*, 73<sup>rd</sup> Edition, CRC press, Boca Raton, 1992.
15. Z. Pan, S.H. Morgan, "*Optical transitions of  $Er^{3+}$  in lead-tellurium-germanate glasses*," J.Lum.75, 301-308 (1997).
16. Z. Pan, S.H. Morgan, "*Raman spectra and thermal analysis of a new lead-tellurium-germanate glass system*", J. Non-Cryst. Sol. 210,130-135 (1997).
17. Data on Kigre MM2 available at <http://www.kigre.com/MM2Datasheet.pdf>

### III. Characterization of Highly Doped Fibers

In the last chapter the successful use of the “Core-Suction” technique for making highly doped fibers based on SF6, Lead-Germanate-Tellurite and MM2 glasses in the core and silica cladding was demonstrated. In this chapter, measurements on these manufactured fibers and one existing high GeO<sub>2</sub> doped fiber obtained from Bell Labs are presented. These measurements include loss, refractive index profile, spontaneous spectrum and elemental analysis. Elemental analysis using an electron microprobe on all of these fibers shows that silica diffuses into the core forming a silicate based core. This also provides a reasonable explanation for lower than the expected index values in the cores of all of these fibers. Table 3.1 lists all the measured fibers with their core and cladding compositions.

**Table 3.1 – List of the Fibers Measured**

Label	Core Glass	R.I	Cladding Glass
Sample S1	27PbO.43GeO <sub>2</sub> .20TeO <sub>2</sub> .10CaCO <sub>3</sub> .0.2 Er <sub>2</sub> O <sub>3</sub>	~1.86	Silica
Sample S3	26PbO.33GeO <sub>2</sub> .30TeO <sub>2</sub> .5CaO.1Nd <sub>2</sub> O <sub>3</sub> .0.5Na <sub>2</sub> CO <sub>3</sub>	~1.91	Silica
Sample S5	27PbO.33GeO <sub>2</sub> .30TeO <sub>2</sub> .10CaCO <sub>3</sub>	~1.91	Silica
Bell Labs Fiber	90GeO <sub>2</sub> .10B <sub>2</sub> O <sub>3</sub>	NA	Pyrex
MM2 Glass Fiber	Alumina. Erbium. Phosphate (actual composition unknown)	NA	Silica

#### 3.1 Loss Measurement by Cut-Back Method

*Splicing of Fabricated Fibers to the Standard Corning SMF-28 fiber pigtail:* To measure the loss spectrum of fabricated fibers, they were fusion spliced to Corning SMF-28 standard single mode fiber pigtails. A commercial splicer (Fitel model S-175) was used to splice the fibers. All the fibers listed in table-1 except the one from Bell labs, were fusion spliced without any difficulty. Splice losses of better than 0.3 dB were measured by the splicer in all cases. The fiber from Bell labs could not be spliced to any standard fiber because of its Pyrex cladding which has much lower melting temperature than that of the silica cladding of standard fibers. So the loss of this fiber could not be measured.

Some of the fabricated fibers were of non-standard size which created difficulty in cleaving since the best cleaver (JDS Fitel model S-315) is designed for standard 125 micron cladding fibers. In some of the cases good cleaves were obtained with a Fujikura ultrasonic cleaver while in other cases manual cleaving worked well.

*Sample S1 fiber:* The loss spectrum of this fiber was measured in about 1.5 meters length with the cutback technique by the use of an optical spectrum analyzer and a high power tungsten-filament white light source. Loss of approximately 0.3 dB/cm was measured at the 1550 nm wavelength. A strong erbium ion absorption peak having loss of about 0.6 dB/cm was found at 1535 nm. Another characteristic peak of erbium ions can be seen at 980 nm showing a loss of 0.35 dB/cm. The loss spectrum of this fiber can be seen in figure 3.1.

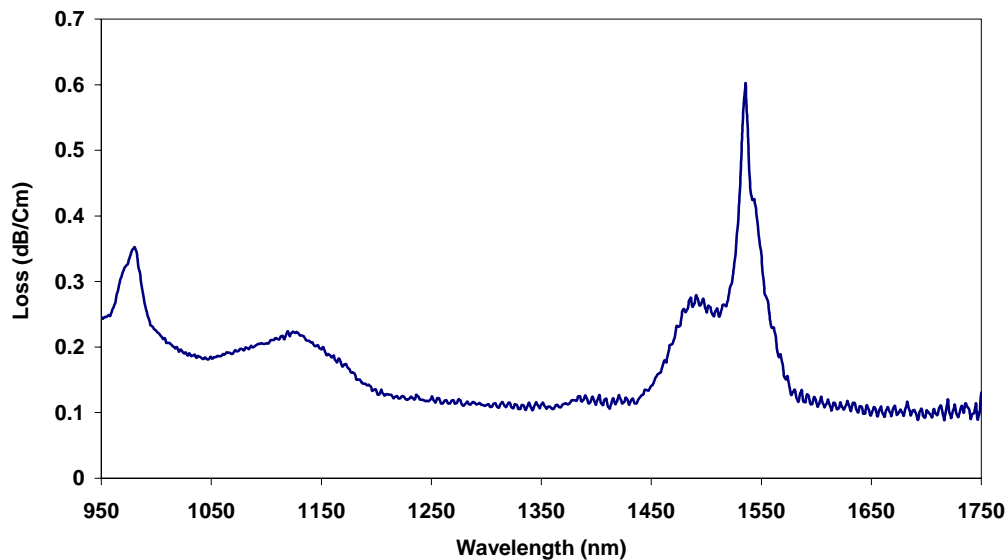


***Figure 3.1 - Loss Spectrum of Sample 1 Fiber***

*Sample S3 fiber:* Using a commercial fusion splicer this fiber was easily spliced to a standard Corning SMF-28 single mode fiber pigtail to measure the loss spectrum. The loss spectrum of this fiber was measured in about 2 meters length with the cutback technique using an optical spectrum analyzer and a tungsten-filament high power white

light source as before. The minimum loss was 4.7 dB/m ~ 1300 nm. There is a strong absorption peak present at 1590 nm having loss of ~ 11.3 dB/m. The loss spectrum of this fiber can be seen in figure 3.2.

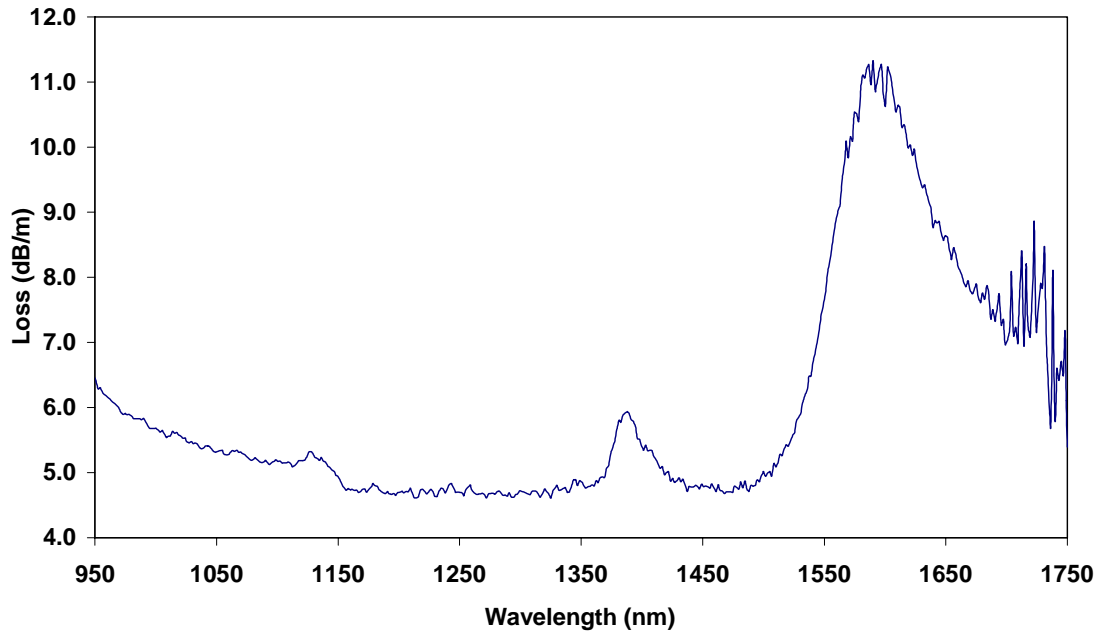


**Figure 3.2 - Loss Spectrum of Sample 3 Fiber**

*Sample S5 fiber:* As before using a commercial fusion splicer this fiber was easily spliced to a standard Corning SMF-28 single mode fiber pigtail to measure the loss spectrum. The loss spectrum of this fiber was measured in about 2 meters length with the cutback technique using an optical spectrum analyzer and an erbium amplified spontaneous emission (ASE) source. The tungsten-filament source was unavailable at the time of these measurements, so the loss spectrum could only be measured over the 1550 nm band of the high power Erbium ASE source. The loss spectrum of this fiber can be seen in figure 3.3. The minimum loss was ~ 0.35 dB/m was measured at ~ 1580 nm wavelength.

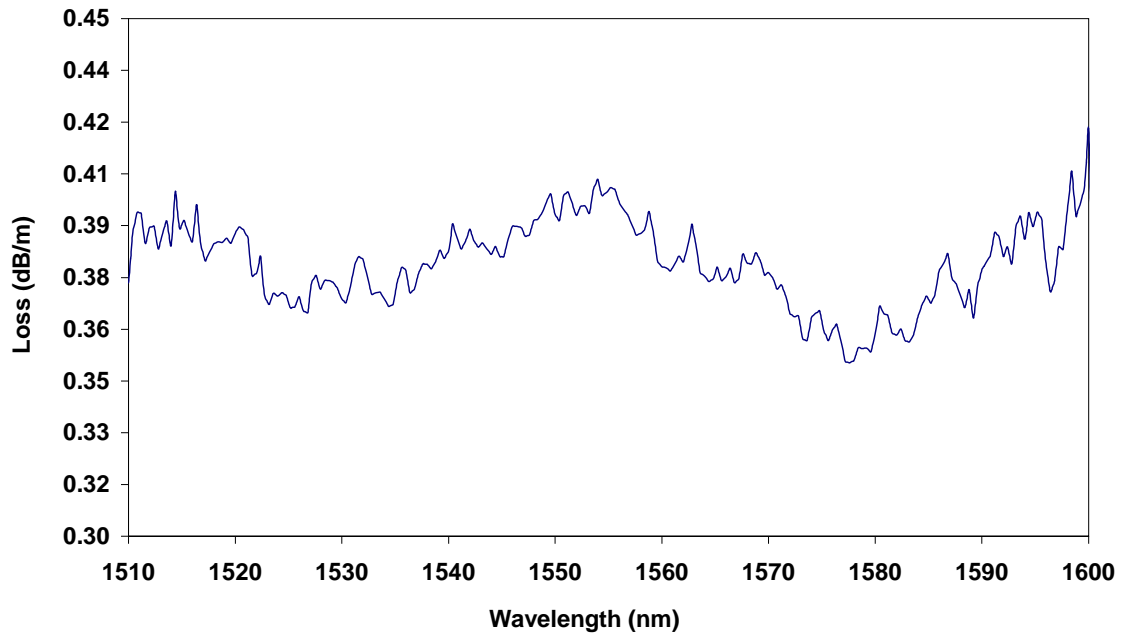


***Figure 3.3- Loss Spectrum of Sample 5 Fiber***

*MM2 Glass fiber:* Using a commercial fusion splicer 5 cm length of MM2 fiber was easily spliced to a standard Corning SMF-28 single mode fiber pigtail to measure the loss spectrum. The loss spectrum of this fiber was measured with the cutback technique using an optical spectrum analyzer and a low power tungsten-filament white light source as before. The loss spectrum of this fiber can be seen in figure 3.4. A strong erbium ion absorption peak having a loss of about 1.54 dB/cm was found at 1535 nm. Another characteristic peak of erbium ions absorption can be seen at 980 nm showing a loss of 0.96 dB/cm.

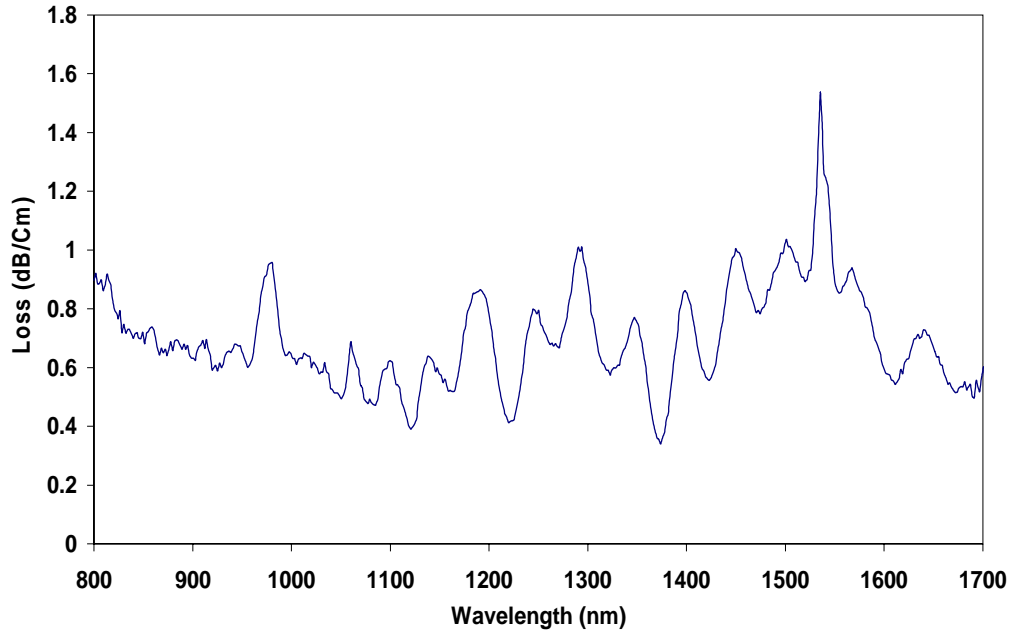


**Figure 3.4 -Loss Spectrum of MM2 glass Fiber (measured on 5 cm length)**

### 3.2 Refractive Index Profile Measurements

*Sample S1 Fiber:* The refractive index profile of this fiber was measured with the York S-14 profiler. This profile can be seen in figure 3.5. (It should be noted that S-14 used for the index profile measurement shows 11% lower than the actual value, which was learned from the measurements made at OFS labs on the same fibers using their profiler.)

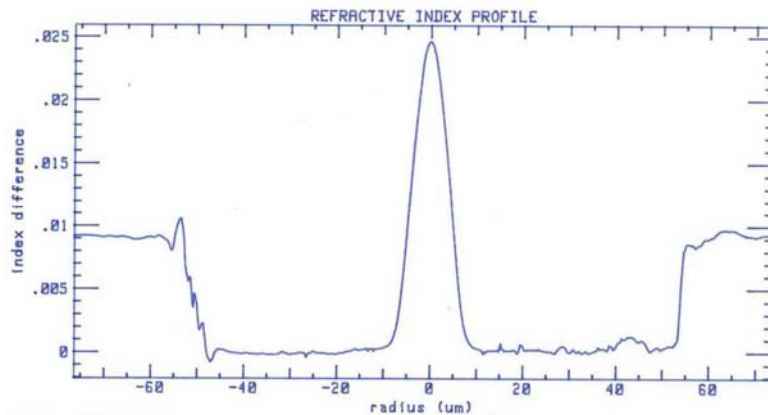


**Figure 3.5 - Refractive index profile of the fiber fabricated by “Core-Suction”**

**Technique using Sample 1 as the core material**

Figure 3.5 shows a large index difference  $\sim 0.028$  (after 11% correction) between the core and the cladding. That gives a core index of  $\sim 1.485$  which is much lower than that of the starting core material index of  $\sim 1.86$ . This huge difference in the values of the refractive index of the starting core glass and the fiber core glass could be because of two possibilities. First the profiler is not set up for extremely large core indices and it is likely that the actual core index is much larger than indicated in the figure. Secondly, there is the possibility of silica diffusion into the core or core glass components diffusing into the silica cladding. This will be discussed in the next section of elemental analysis of this fiber.

*Sample S3 Fiber:* The refractive index profile of this fiber was measured with the York S-14 profiler as before. This profile can be seen in figure 3.6.

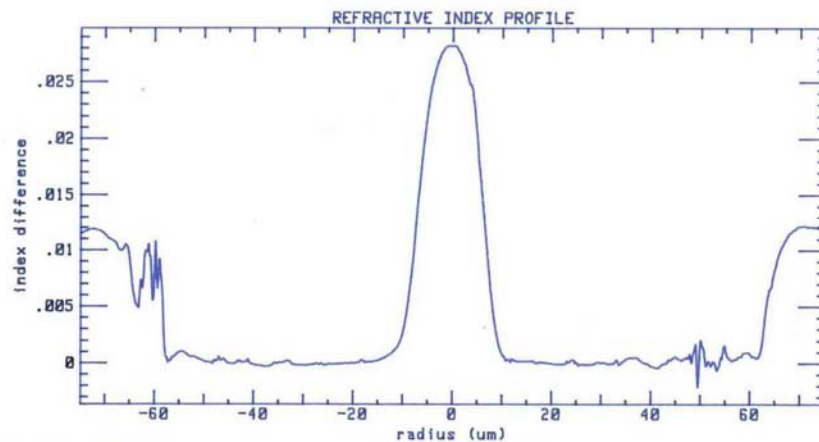


***Figure 3.6- Refractive index profile of the fiber with Sample 3 core glass in silica cladding tube***

Figure 3.6 shows a large index difference  $\sim 0.029$  (after 11% correction) between the core and the cladding. This gives a core index of  $\sim 1.489$  which is much lower than that of the starting core material index of  $\sim 1.86$  as in the case of sample S1 fiber. This huge difference in the values of the refractive index of the starting core glass and the fiber core glass could be because of the same reasons as discussed earlier in the case of sample S1 fiber.



*Bell Labs Fiber:* Figure 3.7 shows the cross section of the Bell Labs fiber having a core diameter of  $\sim 4$  micron surrounded by a cladding of a diameter of  $\sim 150$  micron.

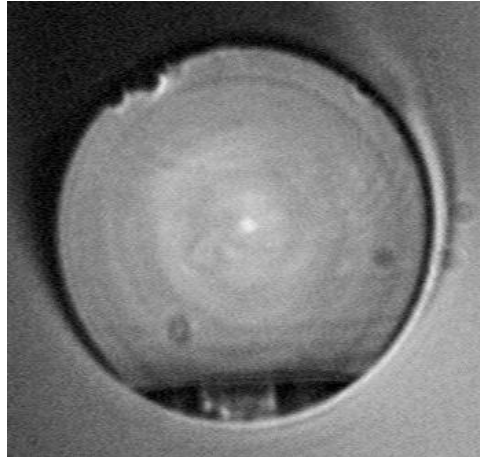


**Figure 3.7- Cross Section of the Bell Labs Fiber**

The refractive index profile of this fiber was measured by A. Yablon at OFS Labs. This profile can be seen in figure 3.8 which shows a large index difference of 0.047 between the core (R.I.-1.5041) and the cladding (R.I.-1.45701). This index difference is not as large as expected from the refractive index values of the starting materials.

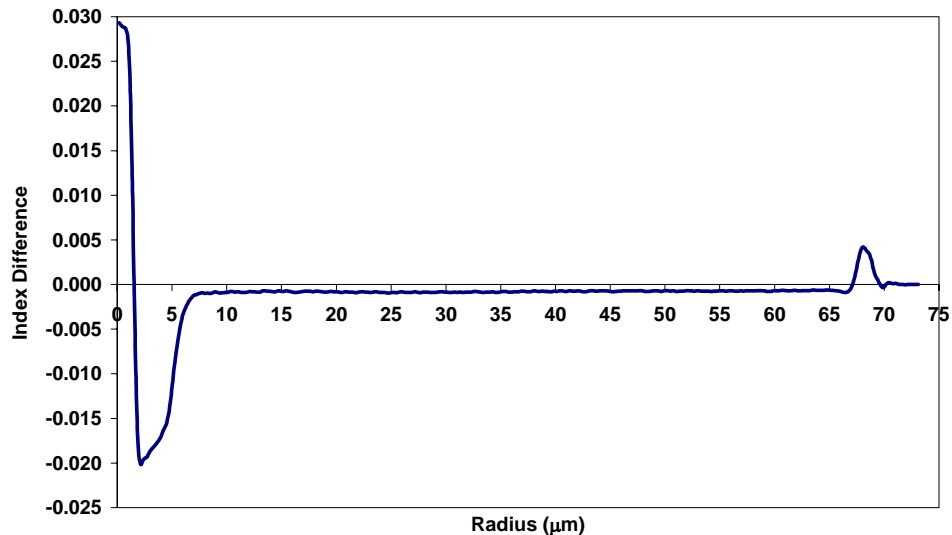


**Figure 3.8- Refractive index profile of the Bell Labs Fiber**

It is likely that there is an out-diffusion of  $\text{GeO}_2$  from the core into the cladding or in-diffusion of silica from cladding to the core. This diffusion is discussed in the next

section of elemental analysis of this fiber. Index profiles for sample S5 and MM2 glass fiber couldn't be measured because of the time constraints.

### 3.3 Electron Micro Probe Analysis (EMPA) for Dopant Concentrations

Electron microprobe analysis (EMPA) is a non-destructive method for determining the elemental composition of tiny amounts of solid materials. EMPA uses a high-energy focused beam of electrons to generate X-rays characteristic of the elements within a sample. The characteristic X-rays are detected at particular wavelengths, and their intensities measured. Chemical composition is determined by comparing the intensity of X-rays from standards (known composition) with those from unknown materials. To check the core and the cladding constituents in the fabricated fibers **CAMECA SX50 Electron Microprobe** system in Geosciences Department at Virginia Tech was used.

*Sample Preparation for the Electron Microprobe:* Two sets of fiber samples for electron microprobe analysis were prepared by using a plastic mold which produces a sample which fits on the mount of the electron microprobe system. Buehler's two part (Hardener and Resin) epoxy called Epo-Thin was used. Hardener and Resin were mixed in a certain ratio to create the epoxy which was poured into the plastic mold. Fiber samples were hung from the top into the plastic mold, filled with the epoxy. This whole setup was left for 18 hours to cure the epoxy. The plastic mold was then stripped off to get the final sample for the electron microprobe. This sample was then optically polished using a sequence of different emery sizes.

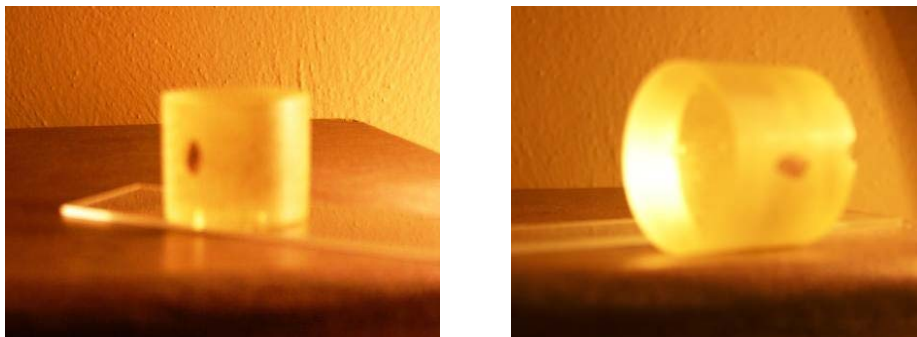


*Figure 3.9 – Photographs of the Electron Microprobe Samples  
(with 5 fiber samples in the middle)*

Figure 3.9 shows the sample prepared for the electron microprobe analysis. This sample has 5 different fiber samples in the middle (not visible in the sample). Figure 3.10 shows the schematic diagram of the cross-sections of 2 electron microprobe samples with the fibers in the middle, labeled EMPA#1 and EMPA#2.

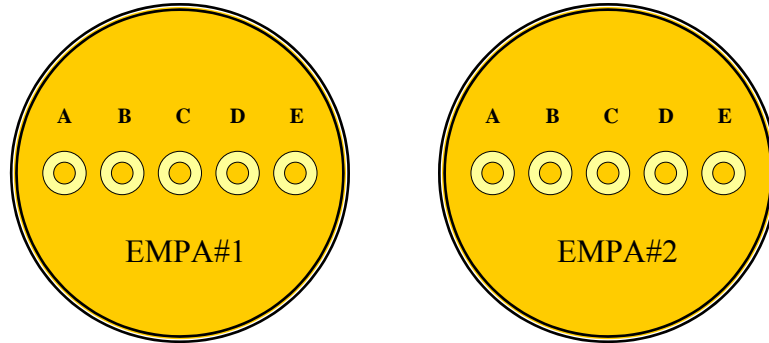


**Figure 3.10 –Schematic diagram of the Cross-Sections of the Electron Microprobe Samples (with 5 fiber labeled A,B,C,D and E in the middle)**

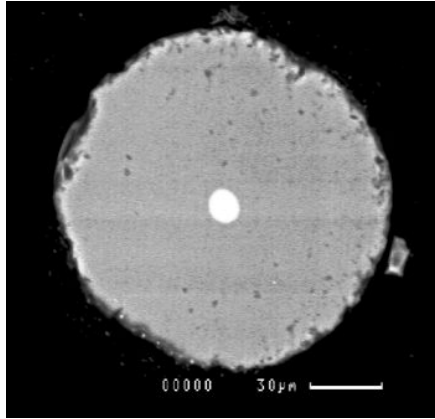
Fibers in both the electron probe samples EMPA#1 and EMPA#2 are similar but taken from the different portion of the original fibers. Table 2 lists all the fibers with their starting glass compositions, analyzed by the electron microprobe.

**Table 3.2 – List of the Fibers Analyzed by Electron Microprobe**

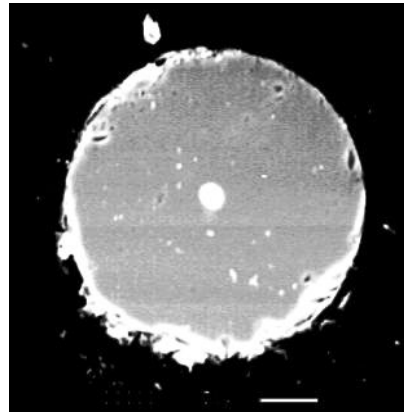
Fiber Label	Glass Label	Core Glass
<b>A</b>	Sample S1	27PbO.43GeO <sub>2</sub> .20TeO <sub>2</sub> .10CaC O <sub>3</sub> .0.2 Er <sub>2</sub> O <sub>3</sub>
<b>B</b>	Sample S3	26PbO.33GeO <sub>2</sub> .30TeO <sub>2</sub> .5CaO.1Nd <sub>2</sub> O <sub>3</sub> .0.5Na <sub>2</sub> CO <sub>3</sub>
<b>C</b>	Sample S5	27PbO.33GeO <sub>2</sub> .30TeO <sub>2</sub> .10CaCO <sub>3</sub>
<b>D</b>	MM2 Glass	Alumina. Erbium. Phosphate (actual composition unknown)
<b>E</b>	Sample S3	26PbO.33GeO <sub>2</sub> .30TeO <sub>2</sub> .5CaO.1Nd <sub>2</sub> O <sub>3</sub> .0.5Na <sub>2</sub> CO <sub>3</sub>

Prior to elemental analysis and imaging, these electron probe samples EMPA#1 and EMPA#2 were coated with 250-300 angstrom carbon layers to remove the static charges on them.

The coated samples EMPA#1 and EMPA#2 were then SEM imaged using **Camscan2** for each of the fiber samples. SEM images of all the fibers labeled “A” to “E” in both the microprobe samples EMPA#1 and EMPA#2 can be seen in the figures 3.11 through 3.15.

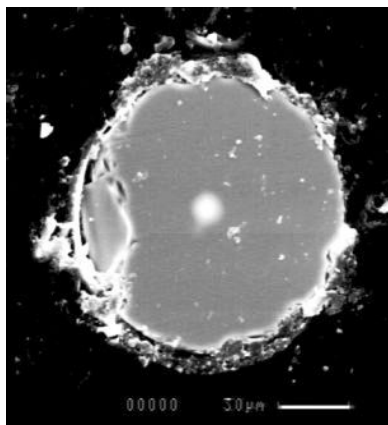


Core Diameter – 11 micron  
Cladding Diameter – 146 micron

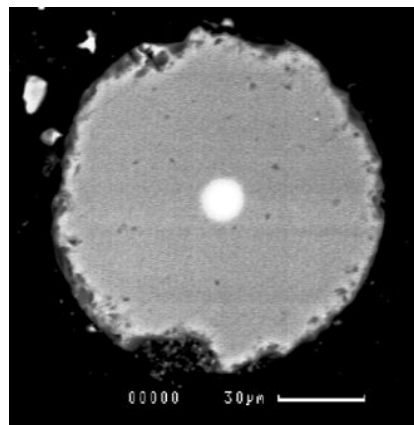


Core Diameter – 12 micron  
Cladding Diameter – 152 micron

***Figure 3.11- SEM images of Fiber Samples labeled ‘A’s in EMPA#1 and EMPA#2***

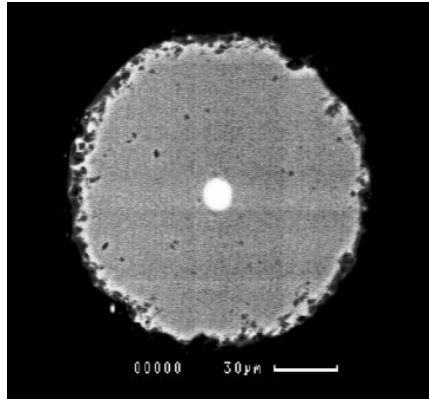


Core Diameter – 14 micron  
Cladding Diameter – 118 micron

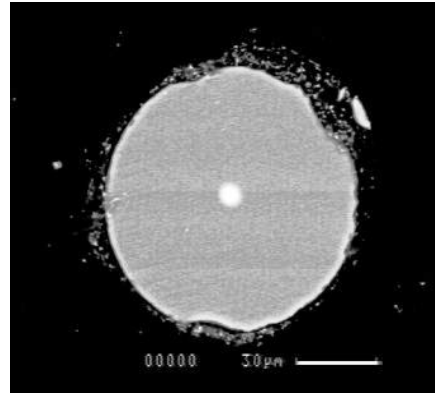


Core Diameter – 13 micron  
Cladding Diameter – 117 micron

***Figure 3.12- SEM images of Fiber Samples labeled ‘B’s in EMPA#1 and EMPA#2***

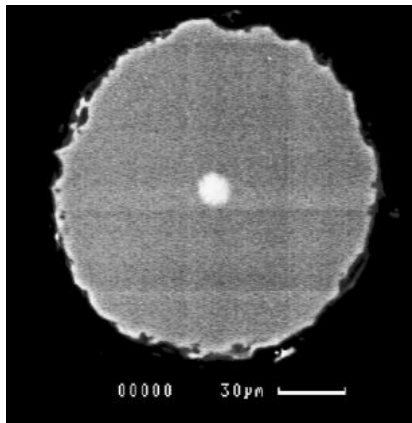


Core Diameter – 12 micron  
Cladding Diameter – 147 micron

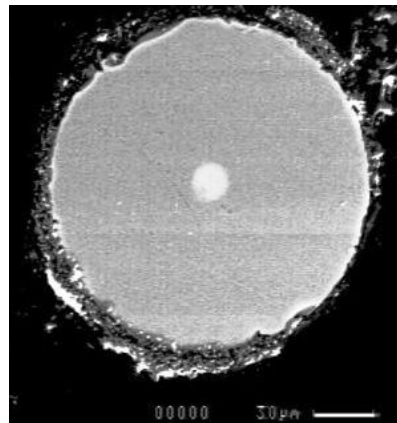


Core Diameter – 8 micron  
Cladding Diameter – 95 micron

*Figure 3.13- SEM images of Fiber Samples labeled 'C's in EMPA#1 and EMPA#2*

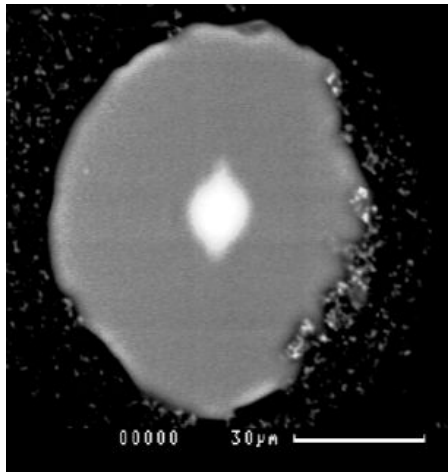


Core Diameter – 13 micron  
Cladding Diameter – 152 micron



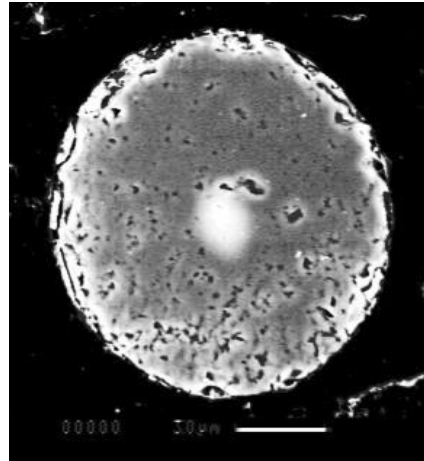
Core Diameter – 15 micron  
Cladding Diameter – 155 micron

*Figure 3.14- SEM images of Fiber Samples labeled 'D's in EMPA#1 and EMPA#2*



Core Diameter – 10 micron

Cladding Diameter – 78 micron



Core Diameter – 16 micron

Cladding Diameter – 118 micron

**Figure 3.15- SEM images of Fiber Samples labeled ‘E’s in EMPA#1 and EMPA#2**

Fibers labeled “A” to “E” in electron microprobe samples EMPA#1 and EMPA#2 were further analyzed for their elemental makeup in the cores and the core-cladding boundary using the **CAMECA SX50 Electron Microprobe** system. Each fiber end was scanned for elemental makeup in horizontal (X) and vertical (Y) directions. In most of the cases the electron beam was focused at three points inside the core and one point in the cladding on each side of the core, resulting in 5 points scanned on each of the fibers. Each scan point was focused to about 3 microns and the scan points were separated by 3 microns from each other. In some cases the cores were scanned at more than 3 (4 to 6) points, depending on the core size. The resulting elemental make up at every scan point (in core and cladding) of the fiber was recorded for each of the fibers in samples EMPA#1 and EMPA#2.

Tables 3.3 through 3.12 summarizes the dopants concentrations (in terms of their weight percentage) at each scan point in the fibers labeled “A” to “E” in the samples EMPA#1 and EMPA#2. The main dopants profiles from these tables are plotted in figures 3.16 through 3.35. In these figures CR0, CR+, CR- represents the scan points in the core, CR0 at the center of the core, CR+ on right of the center of the core and the CR- on the left side of the center of the core. CL+ and CL- represent the scan points in the cladding on right and left side of the core center respectively. CR1, CR2, CR3, CR4 etc. represent the scan point numbers in the core when more than 3 points were scanned in the core.

**Table 3.3- Elemental Make Up of Fiber “A” in Sample EMPA#1**

		SiO2	GeO2	TeO2	Er2O3	CaO	PbO	Total
<b>AH1</b>	<b>1</b>	<b>97.35</b>	<b>0.05</b>	<b>0.00</b>	<b>0.00</b>	<b>0.03</b>	<b>0.39</b>	97.87
	<b>2</b>	<b>84.03</b>	<b>4.70</b>	<b>0.00</b>	<b>0.04</b>	<b>0.77</b>	<b>8.06</b>	97.69
	<b>3</b>	<b>70.24</b>	<b>9.50</b>	<b>0.00</b>	<b>0.13</b>	<b>1.53</b>	<b>14.00</b>	95.57
	<b>4</b>	<b>81.05</b>	<b>5.05</b>	<b>0.00</b>	<b>0.11</b>	<b>0.71</b>	<b>8.55</b>	95.54
	<b>5</b>	<b>97.30</b>	<b>0.02</b>	<b>0.04</b>	<b>0.13</b>	<b>0.02</b>	<b>0.29</b>	97.85
<b>AV1</b>	<b>1</b>	<b>97.68</b>	<b>0.01</b>	<b>0.00</b>	<b>0.01</b>	<b>0.00</b>	<b>0.02</b>	97.86
	<b>2</b>	<b>88.96</b>	<b>3.57</b>	<b>0.06</b>	<b>0.00</b>	<b>0.60</b>	<b>6.12</b>	99.36
	<b>3</b>	<b>67.90</b>	<b>10.34</b>	<b>0.02</b>	<b>0.31</b>	<b>1.75</b>	<b>15.55</b>	96.08
	<b>4</b>	<b>78.02</b>	<b>6.37</b>	<b>0.04</b>	<b>0.20</b>	<b>0.98</b>	<b>10.46</b>	96.20
	<b>5</b>	<b>95.85</b>	<b>0.20</b>	<b>0.00</b>	<b>0.03</b>	<b>0.07</b>	<b>0.89</b>	97.11

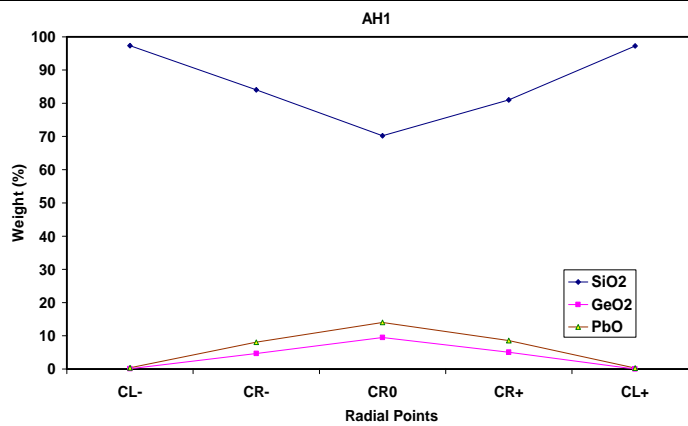


**Figure 3.16 - Horizontal Axis Profile of Fiber “A” in Sample EMPA#1**

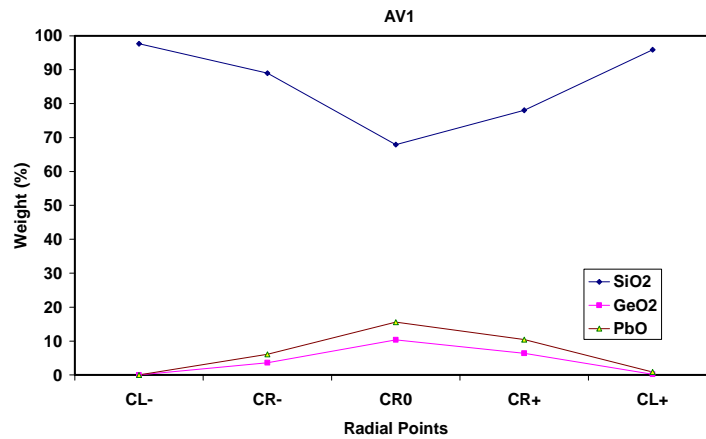


**Figure 3.17 - Vertical Axis Profile of Fiber “A” in Sample EMPA#1**

- Main Observations:*
- 1) No TeO<sub>2</sub> present in the core.
  - 2) SiO<sub>2</sub> diffuses into the core forming a silicate core comprising > 65% of SiO<sub>2</sub> in the center. SiO<sub>2</sub> percentage increases away from the core center.
  - 3) There is no diffusion of GeO<sub>2</sub> or PbO from the core to the cladding.

**Table 3.4- Elemental Make Up of Fiber “A” in Sample EMPA#2**

		SiO2	GeO2	TeO2	Er2O3	CaO	PbO	Total
<b>AH2</b>	1	96.24	0.04	0.00	0.01	0.06	0.31	96.73
	2	79.13	5.06	0.01	0.01	0.90	8.89	94.10
	3	64.43	8.81	0.04	0.12	1.45	14.22	89.22
	4	68.13	9.83	0.12	0.15	1.54	14.32	94.23
	5	97.59	0.00	0.00	0.00	0.00	0.00	97.69
<b>AV2</b>	1	96.68	0.00	0.00	0.04	0.04	0.11	96.99
	2	87.24	2.22	0.02	0.00	0.42	4.57	94.57
	3	86.05	2.71	0.03	0.05	0.50	5.31	94.80
	4	91.38	1.18	0.01	0.00	0.24	2.90	97.75
	5	97.37	0.00	0.04	0.02	0.01	0.02	97.52

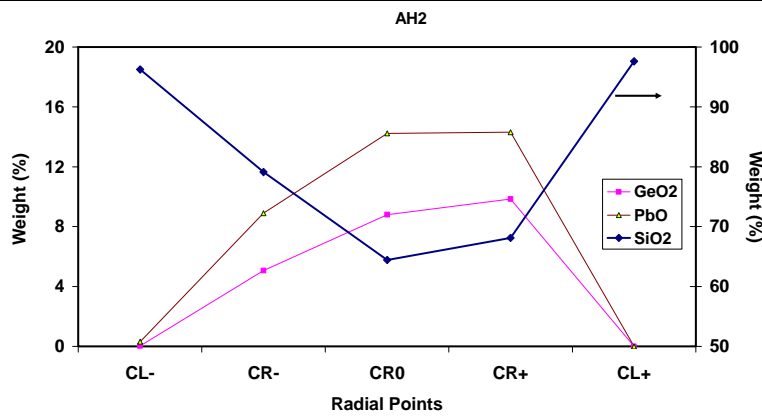


**Figure 3.18 - Horizontal Axis Profile of Fiber “A” in Sample EMPA#2**

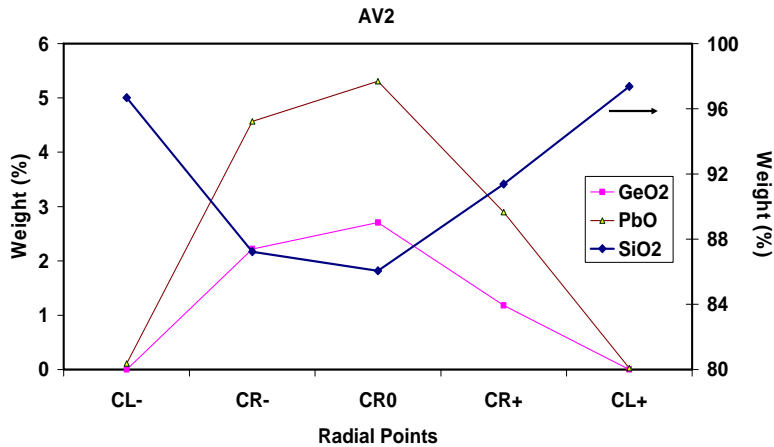


**Figure 3.19 - Vertical Axis Profile of Fiber “A” in Sample EMPA#2**

- Main Observations:*
- 1) No  $\text{TeO}_2$  present in the core.
  - 2)  $\text{SiO}_2$  diffuses into the core forming a silicate core comprising  $> 65\%$  of  $\text{SiO}_2$  in the center.  $\text{SiO}_2$  percentage increases away from the core center.
  - 3) There is no diffusion of  $\text{GeO}_2$  or  $\text{PbO}$  from the core to the cladding.



**Table 3.5- Elemental Make Up of Fiber “B” in Sample EMPA#1**

		SiO2	GeO2	TeO2	Nd2O3	CaO	PbO	Na2O	Total
<b>BH1</b>	<b>1</b>	<b>92.91</b>	<b>0.45</b>	<b>0.02</b>	<b>0.10</b>	0.23	<b>3.00</b>	<b>0.10</b>	96.89
	<b>2</b>	<b>83.58</b>	<b>2.92</b>	<b>0.03</b>	<b>0.58</b>	0.58	<b>8.08</b>	<b>0.11</b>	95.92
	<b>3</b>	<b>79.82</b>	<b>4.42</b>	<b>0.04</b>	<b>0.89</b>	0.80	<b>10.26</b>	<b>0.13</b>	96.44
	<b>4</b>	<b>87.54</b>	<b>1.75</b>	<b>0.02</b>	<b>0.46</b>	0.47	<b>6.41</b>	<b>0.15</b>	96.89
	<b>5</b>	<b>97.49</b>	<b>0.02</b>	<b>0.07</b>	<b>0.00</b>	0.01	<b>0.22</b>	<b>0.05</b>	97.94
<b>BV1</b>	<b>1</b>	<b>97.27</b>	<b>0.00</b>	<b>0.00</b>	<b>0.07</b>	0.00	<b>0.06</b>	<b>0.06</b>	97.51
	<b>2</b>	<b>89.33</b>	<b>0.87</b>	<b>0.04</b>	<b>0.23</b>	0.32	<b>4.59</b>	<b>0.13</b>	95.58
	<b>3</b>	<b>80.64</b>	<b>3.83</b>	<b>0.03</b>	<b>0.47</b>	0.77	<b>9.58</b>	<b>0.16</b>	95.53
	<b>4</b>	<b>83.18</b>	<b>3.38</b>	<b>0.04</b>	<b>0.81</b>	0.73	<b>8.41</b>	<b>0.13</b>	96.80
	<b>5</b>	<b>94.22</b>	<b>0.35</b>	<b>0.03</b>	<b>0.11</b>	0.18	<b>2.43</b>	<b>0.12</b>	97.62

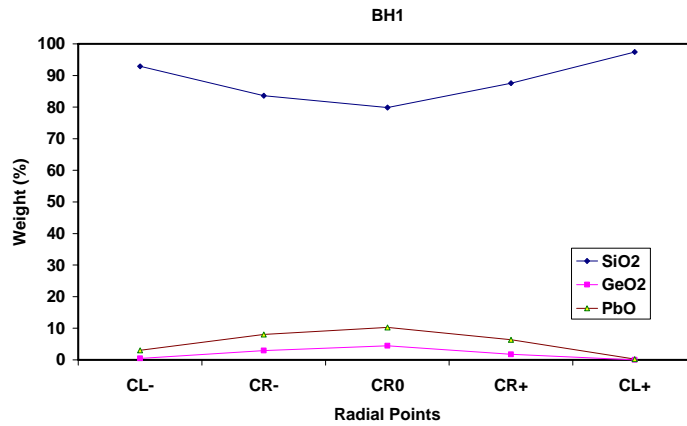


**Figure 3.20 - Horizontal Axis Profile of Fiber “B” in Sample EMPA#1**

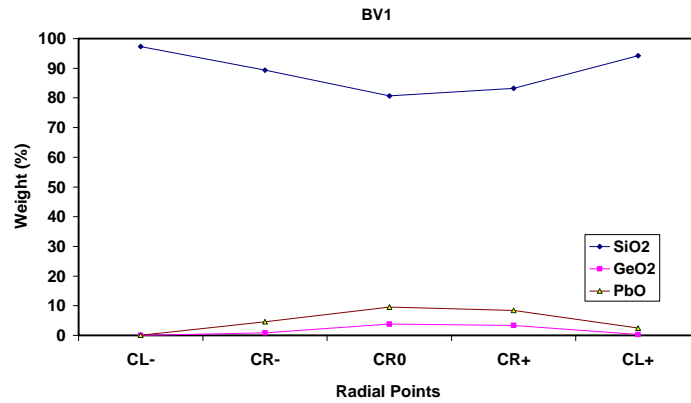


**Figure 3.21 - Vertical Axis Profile of Fiber “B” in Sample EMPA#1**

- Main Observations:*
- 1) No TeO<sub>2</sub> present in the core.
  - 2) SiO<sub>2</sub> diffuses into the core forming a silicate core comprising > 80% of SiO<sub>2</sub> in the center. SiO<sub>2</sub> percentage increases away from the core center.
  - 3) There is no diffusion of GeO<sub>2</sub> or PbO from the core to the cladding.

**Table 3.6- Elemental Make Up of Fiber “B” in Sample EMPA#2**

		SiO <sub>2</sub>	GeO <sub>2</sub>	TeO <sub>2</sub>	Nd <sub>2</sub> O <sub>3</sub>	CaO	PbO	Na <sub>2</sub> O	Total
<b>BH2</b>	1	96.77	0.00	0.00	0.00	0.03	0.30	0.06	97.26
	2	89.45	0.91	0.01	0.28	0.33	4.90	0.16	96.10
	3	82.64	3.14	0.03	0.51	0.67	8.25	0.24	95.81
	4	84.94	3.17	0.03	0.31	0.60	8.47	0.27	97.91
	5	97.69	0.03	0.00	0.05	0.00	0.08	0.07	97.97
<b>BV2</b>	1	96.37	0.00	0.03	0.05	0.02	0.06	0.04	96.77
	2	95.59	0.06	0.07	0.10	0.09	0.90	0.11	96.98
	3	88.40	1.21	0.04	0.12	0.36	5.19	0.14	95.52
	4	92.84	0.35	0.00	0.17	0.19	2.77	0.07	96.53
	5	95.67	0.06	0.04	0.00	0.06	1.00	0.06	96.92

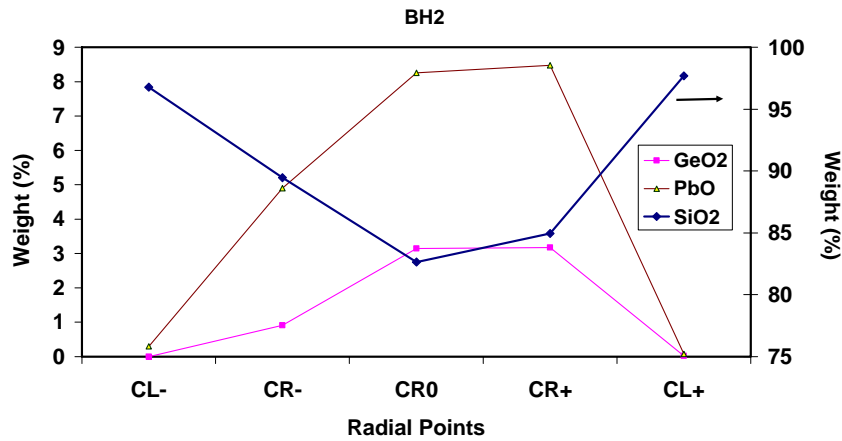


**Figure 3.22 - Horizontal Axis Profile of Fiber “B” in Sample EMPA#2**

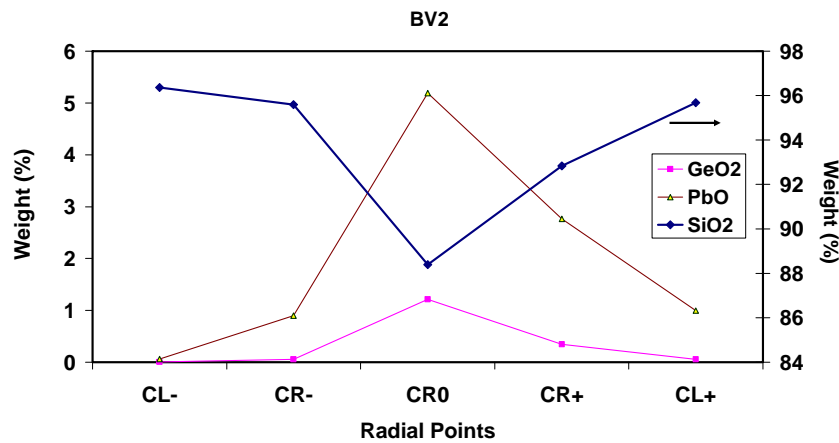


**Figure 3.23 - Vertical Axis Profile of Fiber “B” in Sample EMPA#2**

- Main Observations:*
- 1) No TeO<sub>2</sub> present in the core.
  - 2) SiO<sub>2</sub> diffuses into the core forming a silicate core comprising > 80% of SiO<sub>2</sub> in the center. SiO<sub>2</sub> percentage increases away from the core center.
  - 3) There is no diffusion of GeO<sub>2</sub> or PbO from the core to the cladding.

**Table 3.7- Elemental Make Up of Fiber “C” in Sample EMPA#1**

		SiO2	GeO2	TeO2	CaO	PbO	Total
<b>CH1</b>	1	96.54	0.15	0.00	0.09	1.26	98.23
	2	83.32	4.88	0.04	0.55	8.28	97.95
	3	80.62	6.00	0.01	0.61	9.70	97.76
	4	91.46	1.17	0.03	0.17	3.75	96.71
	5	97.02	0.00	0.00	0.01	0.36	97.64
<b>CV1</b>	1	95.69	0.09	0.00	0.08	1.21	97.36
	2	85.40	3.39	0.04	0.37	7.13	96.92
	3	79.53	6.22	0.00	0.58	9.77	96.89
	4	86.01	3.72	0.00	0.44	6.74	97.55
	5	96.44	0.04	0.04	0.05	0.91	97.59

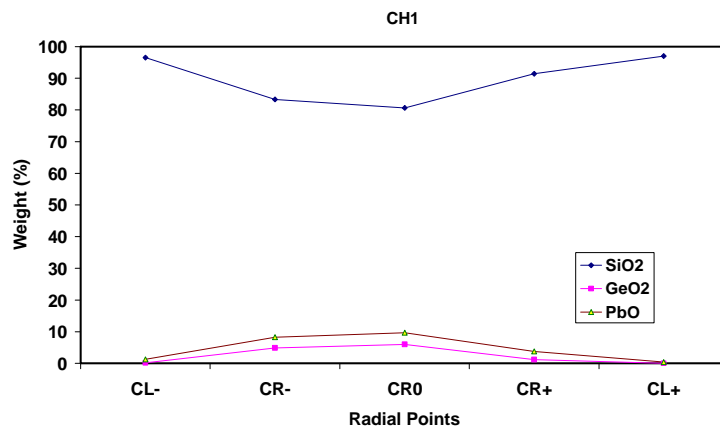


**Figure 3.24 - Horizontal Axis Profile of Fiber “C” in Sample EMPA#1**

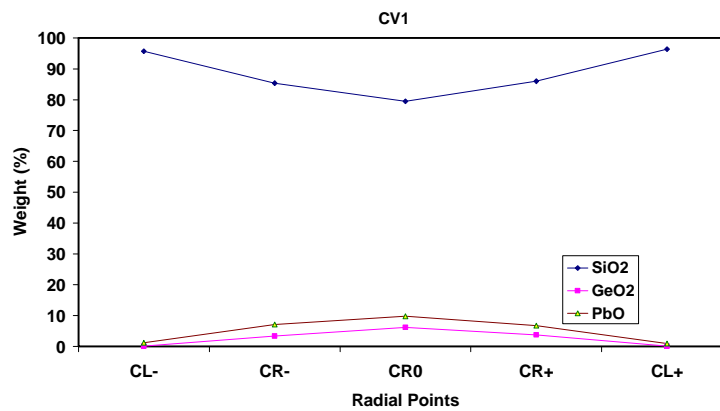


**Figure 3.25 - Vertical Axis Profile of Fiber “C” in Sample EMPA#1**

- Main Observations:**
- 1) No TeO<sub>2</sub> present in the core.
  - 2) SiO<sub>2</sub> diffuses into the core forming a silicate core comprising > 80% of SiO<sub>2</sub> in the center. SiO<sub>2</sub> percentage increases away from the core center.
  - 3) There is no diffusion of GeO<sub>2</sub> or PbO from the core to the cladding.

**Table 3.8- Elemental Make Up of Fiber “C” in Sample EMPA#2**

		SiO <sub>2</sub>	GeO <sub>2</sub>	TeO <sub>2</sub>	CaO	PbO	Total
<b>CH2</b>	1	97.29	0.02	0.00	0.00	0.00	97.46
	2	87.15	3.30	0.07	0.39	6.63	98.11
	3	85.93	3.11	0.02	0.37	6.22	96.21
	4	96.71	0.00	0.01	0.03	0.05	96.89
<b>CV2</b>	1	96.16	0.02	0.01	0.03	0.41	96.69
	2	92.33	0.83	0.01	0.13	2.57	96.12
	3	95.90	0.08	0.05	0.05	0.69	96.93
	4	97.59	0.01	0.01	0.01	0.01	97.83

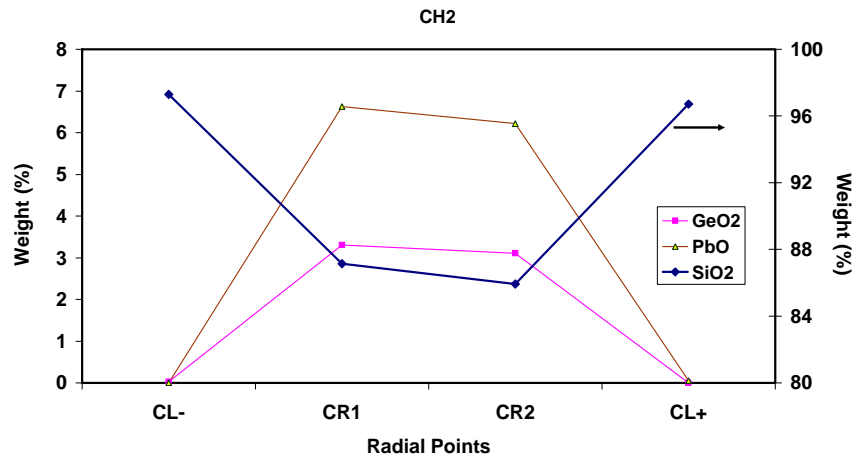


**Figure 3.26 - Horizontal Axis Profile of Fiber “C” in Sample EMPA#2**

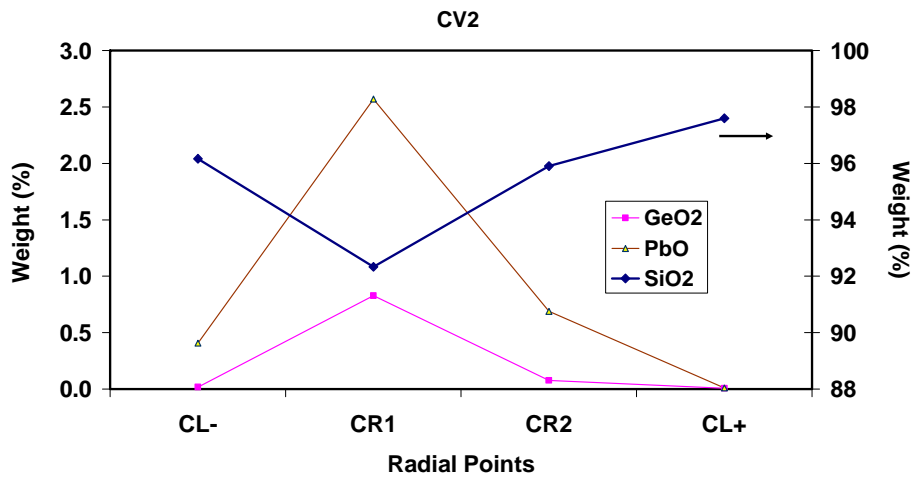


**Figure 3.27 -Vertical Axis Profile of Fiber “C” in Sample EMPA#2**

- Main Observations:**
- 1) No TeO<sub>2</sub> present in the core.
  - 2) SiO<sub>2</sub> diffuses into the core forming a silicate core comprising > 86% of SiO<sub>2</sub> in the center. SiO<sub>2</sub> percentage increases away from the core center.
  - 3) There is no diffusion of GeO<sub>2</sub> or PbO from the core to the cladding.

**Table 3.9- Elemental Make Up of Fiber “D” in Sample EMPA#1**

		P2O5	SiO2	Al2O3	Er2O3	Total
<b>DH1</b>	<b>1</b>	5.54	90.29	0.76	0.01	96.79
	<b>2</b>	9.67	55.70	7.06	0.83	93.54
	<b>3</b>	1.32	53.84	7.75	0.77	93.74
	<b>4</b>	8.27	58.14	6.78	0.70	93.96
	<b>5</b>	8.52	73.15	4.22	0.30	96.35
	<b>6</b>	0.71	96.24	0.21	0.00	97.23
<b>DV1</b>	<b>1</b>	8.07	87.02	1.97	0.20	97.34
	<b>2</b>	4.52	63.80	5.89	0.52	94.85
	<b>3</b>	8.64	57.61	6.99	0.48	93.92
	<b>4</b>	8.94	57.49	6.89	0.70	94.09
	<b>5</b>	7.80	75.32	3.30	0.31	96.88
	<b>6</b>	0.48	96.93	0.08	0.08	97.62

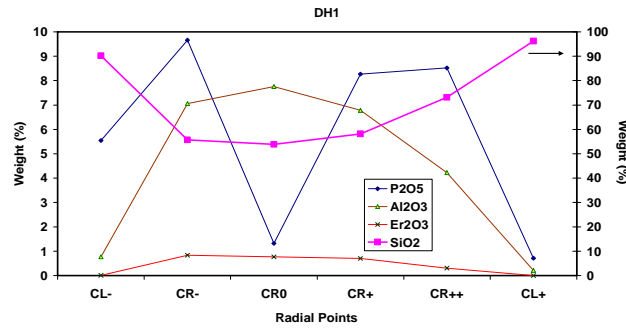


**Figure 3.28 -Horizontal Axis Profile of Fiber “D” in Sample EMPA#1**

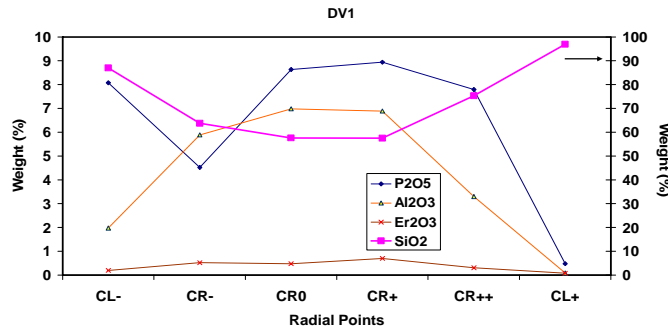


**Figure 3.29 -Vertical Axis Profile of Fiber “D” in Sample EMPA#1**

- Main Observations:**
- 1) No diffusion of  $Er_2O_3$  from the core into the cladding.
  - 2)  $SiO_2$  diffuses into the core forming a silicate core comprising > 50% of  $SiO_2$  in the center.  $SiO_2$  percentage increases away from the core center.
  - 3) There is no diffusion of  $GeO_2$  or  $PbO$  from the core to the cladding.
  - 4) There is some out diffusion of  $P_2O_5$  from the core into the cladding.
  - 5) Small diffusion of  $Al_2O_3$  from the core into the cladding.

**Table 3.10- Elemental Make Up of Fiber “D” in Sample EMPA#2**

		P2O5	SiO2	Al2O3	Er2O3	Total
DH2	1	8.38	86.69	0.97	0.09	96.21
	2	24.35	63.65	4.91	0.58	93.62
	3	27.61	56.90	6.69	0.68	92.01
	4	31.22	52.59	7.83	0.82	92.56
	5	30.85	53.23	7.77	0.81	92.82
	6	27.44	58.71	6.66	0.74	93.66
	7	0.25	96.91	0.08	0.00	97.27
DV2	1	4.82	91.17	0.93	0.06	97.03
	2	25.55	61.49	6.07	0.77	93.92
	3	30.58	53.30	7.79	0.80	92.58
	4	30.39	53.96	7.40	0.90	92.76
	5	29.01	56.19	6.70	0.60	92.68
	6	24.95	63.53	4.99	0.56	94.13
	7	9.77	85.49	1.27	0.10	96.64

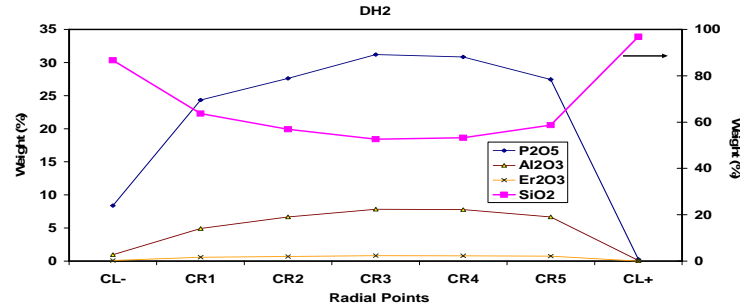


**Figure 3.30 -Horizontal Axis Profile of Fiber “D” in Sample EMPA#2**

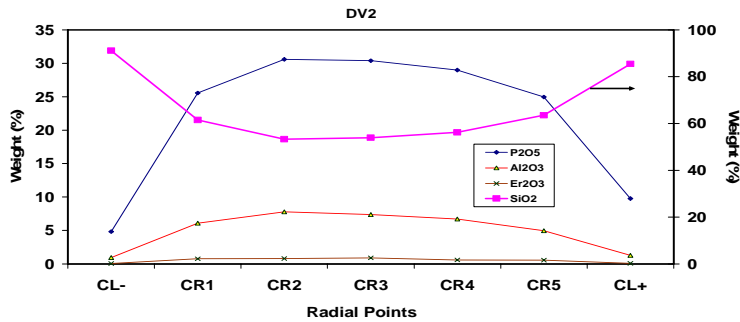


**Figure 3.31 -Vertical Axis Profile of Fiber “D” in Sample EMPA#2**

- Main Observations:**
- 1) No diffusion of  $Er_2O_3$  from the core into the cladding.
  - 2)  $SiO_2$  diffuses into the core forming a silicate core comprising  $> 50\%$  of  $SiO_2$  in the center.  $SiO_2$  percentage increases away from the core center.
  - 3) There is no diffusion of  $GeO_2$  or  $PbO$  from the core to the cladding.
  - 4) There is some out diffusion of  $P_2O_5$  from the core into the cladding.
  - 5) Small diffusion of  $Al_2O_3$  from the core into the cladding.

**Table 3.11- Elemental Make Up of Fiber “E” in Sample EMPA#1**

		SiO <sub>2</sub>	GeO <sub>2</sub>	TeO <sub>2</sub>	Nd <sub>2</sub> O <sub>3</sub>	CaO	PbO	Na <sub>2</sub> O	Total
<b>EH1</b>	<b>1</b>	<b>94.23</b>	<b>0.27</b>	<b>0.00</b>	<b>0.07</b>	0.14	<b>1.87</b>	0.06	96.71
	<b>2</b>	<b>89.39</b>	<b>2.06</b>	<b>0.03</b>	<b>0.33</b>	0.36	<b>4.16</b>	0.06	96.54
	<b>3</b>	<b>85.87</b>	<b>4.52</b>	<b>0.03</b>	<b>0.66</b>	0.44	<b>5.65</b>	0.07	97.51
	<b>4</b>	<b>87.03</b>	<b>3.50</b>	<b>0.02</b>	<b>0.38</b>	0.34	<b>4.65</b>	0.07	96.15
	<b>5</b>	<b>93.56</b>	<b>0.41</b>	<b>0.05</b>	<b>0.12</b>	0.13	<b>2.10</b>	0.03	96.57
<b>EV1</b>	<b>1</b>	<b>95.82</b>	<b>0.02</b>	<b>0.03</b>	<b>0.00</b>	0.04	<b>0.47</b>	0.02	96.50
	<b>2</b>	<b>88.43</b>	<b>2.70</b>	<b>0.00</b>	<b>0.24</b>	0.30	<b>4.01</b>	0.05	95.87
	<b>3</b>	<b>84.41</b>	<b>4.67</b>	<b>0.02</b>	<b>0.59</b>	0.47	<b>5.56</b>	0.03	95.91
	<b>4</b>	<b>87.59</b>	<b>3.70</b>	<b>0.02</b>	<b>0.62</b>	0.40	<b>4.67</b>	0.08	97.24
	<b>5</b>	<b>93.46</b>	<b>1.01</b>	<b>0.00</b>	<b>0.15</b>	0.23	<b>2.54</b>	0.04	97.52

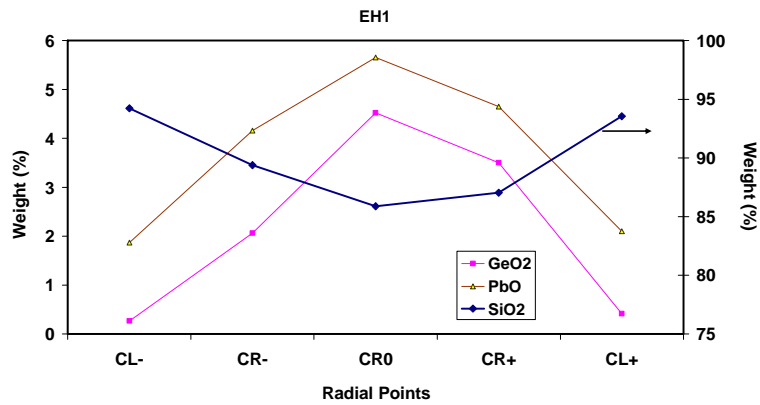


**Figure 3.32 - Horizontal Axis Profile of Fiber “E” in Sample EMPA#1**

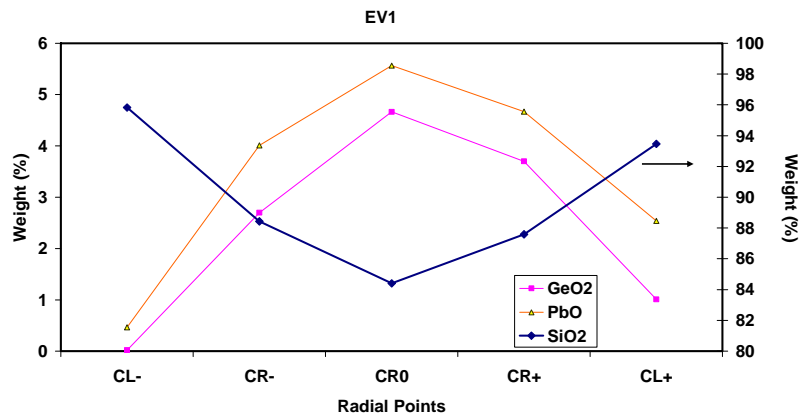


**Figure 3.33 - Vertical Axis Profile of Fiber “E” in Sample EMPA#1**

- Main Observations:**
- 1) No TeO<sub>2</sub> present in the core.
  - 2) SiO<sub>2</sub> diffuses into the core forming a silicate core comprising > 80% of SiO<sub>2</sub> in the center. SiO<sub>2</sub> percentage increases away from the core center.
  - 3) There is no diffusion of GeO<sub>2</sub> or PbO from the core to the cladding.

*Table 3.12- Elemental Make Up of Fiber “E” in Sample EMPA#2*

		SiO <sub>2</sub>	GeO <sub>2</sub>	TeO <sub>2</sub>	Nd <sub>2</sub> O <sub>3</sub>	CaO	PbO	Na <sub>2</sub> O	Total
<b>EH2</b>	1	95.94	0.00	0.00	0.07	0.04	0.24	0.03	96.41
	2	92.73	0.65	0.00	0.10	0.19	2.77	0.06	96.55
	3	87.31	3.15	0.01	0.33	0.25	4.43	0.08	95.37
	4	85.19	4.77	0.05	0.50	0.38	5.31	0.07	96.40
	5	85.86	3.98	0.03	0.41	0.44	4.94	0.06	96.14
	6	88.90	2.14	0.01	0.44	0.39	4.12	0.05	96.31
	7	94.68	0.00	0.02	0.00	0.07	0.69	0.02	95.72
	8	96.23	0.00	0.09	0.08	0.04	0.00	0.01	96.66
<b>EV2</b>	1	96.34	0.00	0.00	0.09	0.02	0.31	0.05	96.90
	2	92.53	0.65	0.00	0.21	0.18	2.47	0.04	96.27
	3	86.83	3.72	0.00	0.26	0.39	4.81	0.03	96.16
	4	83.95	5.37	0.01	0.39	0.43	5.71	0.03	96.22
	5	86.36	4.40	0.00	0.52	0.38	4.85	0.04	96.69
	6	89.91	2.51	0.00	0.48	0.26	4.00	0.05	97.30
	7	95.19	0.08	0.00	0.01	0.10	1.34	0.05	96.90

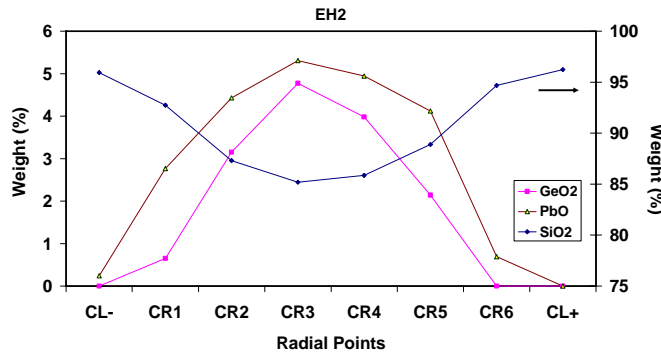


*Figure 3.34 -Horizontal Axis Profile of Fiber “E” in Sample EMPA#2*

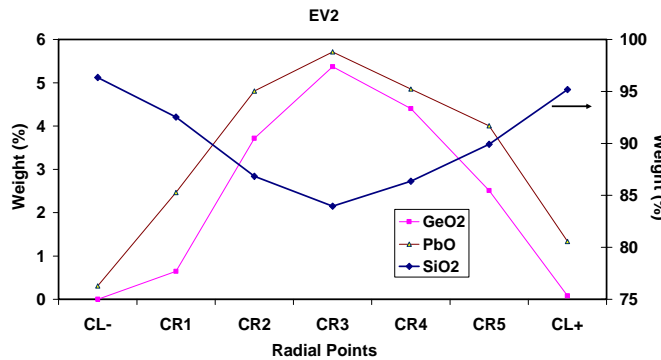


*Figure 3.35 -Vertical Axis Profile of Fiber “E” in Sample EMPA#2*

- Main Observations:*
- 1) No TeO<sub>2</sub> present in the core.
  - 2) SiO<sub>2</sub> diffuses into the core forming a silicate core comprising > 80% of SiO<sub>2</sub> in the center. SiO<sub>2</sub> percentage increases away from the core center.
  - 3) There is no diffusion of GeO<sub>2</sub> or PbO from the core to the cladding.



**Analysis:** In all the cases silica from the cladding diffuses into the core forming a silicate core and silica being the major constituent of the core. TeO<sub>2</sub> had no presence in any of the expected tellurite based cores. There was no out diffusion of GeO<sub>2</sub> or PbO found. P<sub>2</sub>O<sub>5</sub> and Al<sub>2</sub>O<sub>3</sub> were found to diffuse a little from the core into the cladding.

**Bell Labs GeO<sub>2</sub> Core Fiber:**

The index difference profile of the Bell Labs GeO<sub>2</sub> fiber, as shown in Figure 3.36, yielded an index difference between core and clad of 0.047 (delta= 3.08%). Fabrication data on the flow rates of the gases used to fabricate the MCVD preform of the selected fiber should have yielded an expected core composition of 90% GeO<sub>2</sub> and 10%B<sub>2</sub>O<sub>3</sub>. The constituent cross-section of the fiber was analyzed\* with an electron-microprobe system to determine core dopant profiles actually achieved with respect to both Germanium and Silicon. Silica was found to be the major constituent of the core due to the diffusion as before.

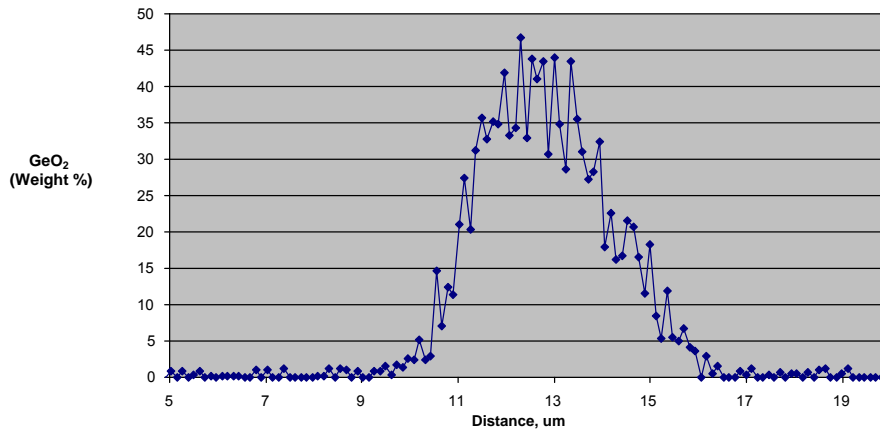


**Figure 3.36 – GeO<sub>2</sub> Concentration (Weight %) Profile of Bell Labs GeO<sub>2</sub> core Fiber**

Figure 3.36 shows Ge concentration profile obtained from the microprobe. Maximum Ge concentration by weight in the core is clearly seen to be less than 45% as opposed to the 90% expected from gas flow analysis. Similarly the Silica concentration in the core was measured to be less than 45%. From the weight % of core constituents, mol % was determined. The core constituent analysis at the center of the core is tabulated in table 3.13.

\* Thanks to Carvel Holton for the measurements

**Table 3.13 - Mole Fraction Analysis for Core of Bell Labs Fiber**

	<b>Mol. Weight</b>	<b>Weight (%) in Fiber Sample</b>	<b>No. of Moles</b>	<b>Mole % in Total Sample</b>
<b>GeO<sub>2</sub></b>	104.61	41.78	0.399	<b>30.01</b>
<b>SiO<sub>2</sub></b>	60.08	41.78	0.695	<b>52.25</b>
<b>B<sub>2</sub>O<sub>3</sub></b>	69.62	16.44	0.236	<b>17.74</b>

The mole% of GeO<sub>2</sub> in the fiber's core was also determined by the measured fiber index profile shown in figure-3.8. Fiber index profile also gave an inferred average GeO<sub>2</sub> concentration in the core of 30 mole%.<sup>1</sup> Thus both methods of obtaining the GeO<sub>2</sub> concentration are in agreement verifying the in-diffusion of silica into the core.

### **3.4 Spontaneous Scattering Spectrum Measurements**

The highly doped fibers fabricated and discussed in this thesis are primarily intended for optical amplification either Raman or Erbium fiber amplifiers. In the case of the erbium doped fibers, the gain spectrum is directly proportional to the spontaneous scattering spectrum. While for Raman fibers (high doping of GeO<sub>2</sub> and/or TeO<sub>2</sub>) the spontaneous spectrum differs from the gain spectrum by the Bose-Einstein population factor,  $n+1$ , where  $n=1/[\exp(h\nu c/k_B T)-1]$ ;  $h$  is Planck's constant,  $\nu$  is the phonon frequency in  $\text{cm}^{-1}$ ,  $k_B$  is the Boltzmann constant,  $T$  is the temperature in degrees Kelvin, and  $c$  is the vacuum velocity of light. For any fiber the gain spectrum can be derived from the spontaneous spectrum. The next section presents the spontaneous scattering measurements made on the fibers mentioned above.

*Measurement Setup:* Spontaneous scattering spectra of all the fibers except the Bell Labs GeO<sub>2</sub> fiber were measured using the following setup shown in figure 3.37. This figure shows the schematic diagram of the experimental setup used which consists of a circulator for pumping the fiber with a pump source. The pump laser used in this setup was a Raman fiber laser peaked at 1486.7 nm which put out a maximum CW power of 2 watts. The backward spontaneous scattered light is coupled to the OSA (optical spectrum analyzer) through the circulator. The spectrum of the backward spontaneous scattered

light is then recorded on OSA. The output end of the experimental fiber is terminated in an index matching fluid to avoid back reflections.

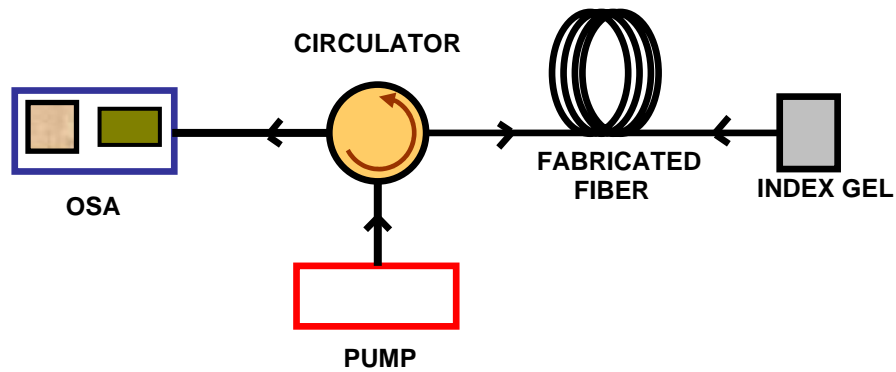


**Figure 3.37 – Schematic Diagram for Spontaneous Scattering Measurement Setup**

*Sample S1 Fiber:*

Using the setup mentioned above and shown in figure 3.37, the spontaneous spectrum in about 30 centimeters length of sample S1 fiber was measured. This spontaneous spectrum is shown in figure 3.38.

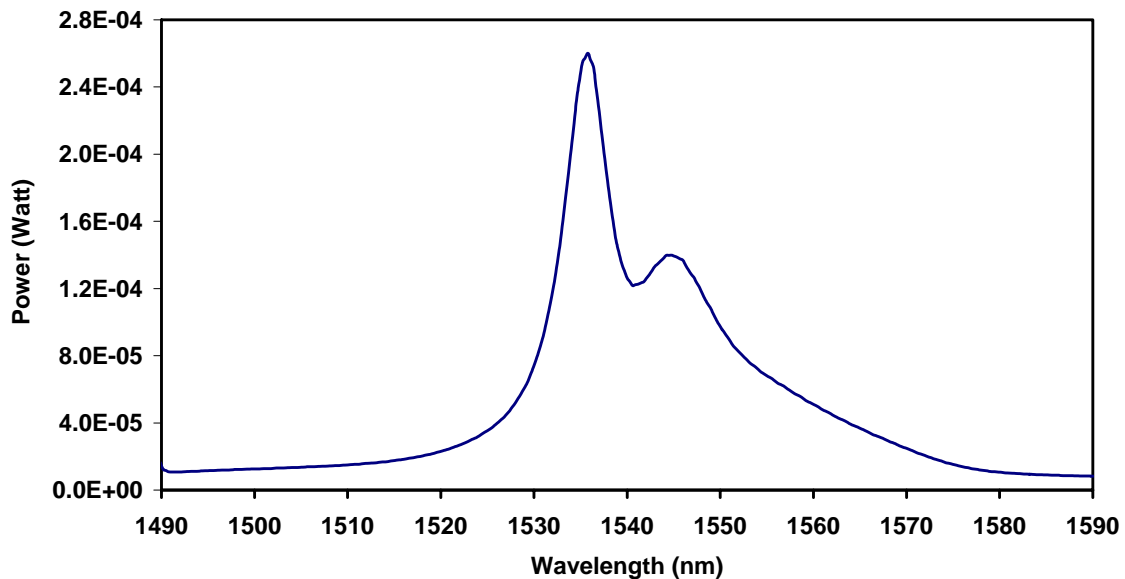


**Figure 3.38 - Spontaneous Scattering Spectrum of 30 cm length of Sample S1 Fiber**

Although this fiber was expected to have high percentages of high Raman scattering constituents like  $\text{GeO}_2$  or  $\text{TeO}_2$  ( $27\text{PbO}.43\text{GeO}_2.20\text{TeO}_2.10\text{CaO}.0.2\text{Er}_2\text{O}_3$ ) the stronger spontaneous spectrum from the Erbium ions dominated the relatively weaker Raman spontaneous spectrum. The well known peak of Erbium ions at 1535 nm can be seen from the spectrum.

*Sample S3 Fiber:*

The same setup shown in figure 3.37 was used to measure the spontaneous spectrum in about 1.5 meter length of sample S3 fiber. This spontaneous spectrum along with the spontaneous spectrum from only the fiber in the circulator is shown in figure 3.39.

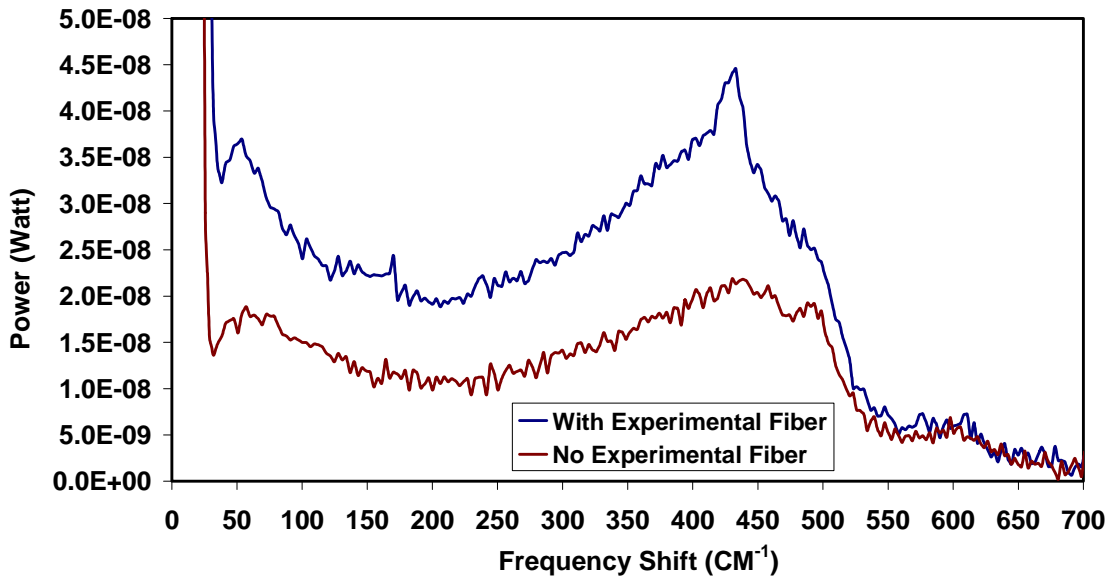


**Figure 3.39 - Spontaneous Scattering Spectrum of Sample S3 Fiber**

The fiber connected to the circulator in the experimental setup is a standard Corning SMF28 fiber with very small amount of  $\text{GeO}_2$  doping and does show a weak Raman spontaneous scattering. This spontaneous Raman spectrum just from the fiber in the setup (without any experimental fiber) is shown in the bottom curve of the figure 3.39. This spectrum has a peak at around  $440\text{ cm}^{-1}$  frequency shift which matches the peak of the silica fiber Raman spectrum. The spontaneous spectrum when sample S3 fiber is included can be seen from the top curve in the same figure 3.39, which shows a higher scattering spectrum with a shifted peak.

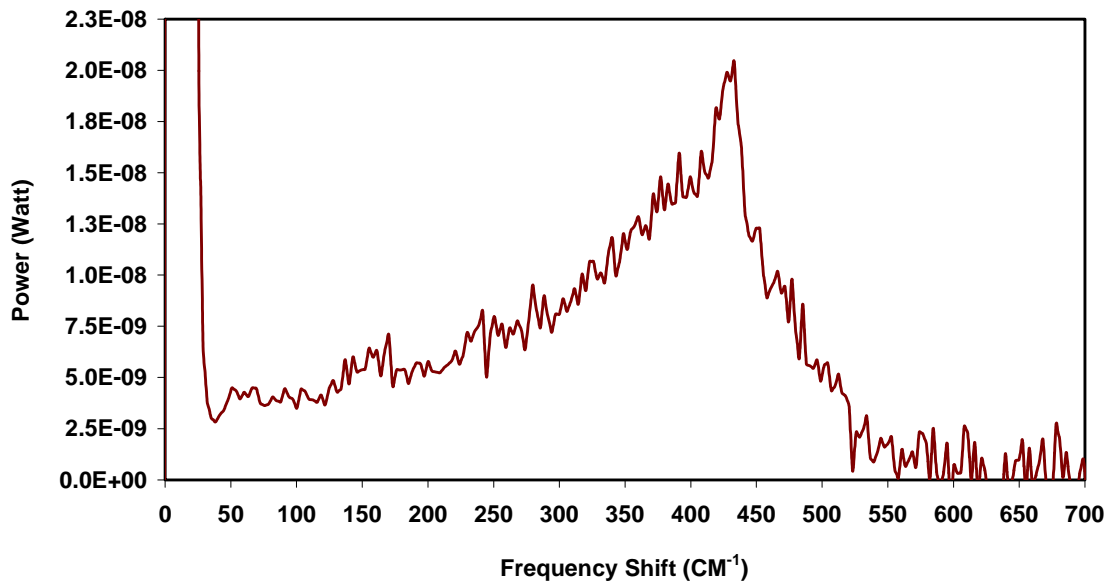


***Figure 3.40 - Raman Gain Spectrum of 1.5 meter length of Sample S3 Fiber***

The bottom curve in figure 3.39 was then subtracted from the top curve to remove the effect of the circulator fiber from the total spontaneous Raman spectrum with the Sample S3 fiber. This was further divided by the Bose-Einstein population factor to derive the Raman gain spectrum of the sample S3 fiber, which is shown in figure 3.40. This spectrum has a peak at  $433\text{ cm}^{-1}$  frequency shift which is in between the peaks of pure  $\text{GeO}_2$  ( $420\text{ cm}^{-1}$ ) and pure  $\text{SiO}_2$  silica ( $440\text{ cm}^{-1}$ ) Raman gain spectra. This indicates the presence of  $\text{GeO}_2$  and  $\text{SiO}_2$  in the core which was verified by the microprobe analysis of this fiber. This peak ( $433\text{ cm}^{-1}$ ) is closer to the  $\text{SiO}_2$  peak ( $440\text{ cm}^{-1}$ ) than that of the  $\text{GeO}_2$  peak ( $420\text{ cm}^{-1}$ ) indicating that silica is the major constituent in the core.

*Sample S5 Fiber:*

The spontaneous Raman spectrum of sample S5 fiber was measured in the same way as the Sample S3 fiber. The length of the fiber used was about 2 meters. This spectrum was further divided by the Bose-Einstein population factor to derive the Raman gain spectrum of the sample S5 fiber, which is shown in figure 3.41.

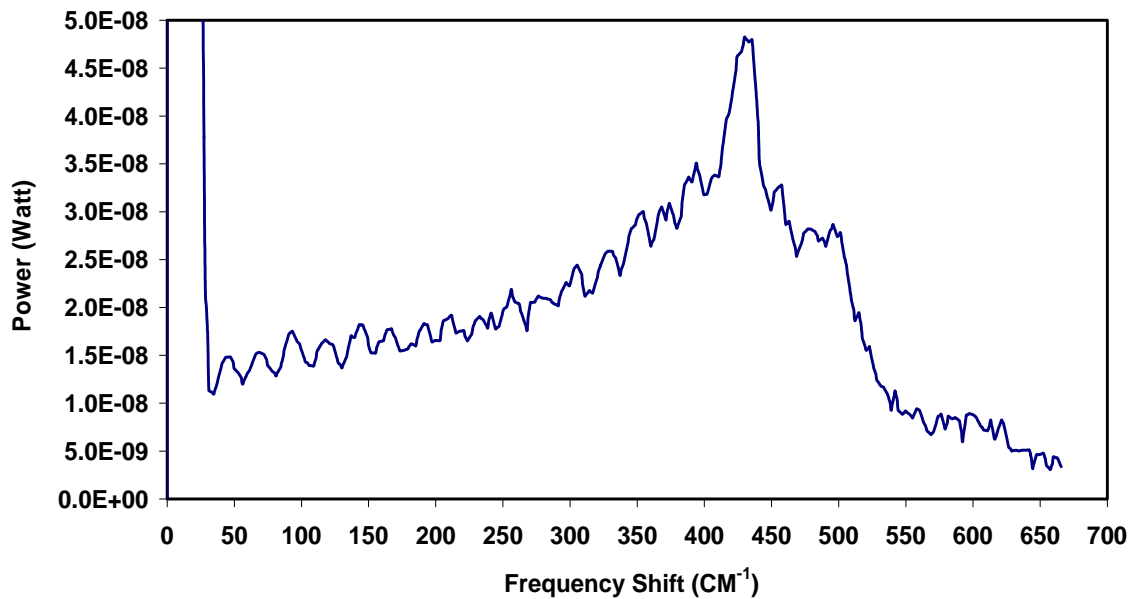


*Figure 3.41- Raman Gain Spectrum of 2 meters length of Sample S5 Fiber*

This spectrum has a peak at  $431\text{ cm}^{-1}$  frequency shift which is in between the peaks of pure  $\text{GeO}_2$  ( $420\text{ cm}^{-1}$ ) and pure  $\text{SiO}_2$  silica ( $440\text{ cm}^{-1}$ ). This indicates the presence of  $\text{GeO}_2$  and  $\text{SiO}_2$  in the core as verified by the microprobe analysis of this fiber. Compared to the peak ( $433\text{ cm}^{-1}$ ) in sample S1 fiber this peak ( $431\text{ cm}^{-1}$ ) is shifted slightly towards the pure  $\text{GeO}_2$  peak ( $420\text{ cm}^{-1}$ ) indicating that this fiber has a lesser  $\text{SiO}_2$  than sample S1 fiber.

*MM2 Glass Fiber:*

The next fiber measured for spontaneous scattering was the fiber fabricated with MM2 glass in the core and a silica cladding. A total of 5 centimeters length of this fiber was used to measure the spontaneous spectrum. This fiber had a very high gain glass in the core and the spontaneous spectrum could be measured in only one centimeter length of this fiber. The spontaneous spectrum measured in 5 centimeters length of this fiber is shown in figure 3.42 which shows the characteristic peak of erbium fibers at 1535 nm. The exact composition of this fiber core glass is unknown but the bump observed at 1560 nm could be due to presence of phosphate in the core glass.

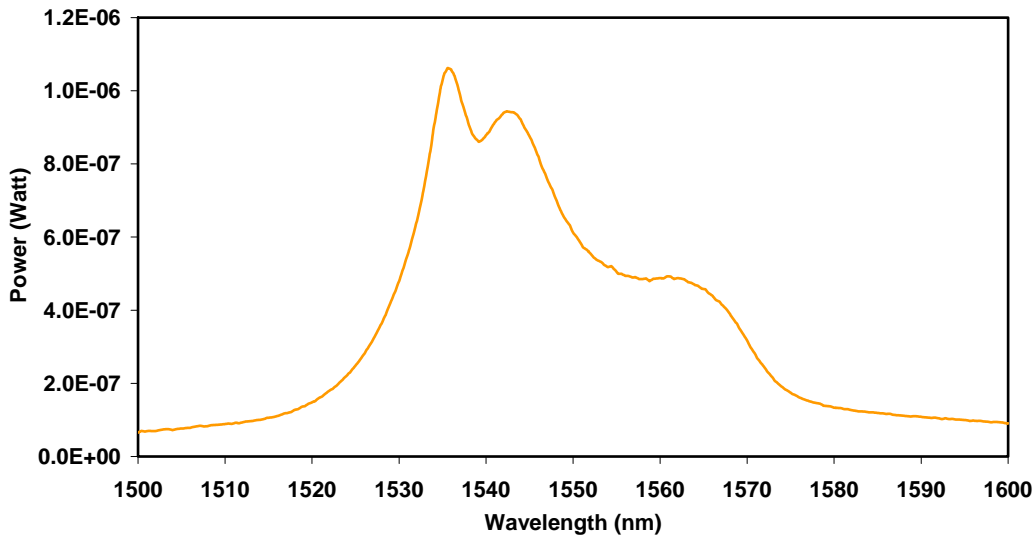


*Figure 3.42 – Spontaneous Spectrum of 5 cm length of MM2 Fiber*

*Bell Labs GeO<sub>2</sub> Fiber:*

This fiber had a GeO<sub>2</sub> core surrounded by a Pyrex cladding which made it impossible to splice it to the standard silica core fiber. Thus this fiber could not be used in the spontaneous spectrum measurement setup shown in figure 3.37. However, the forward spontaneous Raman spectrum was measured using the 514.5 nm line of an Argon ion laser. Green light at 514.5 nm was launched into 5 meters of the GeO<sub>2</sub> fiber with the help of a microscope objective and piezo-controlled stages.

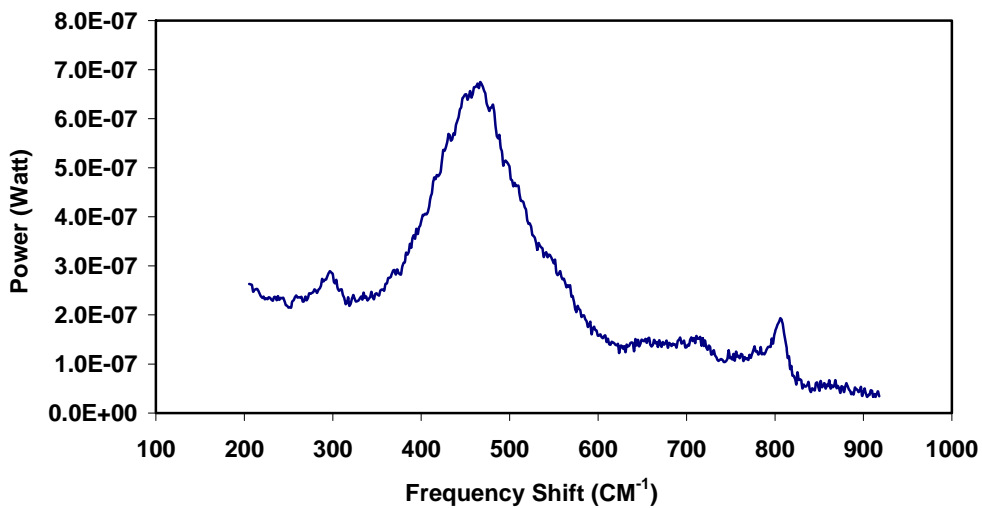


*Figure 3.43 - Spontaneous Raman Spectrum of Bell Labs GeO<sub>2</sub> core fiber, measured using the 514.5 nm line of an Argon ion laser*

The forward spontaneous Raman spectrum was recorded using an OSA. The resulting spectrum is shown in Figure 3.43 which has a peak Raman shift of  $460\text{ cm}^{-1}$ . This is closer to the peak of silica rather than that of pure Germania. The spectral measurement is therefore in qualitative agreement with the predictions based on measured index and concentration in that the dominant constituent is silica.

### 3.5 Summary

In this chapter measurements on fabricated Lead-Germanate-Tellurite and MM2 glasses based fibers and on an existing high  $\text{GeO}_2$ -doped fiber obtained from Bell Labs were presented. These measurements include loss, refractive index profile, elemental analysis and spontaneous spectrum. For all of these fibers, the values of the refractive indices in the core obtained from the refractive index profiles were found to be much lower than that of the index values expected from the starting core material. Elemental analysis using an electron microprobe on all of these fibers showed that silica diffuses into the core forming a silicate based core. This explained the lower-than-expected index values in the cores of all of these fibers. Also in the cores no trace was found of the index raising constituent  $\text{TeO}_2$ . That further explains the lower-than-expected values of the core indices for these fibers. Spontaneous spectra of all of these fibers were measured and found to be closer to pure silica than that of the constituents which also supports the fact that the major constituent of the cores is silica. Also, in the spontaneous spectra measurements no characteristic peaks corresponding to  $\text{TeO}_2$  were found, which reinforces the absence of  $\text{TeO}_2$  in the cores. In the next chapter the fabricated erbium based fibers will be used for making optical amplifiers and their characteristics measured.

### 3.6 Reference

1. Shigeki Sakaguchi and Shin-ichi Todroki, "*Optical properties of  $\text{GeO}_2$  glass and optical fibers*", *Applied Optics*, Vol. 36, No. 27, 20 Sept., 1997, pp. 6809-6814.



## IV. Application of Highly Doped Fibers for Optical Amplification

In the previous chapters fabrication and characterization of highly doped fibers were discussed. Here in this chapter use of the fabricated fibers for the purpose of optical amplification is presented. Out of the fabricated fibers, only erbium based fibers could be used to setup erbium doped fiber amplifiers (EDFAs). A 30 centimeter length of sample S1 fiber was used to setup an EDFA and the gain spectrum and distributed gain behavior of this amplifier measured. Two other EDFAs were setup using 5 cm and 1 cm lengths of MM2 glass fiber and their gain spectrum measured.

It would have been highly desirable to use high GeO<sub>2</sub> based fabricated fibers for the use of optical (Raman) amplification. Unfortunately, because of their smaller lengths (a couple of meters) and larger core diameters, no measurable gain could be seen. However a commercial highly GeO<sub>2</sub> doped dispersion compensated fiber (DCF) from OFS labs was used to setup a Raman amplifier. Table 4.1 lists all the fibers used for setting up the amplifiers.

*Table 4.1 – List of the Fibers Used for Optical Amplifiers*

Label	Core Glass	Cladding Glass	Length Used	Type of Amplification
Sample S1 Fiber	27PbO.43GeO <sub>2</sub> .20TeO <sub>2</sub> .10CaCO <sub>3</sub> .0.2 Er <sub>2</sub> O <sub>3</sub>	Silica	30 cm	Erbium Based
MM2Glass Fiber	Alumina. Erbium. Phosphate (actual composition unknown)	Silica	5 cm	Erbium Based
MM2Glass Fiber	Alumina. Erbium. Phosphate (actual composition unknown)	Silica	1 cm	Erbium Based
OFS Labs Fiber	Highly GeO <sub>2</sub> doped	Silica	4735 meters	Raman Amplification

### 4.1 EDFA using 30 cm length of Sample S1 Fiber

Using the erbium based sample S1 fiber fabricated by the “core-suction” technique an erbium doped fiber amplifier (EDFA) was setup. The schematic diagram of this EDFA setup can be seen in figure 4.1.

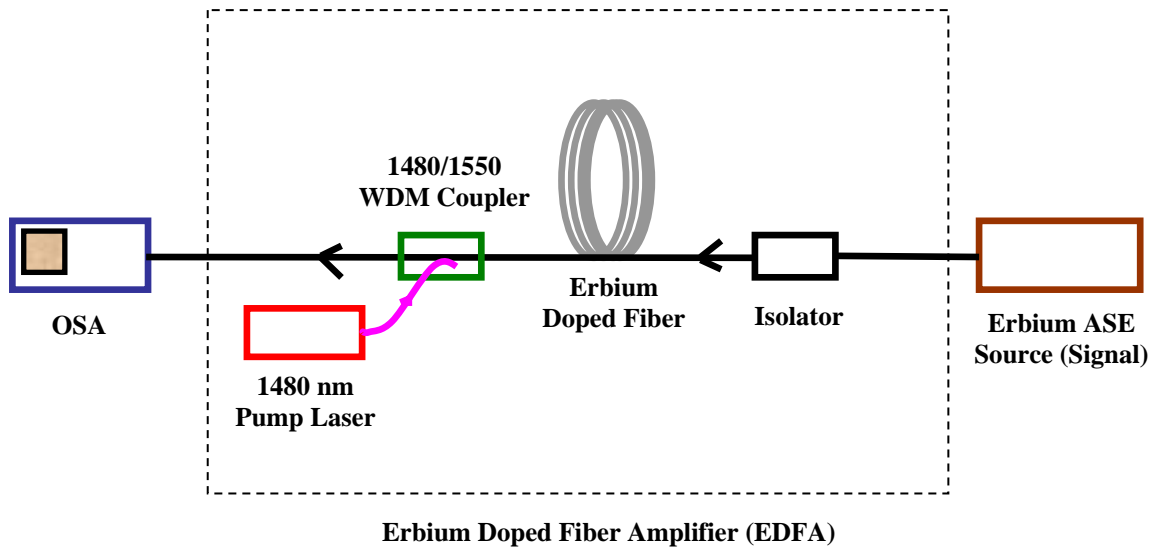


**Figure 4.1- Schematic diagram of the EDFA setup comprising erbium based fiber**

This EDFA setup comprised 30 cm of the fabricated erbium fiber, a wavelength division multiplexer (WDM) coupler, an isolator and a 1480 nm pump laser in the counter-propagating configuration, in which the pump energy travels in the direction opposite to the signal. A WDM coupler was used to combine the input signal and the pump laser. The input signal used in this setup was an Erbium amplified spontaneous emission (ASE) source which has a spectrum spanning over the entire gain spectrum of the erbium fiber.

*Gain Spectrum:* The signal spectrum was measured on optical spectrum analyzer (OSA) first with the pump power off and then pump power on. The gain spectrum of this EDFA was then calculated by the ratio of the signal powers with pump ON and pump OFF. The gain spectrum of this fiber with varying pump current (power) is shown in Figure 4.2. 50 mA current value of pump corresponds to a pump power of ~ 3 mW while 800 mA corresponds to ~ 35 mW.

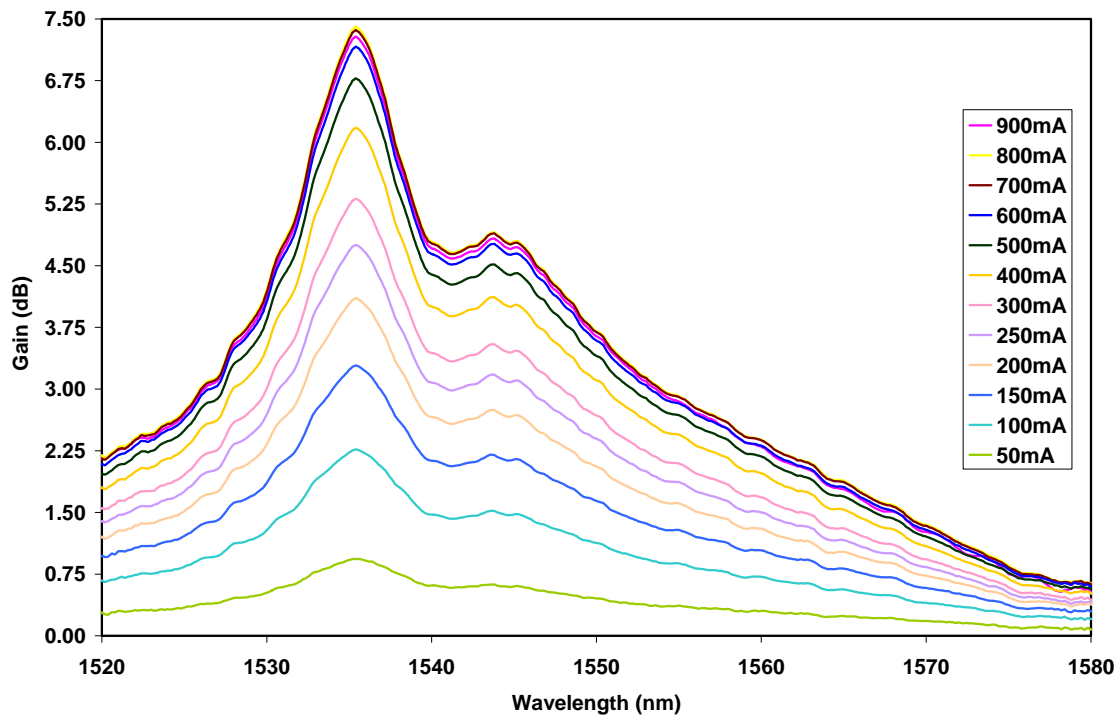


**Figure 4.2- Gain spectrum of the erbium based Sample S1 fiber**

As expected, the gain of the erbium fiber increases with pump power until saturation is reached. A characteristic gain peak of erbium can be seen at 1535 nm with a second peak at 1545 nm. A peak gain of about 7 dB was measured with  $\sim 35$  mW of pump power.

#### **4.2 Distributed Gain Measurement**

The two key parameters of an erbium fiber for its use in an EDFA or EFL (Erbium fiber laser), are gain distribution along the fiber and the ideal length of the doped fiber, which is normally calculated theoretically. The practical determination of the optimum length for maximum gain can be done with a cutback method but it is a destructive technique and very expensive due to the high cost of the Erbium doped fiber. One can check the distributed gain using an optical time domain reflectometer (OTDR) with additional ASE filtering<sup>1</sup>. However, the OTDR is not suitable to measure the gain distribution in typical Erbium-doped fibers (EDF) with lengths of few meters due to its limited dynamic range and spatial resolution (few tens of meters). Furthermore an OTDR can only be used for low-doped fibers.

Among the different techniques to evaluate the distributed gain in active fibers, the technique of coherent optical frequency domain reflectometry (C-OFDR) seems most promising as it is a nondestructive measurement method well matched to the task due to its dynamic range, resolution, and range. Moreover, background light from ASE or residual pump light is strongly rejected due to the coherent detection scheme employed. Successful use of the OFDR technique to measure the distributed gain behavior in active fibers is demonstrated in the literature<sup>2-6</sup>.

#### 4.2.1 Optical Frequency Domain Reflectometer (OFDR): Principle

The coherent OFDR technique is based on the coherent detection of the reflected light signal coming from the fiber under test when the optical frequency of the light source is swept<sup>2-6</sup>. This technique consists of analyzing a beat signal caused by the optical interference between two reflections; one called the reference reflection coming from a local oscillator and another reflection coming from the fiber under test. The schematic diagram of the OFDR setup is shown in figure 4.3. The output of a linearly tunable laser is coupled into the fiber under test using one arm, called test arm, of a 3-dB coupler. The reflection coming from the terminated end of the other arm of the 3-dB coupler provides the reference reflection, or local oscillator.

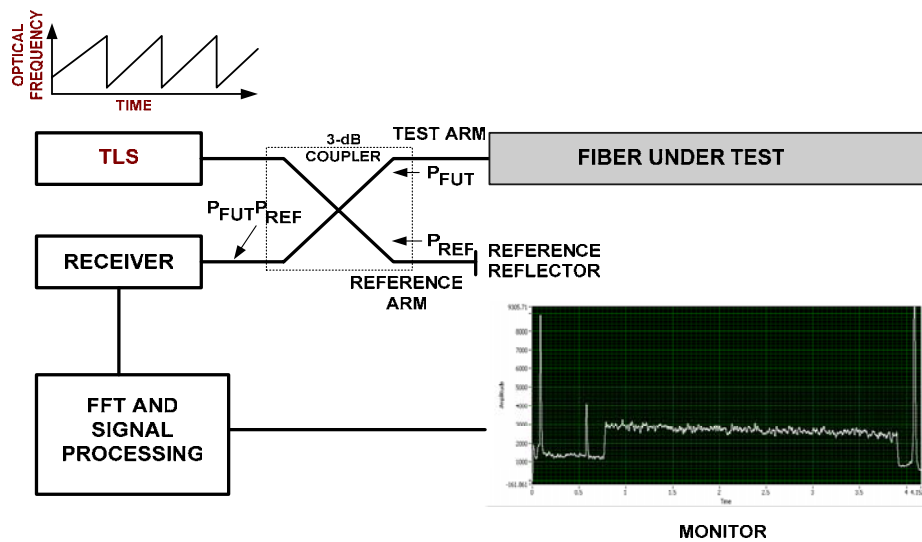


Figure 4.3- Schematic Diagram of an OFDR

The frequency of the laser source is swept linearly so that any optical interference will have a beat frequency proportional to the time delay between the reference and the test arm signals. Since this time delay can be related to the distance in the test fiber where the reflection takes place, one can map the reflections on the distance scale.

#### 4.2.2 Distributed Gain Measurement of Sample S1 Fiber using OBR

The distributed gain measurements were made on the fabricated Erbium doped sample S1 fiber, using the Luna Technologies optical backscatter reflectometer (OBR). The OBR is based on optical frequency domain reflectometry (OFDR) and has an excellent sensitivity of -125 dBm and 75 dB dynamic range<sup>7</sup>. It can measure devices up to 300 meters with no dead zone and with a spatial resolution down to 40 micron.

To measure the distributed gain in the fabricated erbium fiber, a forward pumped EDFA was setup using WDM coupler, sample S1 erbium fiber and a pump laser. The WDM coupler used was designed for multiplexing 1480 and 1550nm wavelengths. The pump laser wavelength was 1480 nm and the pump output power could be varied by varying the drive current.

This EDFA was then connected to the output of the OBR. The schematic diagram of this scheme can be seen in figure 4.4.

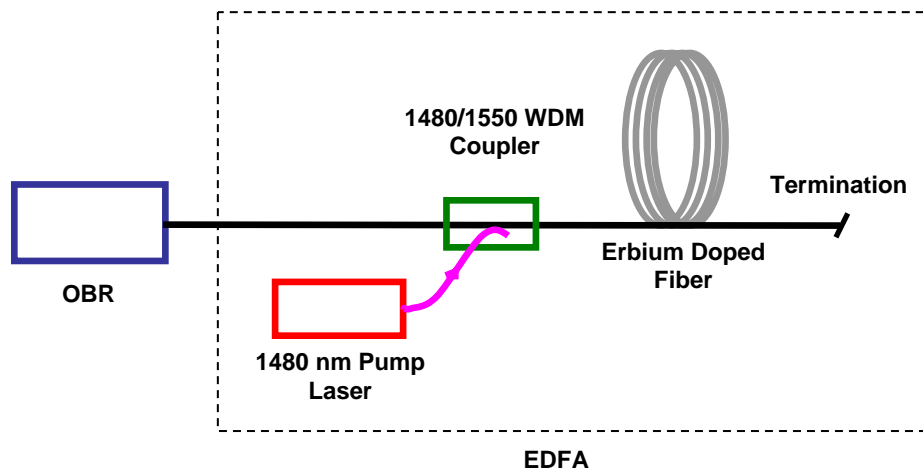


**Figure 4.4- Schematic of OBR use for distributed gain measurement in Erbium fiber**

The OBR swept center frequency was set at the 1535 nm, as that's peak of the erbium fiber gain curve, with a span of 5 nm. The OBR measurement was run on this setup by connecting the output of the OFDR to the 1550 nm port of the WDM coupler. Figure 4.5 shows the results for a fiber of 30 cm in length. The curves show the distributed Rayleigh backscattering as measured by the OBR for different pump powers keeping the OBR signal power constant. The bottommost curve shows the distributed backscattered power with pump power “off” and the top curves show the backscattered power for two different pump powers.

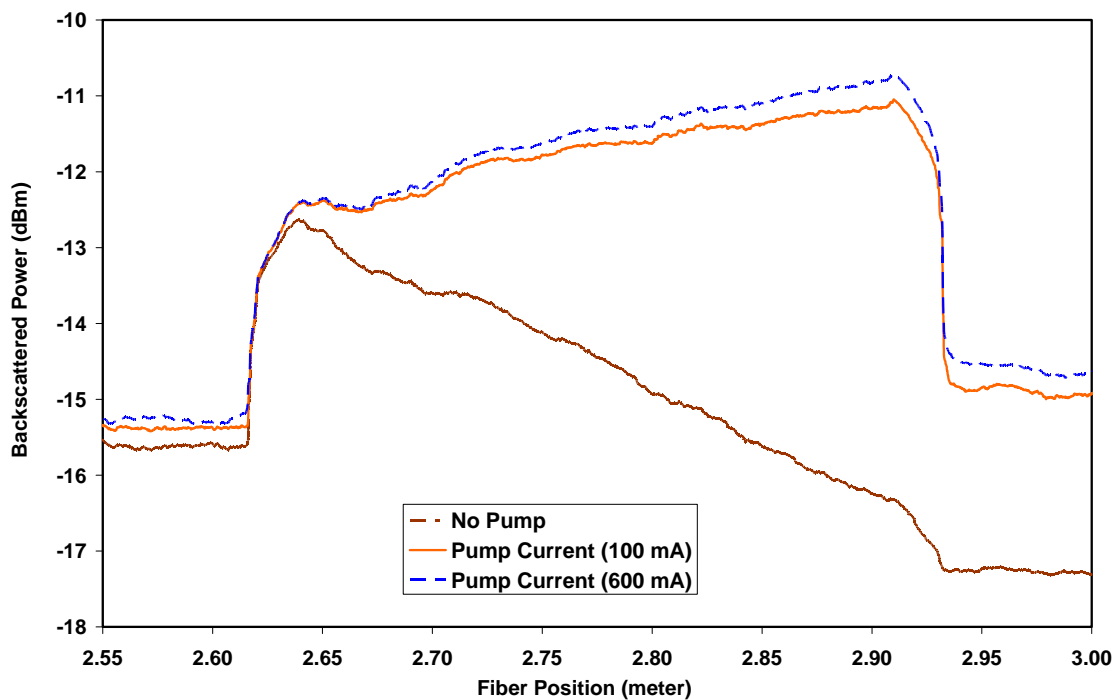


***Figure 4.5 - Distributed gain of fabricated Sample S1 fiber measured using OBR***

At the beginning of the Erbium fiber (2.62 meter mark), a distinctive jump in the Rayleigh scattering level can be observed due to the larger numerical aperture (NA) of the EDF, leading to a larger capturing of the Rayleigh scattered light. As a byproduct, the OBR curves therefore give a good idea of the amount of possible NA mismatches.

For pump switched off, a linear decay (exponential on a linear scale) in the curve within the Erbium fiber (2.62 m –2.92 m) can be observed. This corresponds to the

expected absorption loss of the Er ions in the active fiber at 1535 nm, which can be calculated from the slope. As seen in the other curves, when pump power is switched on, the backscattered signal grows with the length leading to some gain. From these curves, we can observe the location of the peak gain which strongly depends on the pump power and shifts towards the farther positions. The position of peak gain can be used to decide the optimum length of the fiber for fiber amplifier or laser application.

### **4.3 EDFA using 5 cm length of MM2Fiber**

As before, an EDFA was setup using the erbium based MM2 glass fiber fabricated by the “core-suction” technique. The schematic diagram of this EDFA setup can be seen in figure 4.1. This fiber was first spliced to standard fiber pigtails to connect it to the other components like the WDM and isolator of the EDFA setup. The photograph of this fiber spliced with the standard fiber pigtails can be seen in figure 4.6.



***Figure 4.6- Photograph of the 5 cms MM2 glass fiber spliced to standard fiber pigtails***

*Gain Spectrum:* The gain spectrum of this EDFA having 5 cms of MM2 glass fiber was measured as before. Variation of the gain spectrum of this fiber with pump can be seen in Figure 4.7.

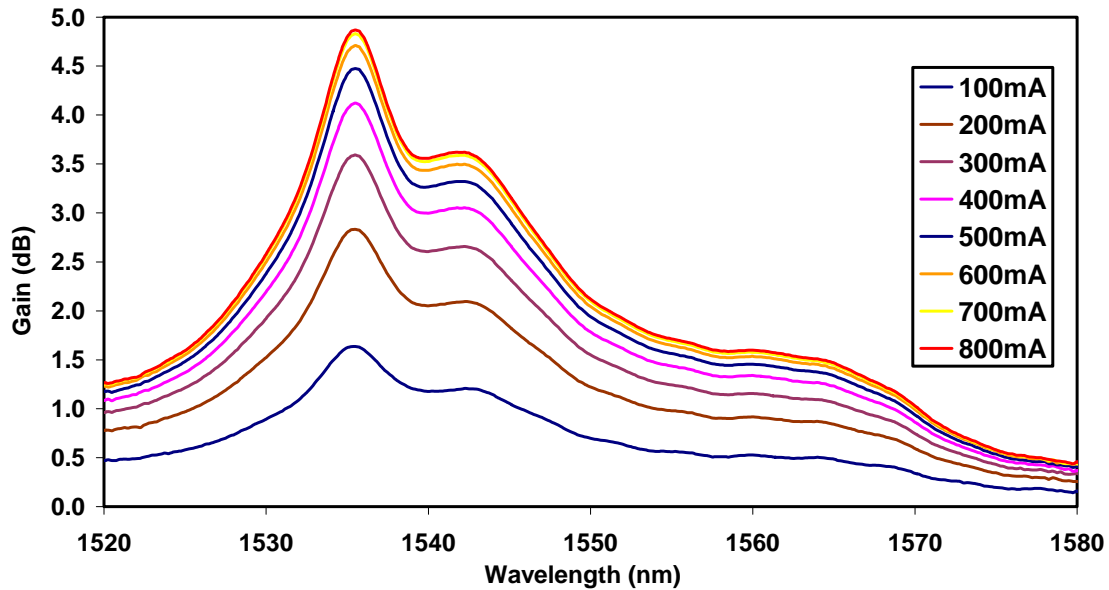


*Figure 4.7 - Gain spectrum of 5 cm length of erbium based MM2 glass fiber*

As before, gain of this fiber increases with pump power until saturation is reached. A characteristic gain peak of erbium can be seen at 1535 nm with a second peak at 1545 nm. Compared to the sample S1 fiber, this fiber has a wider gain spectrum showing one more peak at around 1565 nm which could be because of the phosphate present in the glass (actual composition of this fiber is unknown). At 1535 nm a peak gain of about ~5 dB was measured with ~ 35 mW of pump power.

#### **4.4 EDFA using 1 cm length of MM2Fiber**

As before another EDFA was setup using 1 cm length of erbium based MM2 glass fiber fabricated by the “core-suction” technique. The schematic diagram of this EDFA setup can be seen in figure 1. This fiber was also first spliced to standard fiber pigtailed to connect it to the other components like the WDM and isolator of the EDFA setup. The photograph of this fiber spliced with the standard fiber pigtailed can be seen in figure 4.8.





**Figure 4.8-** Photograph of 1 cm MM2 glass fiber spliced to standard fiber pigtailed

*Gain Spectrum:* The gain spectrum of this EDFA having 1 cm of MM2 glass fiber was measured as before. Variation of the gain spectrum of this fiber with pump can be seen in Figure 4.9.

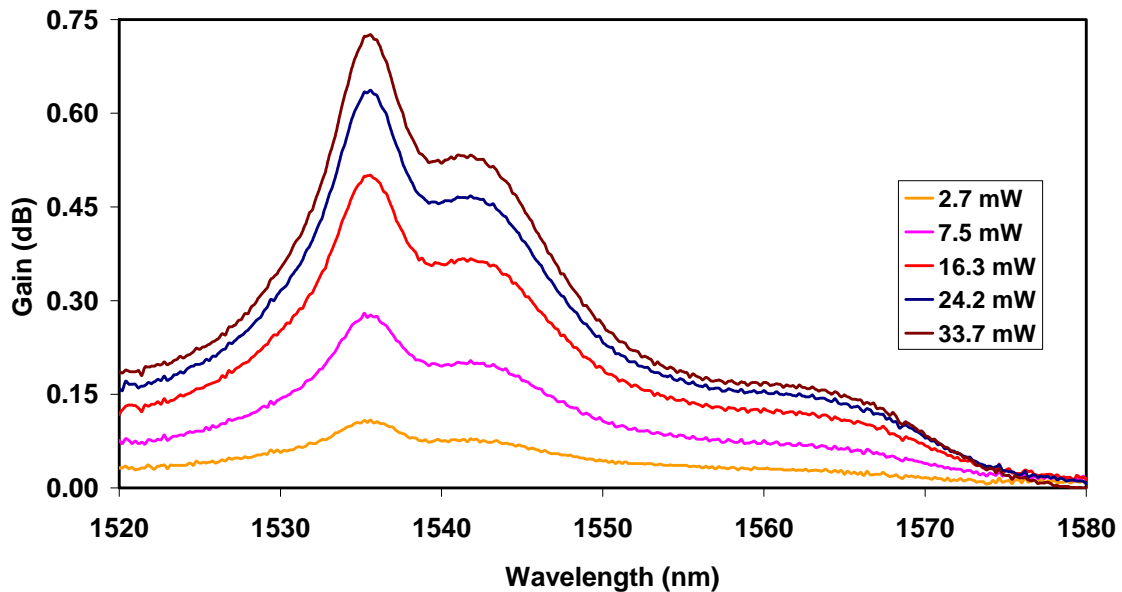


**Figure 4.9-** Gain spectrum of 1 cm length of erbium based MM2 glass fiber

It can be observed from the figure that gain of this fiber increases with pump power until saturation is reached. A characteristic gain peak of erbium can be seen at 1535 nm with a

second at 1545 nm. Compared to the sample S1 fiber, this fiber also shows a wider gain spectrum showing one extra peak at around 1565 nm which could be because of the phosphate present in the core glass. A peak gain of about 0.7 dB was measured at ~ 34 mW of pump power.

#### 4.5 Setup of a Raman Amplifier using commercial (OFS Labs) Dispersion Compensating Fiber (DCF)

The fabricated fibers with high Raman gain constituents like GeO<sub>2</sub> or PbO were not long enough to measure Raman amplification. Also their large core diameter made it impossible to see any Raman shifts. So a commercial dispersion compensated fiber (DCF) from OFS Labs was used to setup a Raman amplifier as shown in figure 4.10.

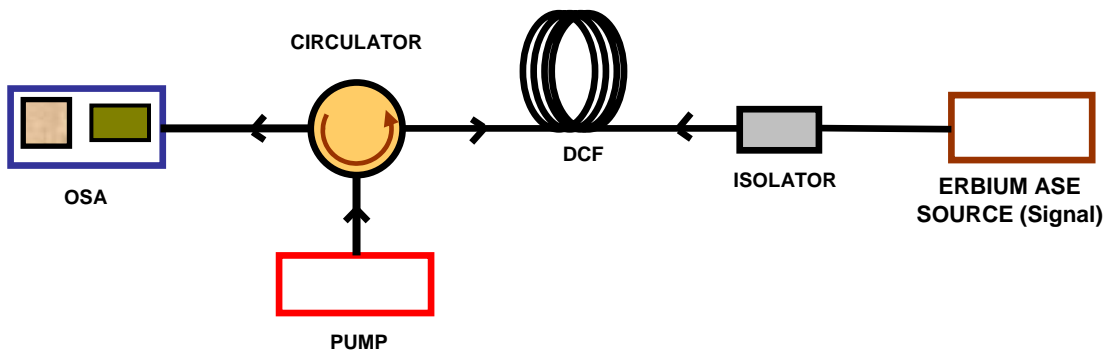


*Figure 4.10 - Schematic diagram of Raman Amplifier comprising OFS DCF*

This Raman amplifier comprised 4735 meters of the DCF, a circulator, an isolator and a 1450 nm pump laser in the counter-propagating configuration, in which the pump energy travels in the direction opposite to the signal. An isolator was used to block the pump power from entering into the signal source. A circulator was used to combine the signal and the pump. The signal used in this setup was an Erbium amplified spontaneous

emission (ASE) source which has spectral output over the 1550 nm band and also covers the peak Stokes shift ( $\sim 432 \text{ cm}^{-1}$  (1547 nm)) of this fiber.

*Gain Spectrum:* Signal spectra of the ASE source were measured on an optical spectrum analyzer (OSA) first with the pump power “off” and then pump power “on”. The bottom curve in the figure 4.11 shows the spectrum of the ASE source when the pump is OFF and the upper curve with the pump power ON. The amplification of this amplifier was then calculated by the ratio of the signal powers at pump ON and pump OFF, which is also shown in the figure 4.11.

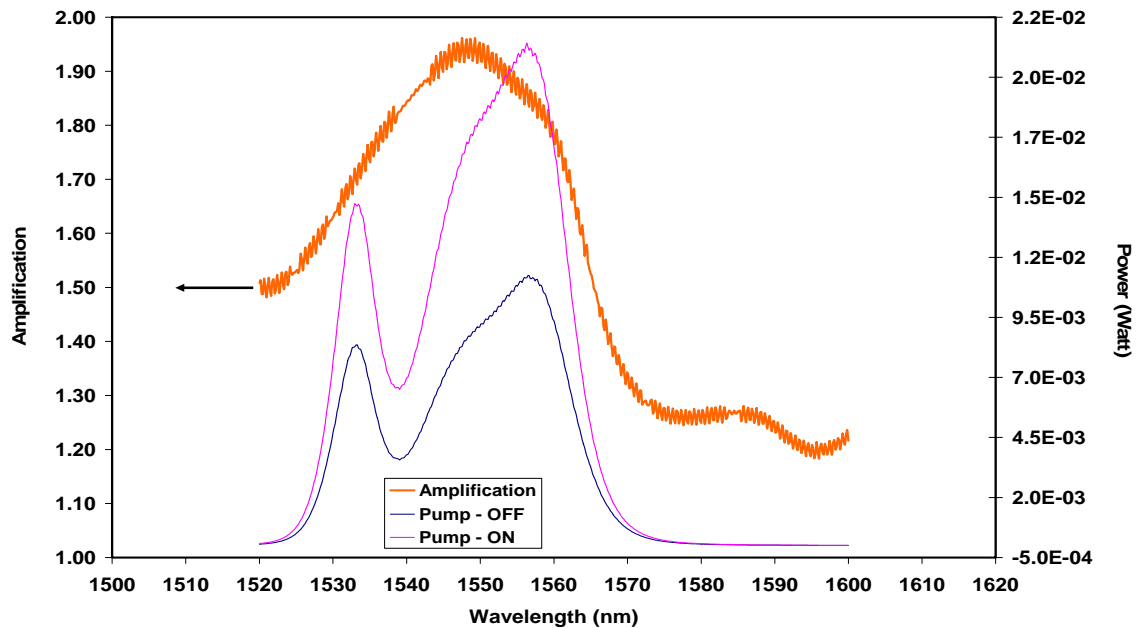


**Figure 4.11 - Amplification Spectrum of the Raman Amplifier setup by OFS DCF**

For this Raman amplifier, the gain with respect to frequency shift can be seen in figure 4.12. This figure shows a Raman gain peak at  $\sim 432 \text{ cm}^{-1}$  Stokes frequency shift. A peak gain of about 3 dB was measured with  $\sim 100 \text{ mW}$  of pump power.

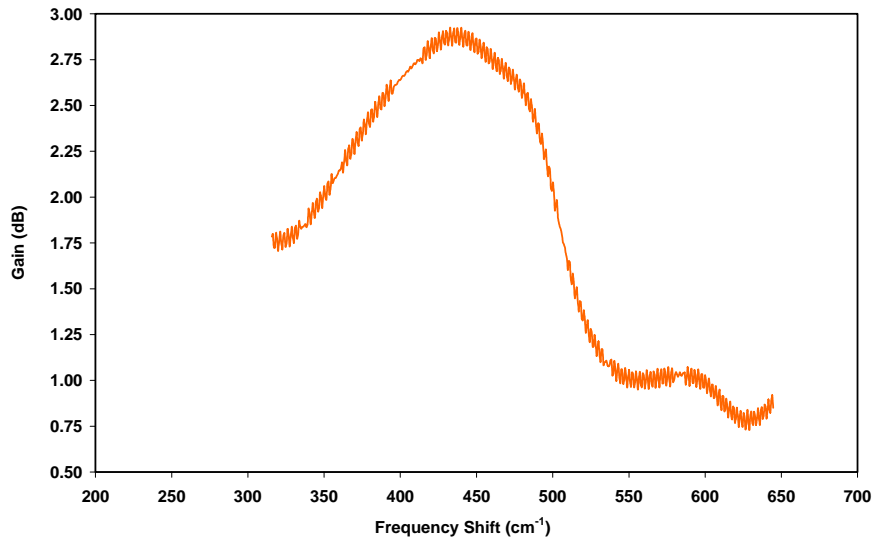


**Figure 4.12- Gain Spectrum of the Raman Amplifier setup by OFS DCF**

#### **4.6 Summary**

In this chapter successful use as EDFAs of the erbium based fibers, fabricated by the “core-suction” technique was presented. Spectral gains of these erbium fibers were measured. A 30 cm length of sample S1 fiber produced a peak gain of about 7 dB with a pump power of ~35 mW. Distributed gain of this fiber was also measured using an OBR. Using the OBR, very accurate distributed gain measurements in Erbium and other doped fibers can be performed very precisely in a rapid and nondestructive way. This information will be very useful in improving the manufacturing process for doped fibers, and designing inexpensive fiber lasers and amplifiers for much better performance. Two other EDFAs were setup using 5 cm and 1 cm lengths of a MM2 glass fiber. A peak gain of ~5 dB was measured in a 5 cm length of MM2 glass fiber, while a 1 cm length gave ~0.7 dB gain with ~35 mW pump power. Distributed gain in these MM2 fiber EDFAs could also be measured. A Raman amplifier was also setup using a commercial DCF, and its gain spectrum measured. A peak gain of ~3dB was measured with ~ 100 mW pump power.

## 4.7 References

1. M. Nakazawa, Y. Kimura, and K. Suzuki, “*Gain-distribution measurement along an ultralong erbium doped fiber amplifier using optical time domain reflectometry,*” *Opt. Lett.*, vol. 15, no. 1, pp. 1200–1202, 1990
2. M. Wegmuller et.al., Wegmuller, M.; Oberson, P.; Guinnard, O.; Huttner, B.; Guinnard, L.; Vinegoni, C.; Gisin, N.; “*Distributed gain measurements in Er-doped fibers with high resolution and accuracy using an optical frequency domain reflectometer*” *Journal of Lightwave Technology*, VOL. 18, NO.-12, December 2000 Page(s):2127 – 2132
3. J. P. von der Weid, R. Passy, B. Huttner, O. Guinnard, and N. Gisin, “*High-resolution distributed-gain measurements in erbium-doped fibers,*” *IEEE Photon. Technol. Lett.*, vol. 10, pp. 949–951, July 1998.
4. J. P. von der Weid, R. Passy, G. Mussy, and N. Gisin, “*On the Characterization of optical fiber network components with optical frequency domain reflectometry,*” *J. Lightwave Technol.*, vol. 15, July 1997.
5. W. Eickhoff and R. Ulrich, “*Optical frequency domain reflectometry in single-mode fiber,*” *Appl. Phys. Lett.*, vol. 39, no. 9, pp. 693–695, 1981.
6. J. P. von der Weid, R. Passy, and N. Gisin, “*Coherent reflectometry of optical fiber amplifiers,*” *IEEE Photon. Technol. Lett.*, vol. 9, pp.1253–1255, Sept. 1997.
7. [http://www.lunatechnologies.com/products/obr/files/OBR\\_description.pdf](http://www.lunatechnologies.com/products/obr/files/OBR_description.pdf) OBR Description , LUNA Technologies.

## V. Calculation of Raman Gain in GeO<sub>2</sub> doped Fibers

Raman amplification in optical fibers is gaining significant interest in optical fiber communication systems for applications like distributed and discrete optical amplifiers and fiber lasers. The fundamental advantage of Raman amplification is that the transmission fiber itself acts as an amplifying medium. The transmission fiber can be a pure silica core fiber, conventional step index fiber with low GeO<sub>2</sub> doping or triangular index dispersion shifted fiber with relatively high GeO<sub>2</sub> doping. These transmission fibers differ mainly in GeO<sub>2</sub> doping levels and effective areas. To calculate the Raman gain in fibers, it is necessary to know the Raman gain characteristics of different fiber types with different GeO<sub>2</sub> doping levels.

In this chapter, Raman gain calculations for pure silica core Sumitomo Z-Plus fiber, a low GeO<sub>2</sub> doped Spectran standard fiber, and a high GeO<sub>2</sub> doped Lucent Truewave fiber are presented. To calculate the Raman gain, first the index profile of the fiber under investigation was measured and mode fields at pump and signal wavelengths calculated. The Raman gain was then calculated by taking the Raman gain coefficient  $g$ , which is a function of GeO<sub>2</sub> doping, into the overlap integral between the pump and the signal mode fields. Polarization dependence of the Raman gain was also taken into account.

### 5.1 Raman Amplification:

If pump power  $P_0$  is launched in a fiber of length  $L$  and  $\alpha_p$  attenuation coefficient at the pump wavelength, the Raman amplification  $G_A$  at the Stokes wavelength (signal) is given by equation [1]<sup>1</sup>:

$$G_A = \exp\left(\frac{gP_0L_{eff}}{A_{eff}}\right) \quad (1)$$

where  $L_{eff}$  is the effective length of the fiber defined as  $L_{eff} = \frac{1 - \exp(-\alpha_p L)}{\alpha_p}$ , which takes into account pump absorption with fiber length;  $g$  is the Raman gain coefficient of the fiber; and  $A_{eff}$  is the effective area of the fiber, which for Raman gain is determined by mode size and the overlap between the pump and the Stokes modes, and defined as:

$$A_{eff} = \frac{\int \psi_p^2 r dr \int \psi_s^2 r dr}{2\pi \int \psi_p^2 \psi_s^2 r dr} \quad (2)$$

Where,  $\Psi_p$  and  $\Psi_s$  represent the mode fields at the pump and the Stokes wavelengths respectively. It can be seen from equation (1) that increasing the value of  $g$  and decreasing  $A_{eff}$  will increase the Raman amplification in fibers. Now equation (1) can be re-written in terms of Raman Gain ( $g/A_{eff}$ ) as:

$$\frac{g}{A_{eff}} = \frac{\ln(G_A)}{P_0 L_{eff}} \quad (3)$$

Where  $G_A$ ,  $P_0$  and  $L_{eff}$  are experimental parameters and can be measured experimentally. Once we have the values of these parameters, using equation (3), we can calculate the value of the Raman gain. So the measurement produces the Raman gain  $g/A_{eff}$ , which is the desired parameter in a practical amplifier.

A measurement of the actual Raman gain coefficient of the material  $g$  is more complicated because the gain coefficient depends on  $GeO_2$  concentration which varies across the index profile. Thus a measurement of  $g/A_{eff}$  and a separate determination of  $A_{eff}$  will not necessarily produce a meaningful value for the Raman gain coefficient of  $GeO_2$  doped silica fiber.

## 5.2 Effect of $GeO_2$ Doping on Raman Gain Coefficient

Germanium doping raises the Raman gain coefficient. The effect is small in standard fibers containing about 4 mole %  $GeO_2$  but can raise the gain by about 50% in dispersion-shifted fibers. The gain is more than doubled in dispersion-compensating fibers. A careful series of measurements have been reported for spontaneous Raman scattering vs.  $GeO_2$  concentration in a  $GeO_2$  doped MCVD preform<sup>2</sup>. It has been shown that the Raman gain coefficient increases linearly with the  $GeO_2$  concentration. The relation between peak Raman gain coefficient  $g_p(GeO_2)$  of  $GeO_2$  doped fibers over pure silica  $g_p(SiO_2)$  and mole %  $GeO_2$  ( $x_{GeO_2}$ ) is given by:

$$g_p(\text{GeO}_2) = \frac{n_2^2}{n_1} g_p(\text{SiO}_2) [1 + 0.08 \times x_{\text{GeO}_2}] \quad (4)$$

where  $n_1$  and  $n_2$  are the refractive indices of  $\text{GeO}_2$  doped silica and pure silica fibers respectively. It is to be noted that the peak Raman gain coefficient of pure silica  $g_p(\text{SiO}_2)$  used in equation (4) already takes the polarization effects (the gain for randomly polarized light being the half that for pump and signal light of the same polarization state) into account.

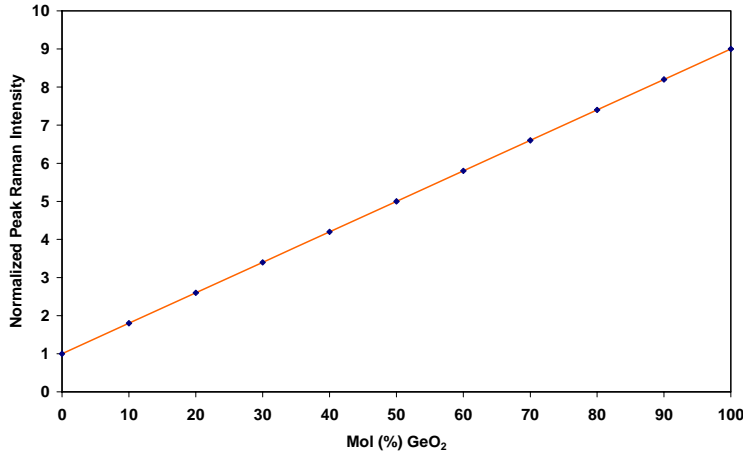


**Figure 5.1- Peak Raman intensity normalized to silica vs. mol %  $\text{GeO}_2$**

Equation (4) is plotted in figure 5.1. Figure 5.1 shows the Raman peak gain intensity normalized to pure silica vs.  $\text{GeO}_2$  concentration, 100 mole %  $\text{GeO}_2$  raises the gain by a factor of 9.0 over pure silica.

In a fiber, the mode field penetrates into the cladding so the effective Raman gain coefficient will be some average over the doping profile, which will be less than the increase in gain from the maximum at the core center. The proper way to include the increase in Raman gain from  $\text{GeO}_2$  doping is to include it in the calculation of the overlap integral<sup>3</sup>. Since Raman Gain ( $g/A_{\text{eff}}$ ) is given by:

$$\frac{g}{A_{\text{eff}}} = g \cdot \frac{\int \psi_p^2 \psi_s^2 r dr}{2\pi \int \psi_p^2 r dr \int \psi_s^2 r dr} \quad (5)$$



where  $\Psi_p, \Psi_s$  are the mode fields at the pump and the signal wavelengths and  $g$  is the Raman gain coefficient. Now the *effective* Raman gain will be given by taking the Raman gain coefficient  $g$  into the overlap integral as follows,

$$\frac{g}{A_{eff}} = \frac{\int \psi_p^2 g(r) \psi_s^2 r dr}{2\pi \int \psi_p^2 r dr \int \psi_s^2 r dr} \quad (6)$$

So, equation (6) can be used to estimate the effective Raman gain in fibers with varying radial  $\text{GeO}_2$  concentration.

### 5.3 Calculation of effective Raman gain for $\text{GeO}_2$ doped fibers

Calculation of the effective Raman gain in a pure silica core fiber and two  $\text{GeO}_2$  doped fibers was made using equation (6). The pump wavelength was taken to be 1450.4 nm which produce peak Raman gain at a signal wavelength  $\sim 1550$  nm. The fibers used for the calculation were Sumitomo Z-PLUS fiber, a standard fiber (STF) from Spectran and Truewave a dispersion shifted fiber (DSF) from Lucent. Z-PLUS is a pure silica core fiber and STF is a low  $\text{GeO}_2$  doped step index fiber; Truewave is relatively high  $\text{GeO}_2$  doped triangular index fiber.

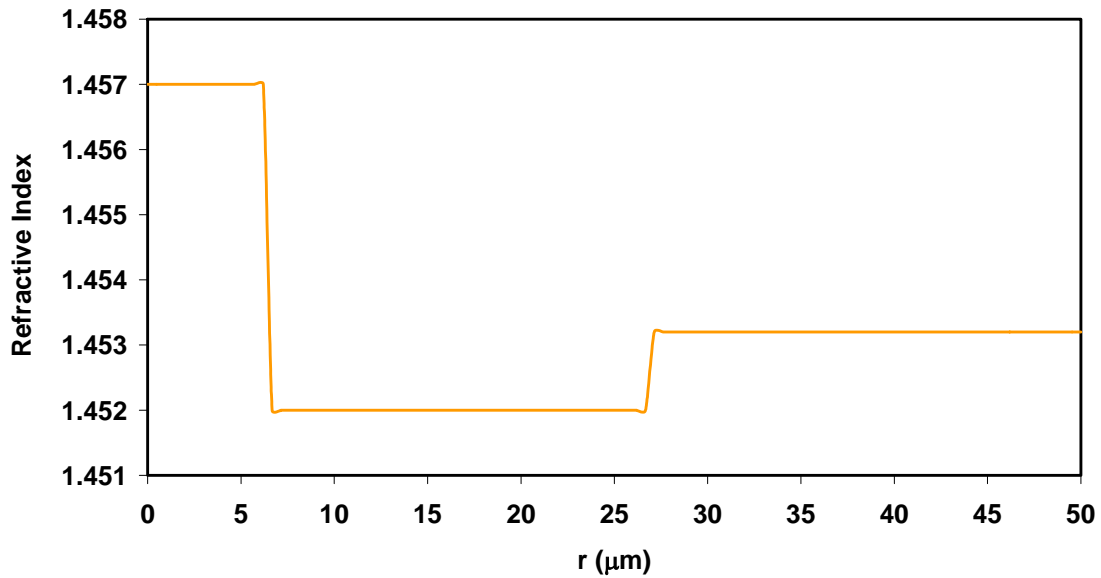


*Figure 5.2- Refractive Index Profile of Sumitomo Z-Plus Fiber*

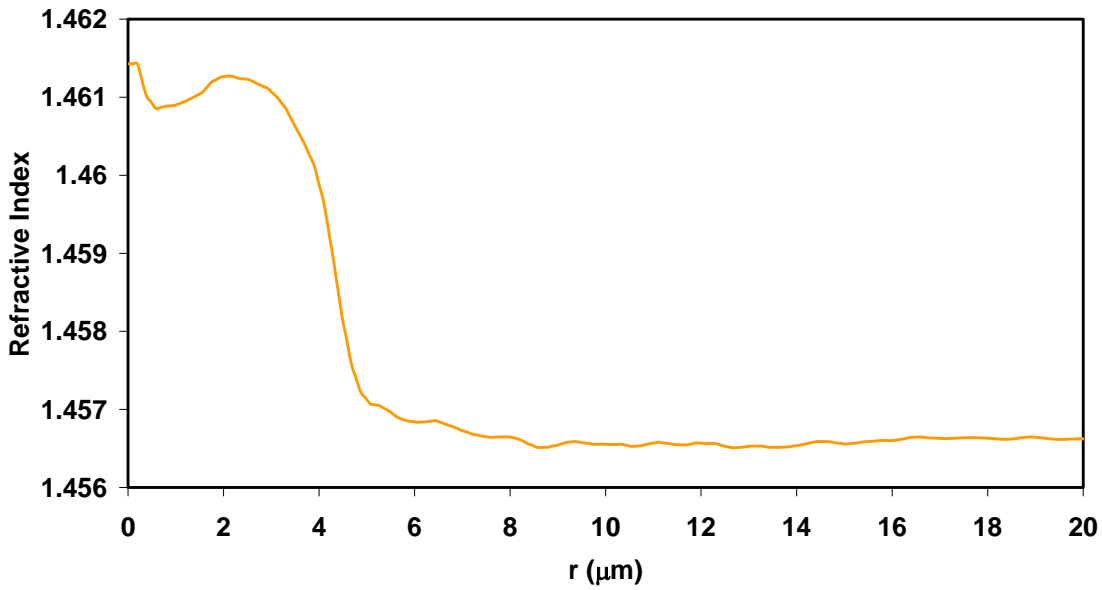


*Figure 5.3- Refractive Index Profile of Spectran Standard Fiber*

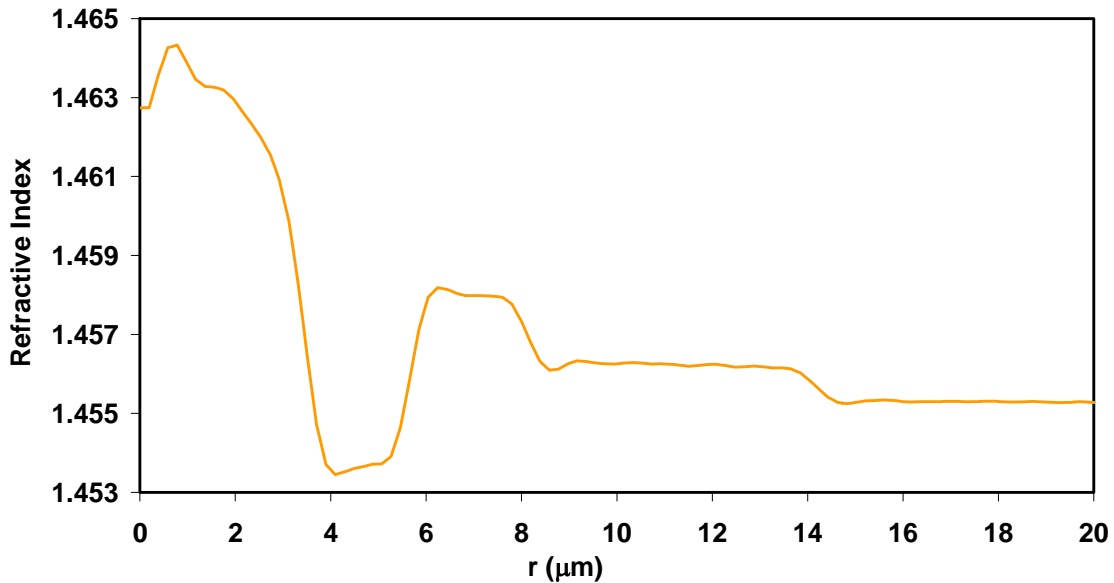


*Figure 5.4- Refractive Index Profile of Lucent Truwave Fiber*

To calculate the effective Raman gain, first of all the refractive index profile of the desired fiber needs to be known. Refractive index profiles for STF and Truwave fibers were measured at OFS Labs by A. Yablon. The profile of the Z-Plus fiber was measured at Virginia Tech with a York fiber index profiler. The profile shown in figure 5.2 has 11% correction as the York profiler measured an index value 11% lower than the actual value. Index profiles for these fibers are shown in figure 5.2 through 5.4.

From the refractive index profile, the radial GeO<sub>2</sub> concentration can be calculated using the relation developed from reference<sup>4</sup>. Relation of refractive index with GeO<sub>2</sub> mol % is plotted in figure 5.5. Consequently, in a fiber once the radial refractive index is known from the refractive index profile, the corresponding radial GeO<sub>2</sub> concentration can be found through the linear relation.

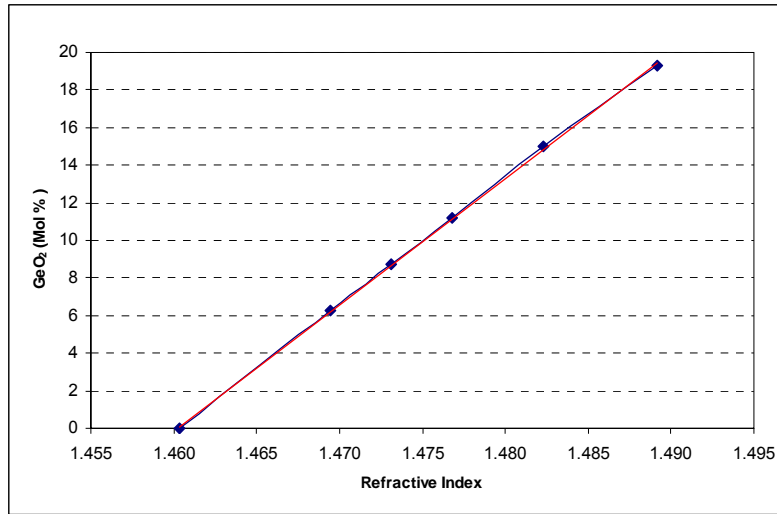


**Figure 5.5- Variation of Mol % GeO<sub>2</sub> with refractive index**

For Spectran STF, peak GeO<sub>2</sub> concentration was calculated to be ~ 3 mol % while Lucent Truewave fiber had a peak concentration of ~ 5 mol%. Once we know the radial GeO<sub>2</sub> mol %, the radial peak Raman gain coefficient  $g_p(\mathbf{r})$  can be calculated using equation (4)

It is to be noted that STF and DSF are single mode at 1450 nm and 1550 nm and support only the fundamental mode LP<sub>01</sub>. From the refractive index profiles of these fibers, using a TELMAC commercial fiber program package, the mode fields  $\Psi_p$  and  $\Psi_s$  at the pump (1450 nm) and the signal (1550 nm) wavelengths were calculated.

From the radial Raman gain coefficient and mode fields  $\Psi_p$  and  $\Psi_s$ , effective Raman gain ( $g/A_{eff}$ ) values for these fibers were calculated using equation (6). For Z-PLUS fiber the effective Raman gain was basically the peak Raman gain for pure silica divided by the effective area of the fiber. Effective area of the Z-PLUS fiber was calculated to be ~ 125

$\mu\text{m}^2$ . For  $\text{GeO}_2$  doped fibers, the procedure of calculating effective Raman Gain ( $g/A_{\text{eff}}$ ) from the fiber refractive index profile is summarized in a flowchart shown in figure 5.6.

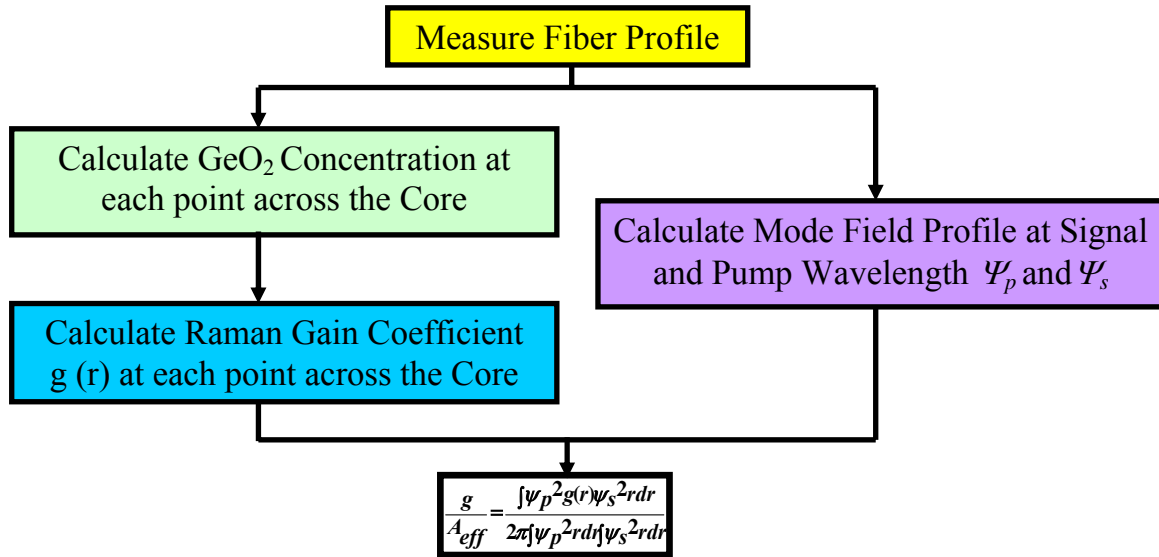


**Figure 5.6- Flowchart for the effective Raman gain calculation**

From the refractive index profiles shown in figure 2 through 4, the calculated effective Raman gain values for Z-PLUS, STF and Truwave are tabulated in table 5.1.

**Table 5.1: Calculated effective Raman gain values for Z-PLUS, STF and Truwave Fibers**

Fiber Type	Calculated Effective Raman Gain ( $\text{km}^{-1}\text{W}^{-1}$ )
Z-PLUS	0.250
STF	0.468
Truwave	0.836

As expected Truwave fiber has the maximum Raman gain because of its high  $\text{GeO}_2$  content and lower effective area. Z-PLUS has the lowest Raman gain because of no  $\text{GeO}_2$  doping.

## 5.4 Summary

Effective Raman gain values were calculated for pure silica core Z-PLUS, a low GeO<sub>2</sub> doped standard fiber and a dispersion shifted fiber with high GeO<sub>2</sub> doping. Raman gain dependence of Raman gain on GeO<sub>2</sub> doping and polarization dependence were taken into account. Truewave fiber showed the maximum Raman gain because of its high GeO<sub>2</sub> content and lower effective area. Z-PLUS had the lowest Raman gain because of no GeO<sub>2</sub> doping. In the next section, the Raman gain is measured experimentally for these fibers and compared with the calculated effective Raman gain values.

## 5.5 References

1. Agarwal G. P., "*Nonlinear Fiber Optics*", Academic Press, Boston 1989
2. S.T. Davey, D.L. Williams, B.J. Ainslie, W.J.M. Rothwell and B. Wakefield, "*Optical gain spectrum of GeO<sub>2</sub>-SiO<sub>2</sub> Raman fibre amplifiers*", IEE proc. Vol. 136, Pt. J. No. 6, December 1989, pp 301-306.
3. R.H. Stolen, "*Issues in Raman Gain measurements*", Technical Digest Symposium on optical Fiber Measurements, 2000, pp.139-142.
4. T. Izawa, N. Shibata and A. Takeda, "*Optical attenuation in pure and doped fused silica in the IR wavelength region*", Applied Physics Letters, Vol. 31, p.33 (1977)

## VI. Measurement of Raman gain in GeO<sub>2</sub> doped Fibers

In the last chapter, Effective Raman gain values were calculated for Sumitomo's pure silica core Z-PLUS fiber, a low GeO<sub>2</sub> doped standard Spectran fiber and a Lucent Truewave dispersion shifted fiber with high GeO<sub>2</sub> doping. The Raman gain dependence of Raman gain on GeO<sub>2</sub> doping and polarization dependence were taken into account. In this chapter the Raman gain is measured experimentally for these fibers and compared with the calculated effective Raman gain values. Raman gain for OFS Labs dispersion shifted fiber (DSF) and dispersion compensated fiber (DCF) is also measured.

### 6.1 Basic Setup of Raman Amplifier

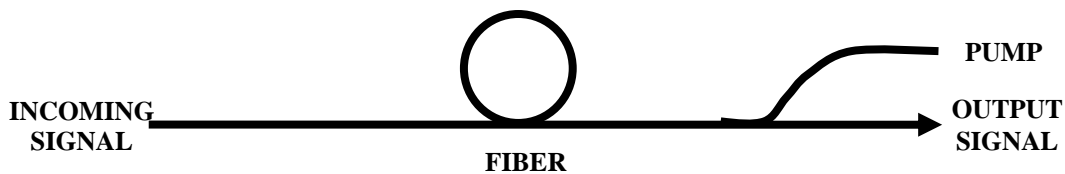


*Figure 6.1 - Basic Setup of Raman Amplifier*

A Raman amplifier basically consists of some means to couple pump and signal light into the same fiber. As shown in figure 6.1, a strong pump light travels down the fiber length along with the weak input signal. The input signal wavelength is set at the Stokes wavelength. The weak signal gets amplified at the cost of the strong pump by a process called stimulated Raman scattering. In practical transmission systems the signal wavelength is usually around 1550 nm and the pump wavelength chosen is around 1450 nm. Raman amplification ( $G_A$ ) in Raman amplifiers is measured by the pump “on” and “off” technique which is basically recording the signal power first when the pump power is “off” and then with the pump “on”.

The ratio of these two signal powers with the pump “on” and pump “off” gives the Raman amplification  $G_A$  in the fiber which is related to the Raman gain  $\frac{g}{A_{eff}}$  by the equation 3 of chapter 5. So from the measurement, value of Raman gain  $g/A_{eff}$  can be obtained which was calculated theoretically in the previous chapter.

## 6.2 Characterization of Fiber Components of the Raman Amplifier Setup

Various fiber components were first characterized for their possible use in the setup for measuring the Raman gain in different fiber types. These components included a 3-dB coupler at 1480 nm, a 1550 nm tap coupler, a 1480/1550 nm WDM coupler, a Circulator, Isolator and attenuators. Characterization of these components is presented below.

**3-dB Coupler:** The schematic diagram of a fused fiber coupler is shown in figure 6.2. Light is launched to the port 1 of the coupler which gets divided between port 2 and port 3. Power values in port 2 and port 3 depends on the coupling ratio, these ports could have equal powers in the case of 3-dB coupler or it could be 10:90 in the case of a 10 dB tap coupler.

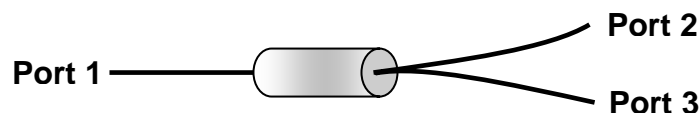


*Figure 6.2 - Schematic Diagram of a Coupler*

A 1480 nm 3-dB coupler was characterized by launching the white light at the input port 1 of the coupler and recording the white light spectra on the port 2 and port 3 on an optical spectrum analyzer (OSA). The output spectra at port 1 and port 2 can be seen in the figure 6.3.

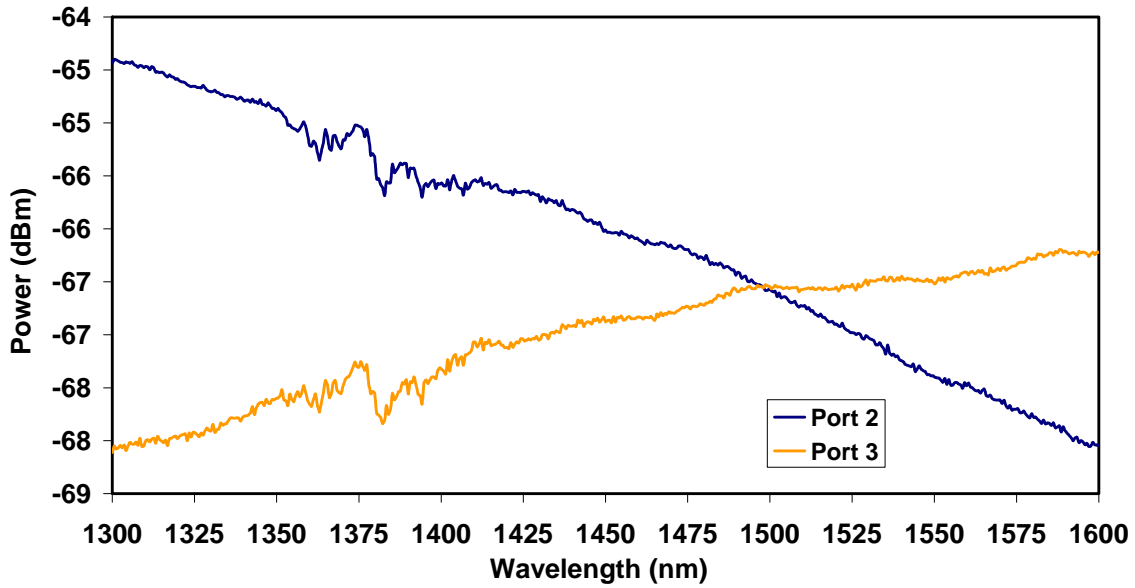


*Figure 6.3 – Output Spectra of a 3-dB 1480 nm Coupler*

It can be seen from the figure 6.3 that this coupler is 3-dB (equal powers in both the output ports) at ~1490 nm as opposed to 1480 nm given in the data sheet of this coupler.

**10-dB Tap Coupler:** A tap coupler is basically used to take a small percent (1-10%) of a signal out to monitor the signal. Figure 6.2 shows the schematic diagram of the same.

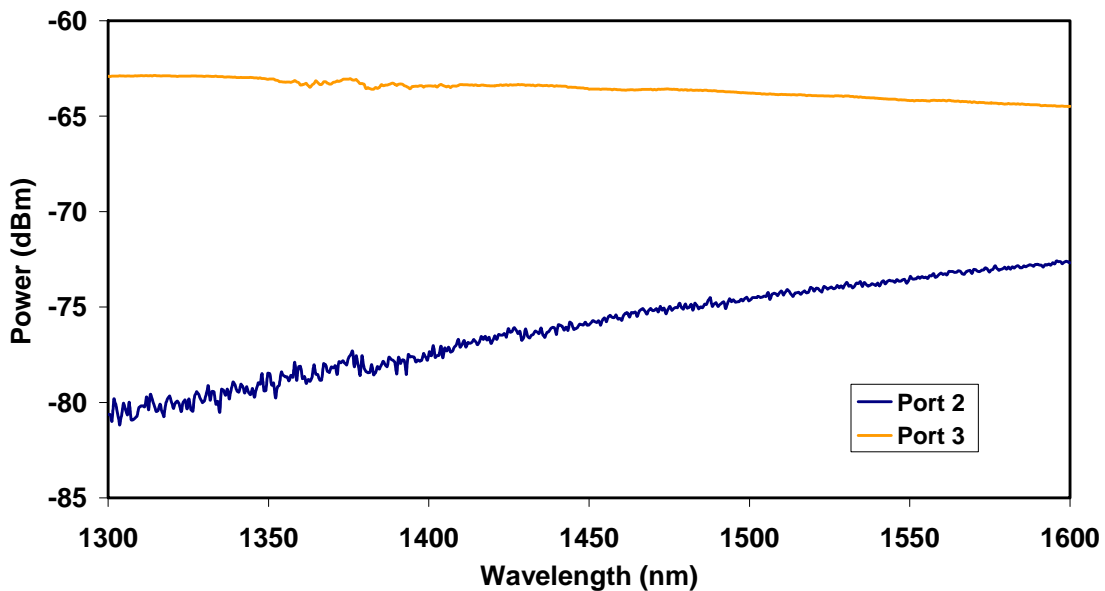


*Figure 6.4 – Output Spectra of a 10-dB Tap Coupler*



As discussed above, a 1550 nm 10-dB coupler was also characterized by launching the white light at the input port 1 of the coupler and recording the white light spectra on the port 2 and port 3 on an optical spectrum analyzer (OSA). The output spectra at port 2 and port 3 can be seen in the figure 6.4. Port 3 is basically the tap port which out couples about 10% of the signal power at 1550 nm.

**WDM Coupler:** A Wavelength Division Multiplexing (WDM) coupler is used to multiplex two or more wavelengths in a single fiber. The WDM coupler characterized here was designed to couple 1480 nm and 1550 nm wavelengths. The schematic diagram of this coupler can be seen in figure 6.2. As before this WDM coupler was also characterized by launching the white light at the input port 1 of the coupler and recording the white light spectra on the port 2 and port 3 on an optical spectrum analyzer (OSA). The output spectra at port 2 and port 3 can be seen in the figure 6.5.

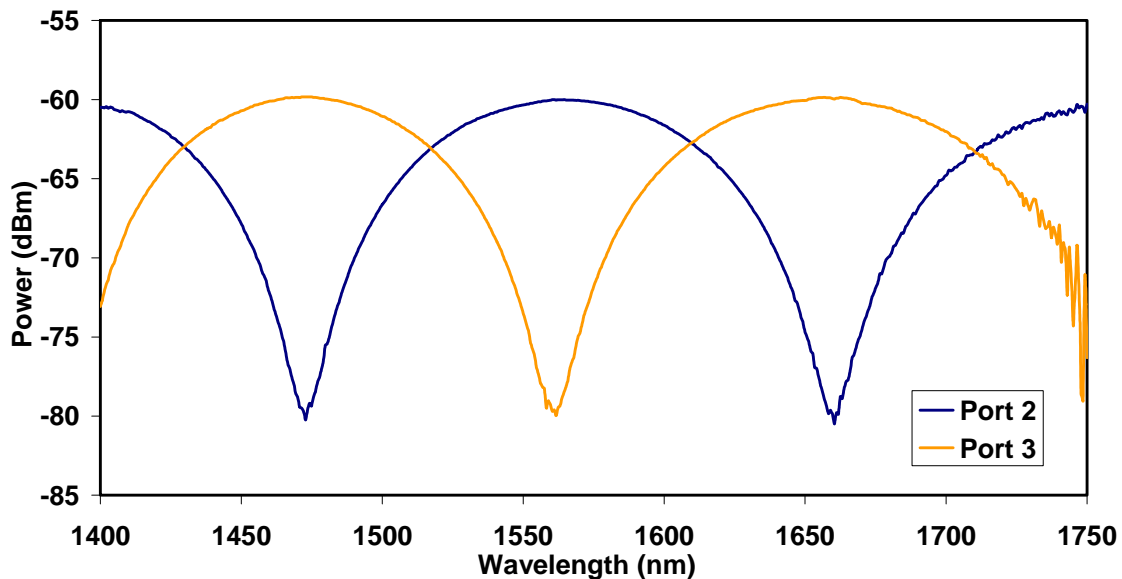


**Figure 6.5 – Output Spectra of a 1480/1550 nm WDM Coupler**

It can be seen from the figure 6.5 that this coupler has coupling peaks basically at 1473 nm and 1562 nm as opposed to 1480 nm and 1550 nm given in the data sheet of this coupler.

**Circulator:** An optical circulator is a non-reciprocal passive device which redirects light from port-to-port sequentially in only one direction. Schematic diagram of an optical circulator is shown in figure 6.6. Light can be coupled from port 1 to port 2 or port 2 to port 3.

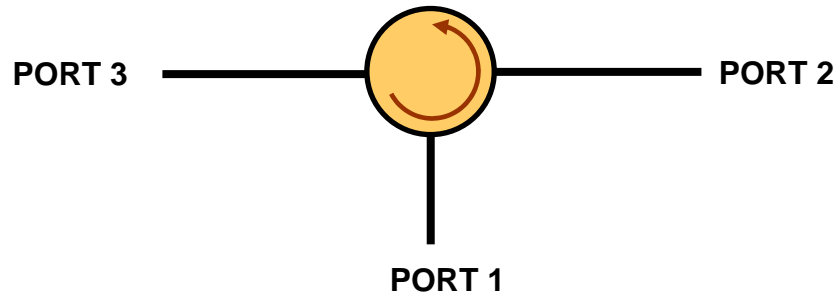


*Figure 6.6 - Schematic Diagram of an Optical Circulator*

To characterize the circulator white light was first launched into the port 1 of the circulator and the spectrum at port 2 was recorded on an OSA. Similarly white light was then launched into port 2 of the circulator and the output spectrum at port 3 was recorded.

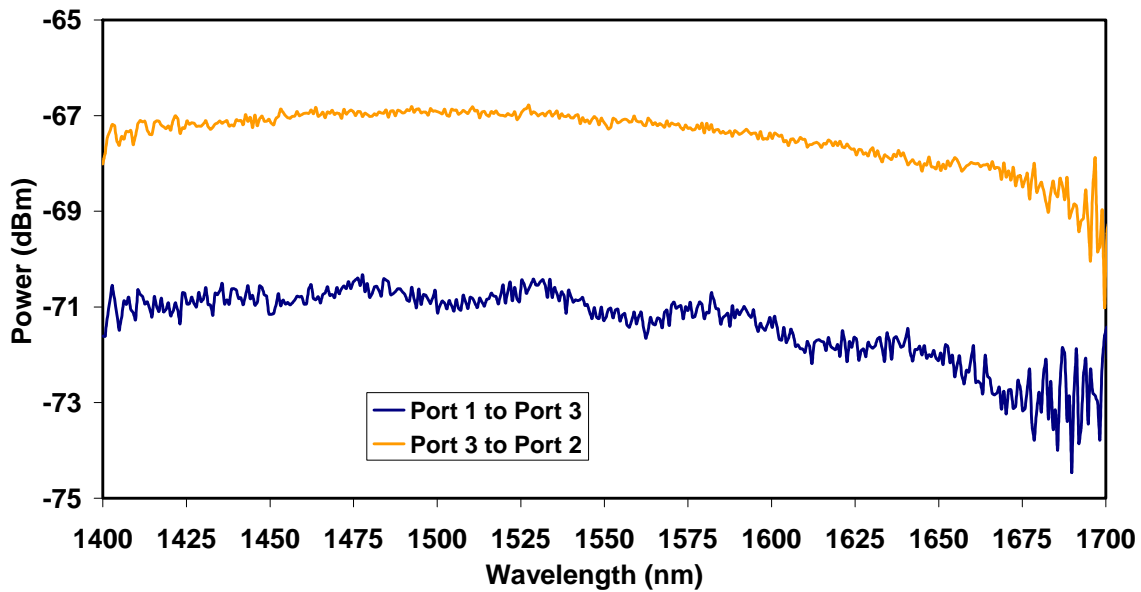


*Figure 6.7 – Output Spectra of an Optical Circulator*

These recorded transmission spectra can be seen in figure 6.7. The power difference in two transmission spectra can be attributed to the different path loss in different directions.

**Isolator:** An isolator is used here to isolate the weak signal laser from the strong pump laser. Strong pump light can affect the weak signal laser by increasing its temperature which leads to a change in the peak signal wavelength (as is shown in the measurement issues section here). The schematic diagram of an optical isolator is shown in figure 6.8.

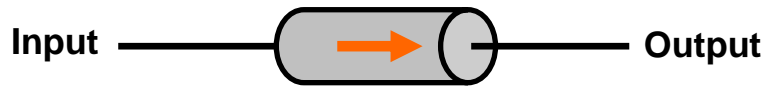


**Figure 6.8 - Schematic Diagram of an Optical Isolator**

The arrow in figure 6.8 indicates the direction in which light can pass, while the light coming opposite to the direction of arrow will be blocked. A 1480 nm isolator was characterized by launching white light first into the direction of arrow (forward) and then opposite to the direction of arrow (backward) and output recorded on an OSA.

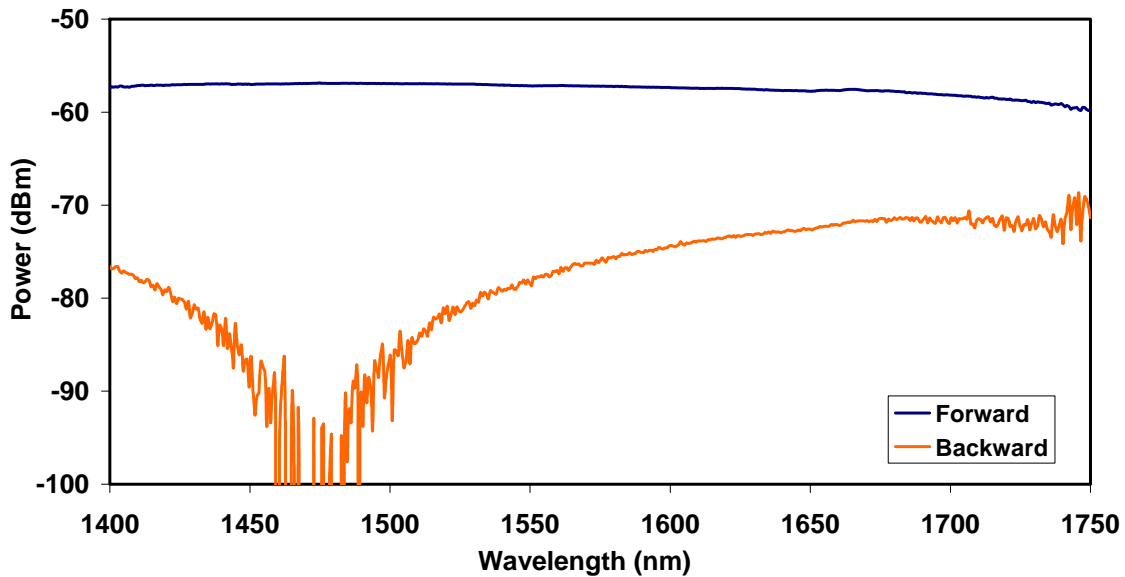


**Figure 6.9 – Spectra of an Optical Isolator in forward and backward directions**

The spectra of this isolator in backward and forward directions can be seen in figure 6.9. At 1480 nm wavelength, compared to the power in the forward direction, a dip of about 40 dB can be seen in the power in backward direction and therefore, this isolator provides an isolation of about 40 dB at 1480 nm.

**Attenuators:** Attenuators were used to attenuate the high pump power so that it can be measured by the powermeter. The detector head on the powermeter could handle a maximum power of about 10 dBm, so it was necessary to attenuate the pump power, which was set at ~20 dBm. The attenuator used was characterized over a 1460 nm – 1580 nm range, which is the range of the tunable laser used to characterize the attenuator. The power of the tunable laser was recorded with and without the attenuator and the difference of the two gave the attenuation spectrum of the attenuator. The attenuation spectrum of this attenuator can be seen in figure 6.10.

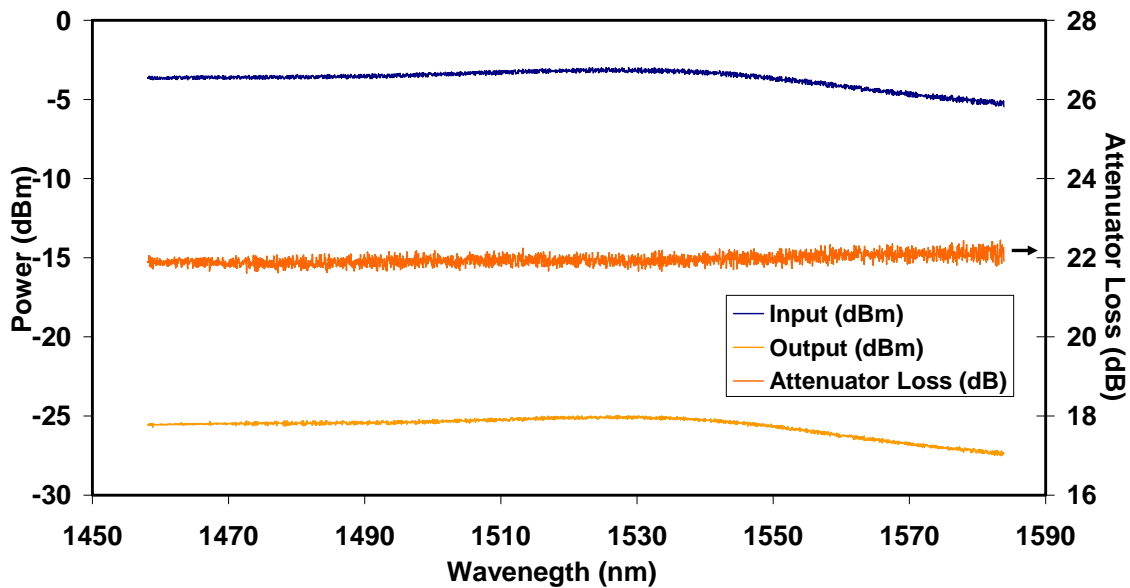


*Figure 6.10 – Attenuation Spectrum of an Optical Attenuator*

It can be seen from the attenuation spectrum in figure 6.10 that the attenuator loss is around 22 dB and very flat over a range of 1460 nm to 1580 nm.

### 6.3 Issues in Raman Gain Measurement

There were various issues in making a setup for accurate Raman gain measurement in different fiber types. These issues included proper selection of a mechanism (coupler or circulator) to couple the pump and signal light into the same fiber, signal wavelength shift with the pump power and the stability of pump and signal power with time. These issues are addressed below and selections of proper components based on them were made for implementing the experimental setup for Raman gain measurements.

### 1) Selection of WDM, 3dB-coupler or Circulator

A 3-dB coupler, a WDM coupler and an optical circulator were tested for their use in coupling pump and signal light into the same fiber. A 1487 nm pump laser was used to pump a pure silica core Sumitomo Z-PLUS fiber using a 3-dB coupler, a WDM coupler and an optical circulator separately. The backward scattered light spectra were recorded on an OSA and are shown in figure 6.11.

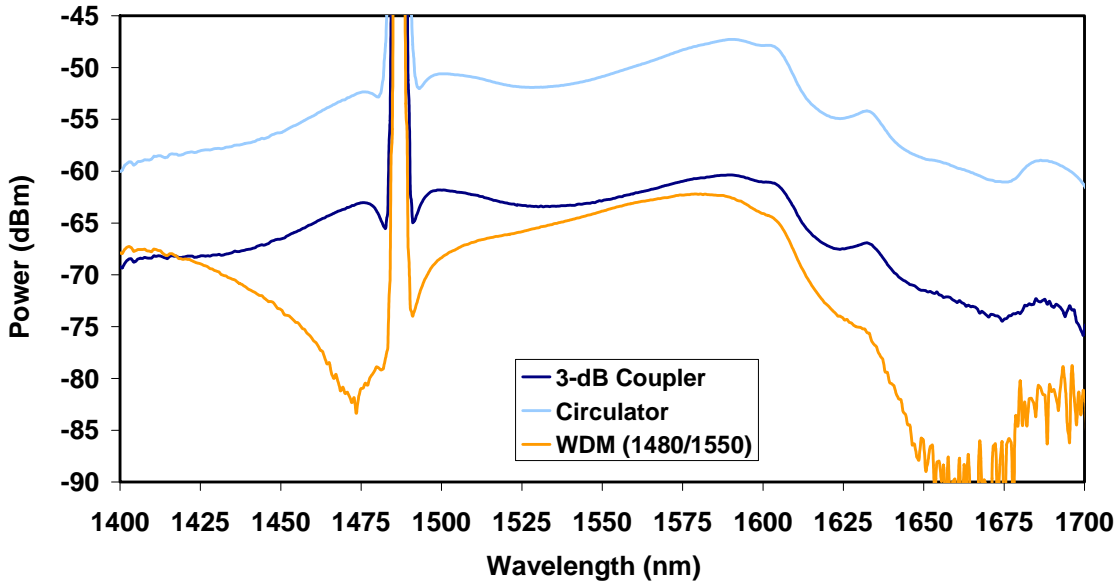


**Figure 6.11 –Raman Spectra of a Z-PLUS fiber obtained using a 3-dB coupler, a WDM Coupler and an Optical Circulator (Pumped at 1487 nm wavelength)**

It can be seen from figure 6.11 that the circulator works the best for measuring the Raman spectra. In the case of a WDM coupler, the Raman spectrum of the fiber is overlapped with the transmission spectrum of the WDM. To measure the actual Raman spectrum of the fiber, this spectrum needs to be corrected for the WDM spectrum. Based on these spectra, it was decided to use a circulator in the Raman gain measurement setup.

### 2) Effect of Isolator

It was found that the peak wavelength of the signal was different when the pump was present than in the absence of the pump. The signal spectrum with and without the isolator is shown in figure 6.12. The peak signal wavelength was 1579.288 nm in the absence of the pump and 1579.444 nm in the presence of pump. That showed that the pump light coupled into the output of the signal laser shifted the signal peak wavelength

by 0.156 nm. Thus for accurate measurements, it is necessary to use an isolator after the signal laser

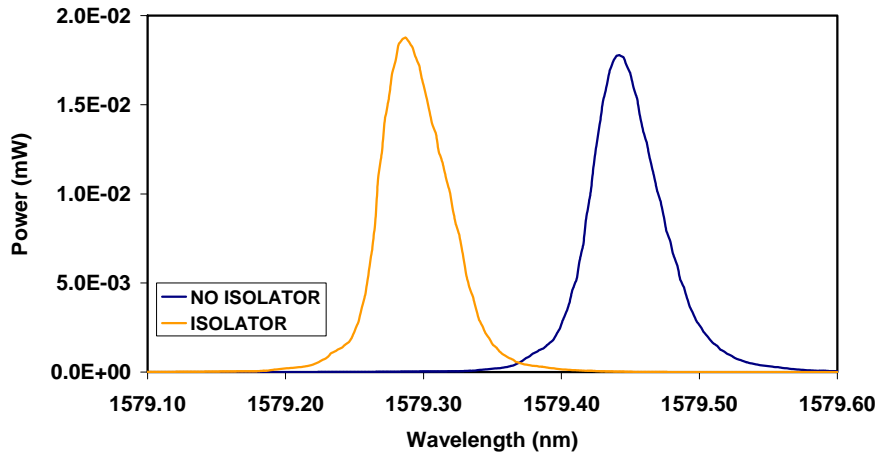


*Figure 6.12 –Signal Spectra with and without Isolator*

### 3) Pump and Signal Power Stability

One of the most important parameters in measuring the accurate Raman gain was the power stability of the signal and the pump over the measurement time period. To check the power stabilities of the pump and the signal, the setup shown in figure 6.13 was implemented.

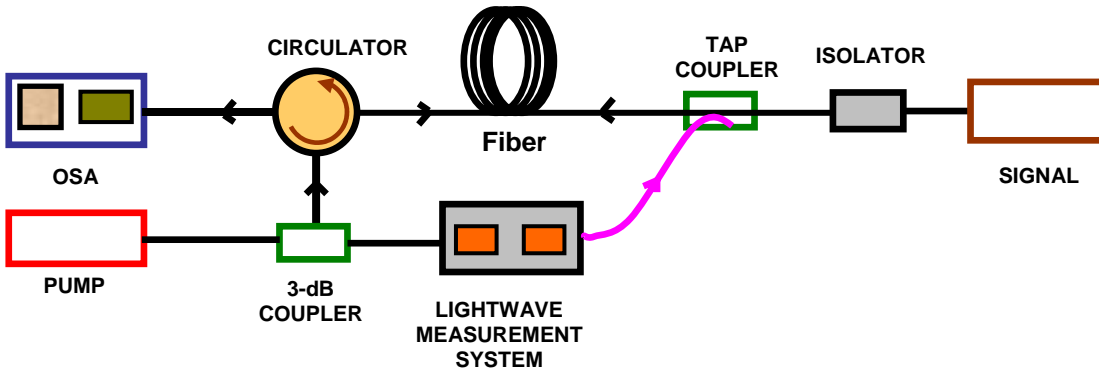


*Figure 6.13 –Schematic Diagram of the Setup for Measuring Power Stability*

This setup includes a lightwave measurement system which has two power detector channels to record the power values with time. One detector was connected to the pump through a 3-dB coupler and the other detector was connected to the signal through a tap coupler. Powers on those two detector channels were recorded over a period of 30 minutes. The stability graphs for the pump and signal power are shown in figure 6.14.

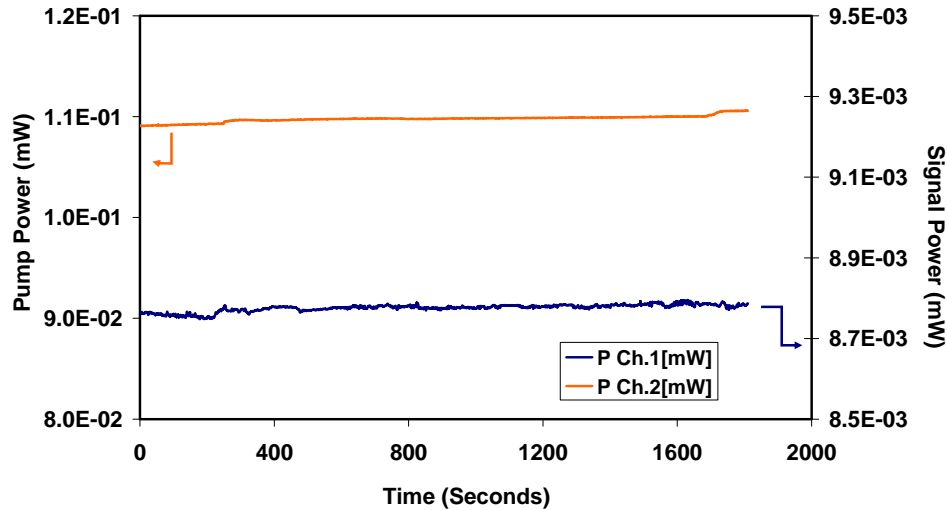


**Figure 6.14 –Power Stability Curves for the Pump and the Signal**

Signal and the pump power were found to be very stable over a period of 30 minutes. Signal power had a standard deviation of  $7.57 \times 10^{-6}$  and the pump power had a standard deviation of  $3.53 \times 10^{-4}$ . These deviation values show a very high stability of the pump and the signal for the Raman gain measurements.

#### **6.4 Characterization of Optical Fibers for the Raman Amplifiers**

There were five different fiber types chosen for making the fiber measurements on them. These fibers varied in their GeO<sub>2</sub> concentration and profile shape. These fibers included pure silica core Sumitomo Z-PLUS fiber, a low GeO<sub>2</sub> doped step index Spectran standard fiber, a high GeO<sub>2</sub> doped Lucent dispersion shifted fiber, another dispersion shifted fiber called Truwave from OFS labs and a very high GeO<sub>2</sub> doped dispersion compensated fibers from OFS labs. These fibers were characterized for their attenuation spectra and Spontaneous Raman spectra, which are presented below.

##### **1) Measurement of Attenuation Spectra of Fibers**

Attenuation spectra of all the fibers were measured by the “cut-back” technique using a white light source and an OSA. First, the white light was launched into the fiber spool under measurement and the output spectrum was recorded on the OSA. The fiber was then cut at about 2 meter distance from the white light source input without disturbing the coupling and the output spectrum measured on OSA. The difference in two spectra, one

at the output end of the fiber and the other at the input end of the fiber after the cut, produced the loss spectrum of the fiber. This loss spectrum, when divided by the total length of the fiber under measurement, gave the attenuation spectrum of the fiber. Attenuation spectra for all the fibers measured are shown in figure 6.15 through 6.19.

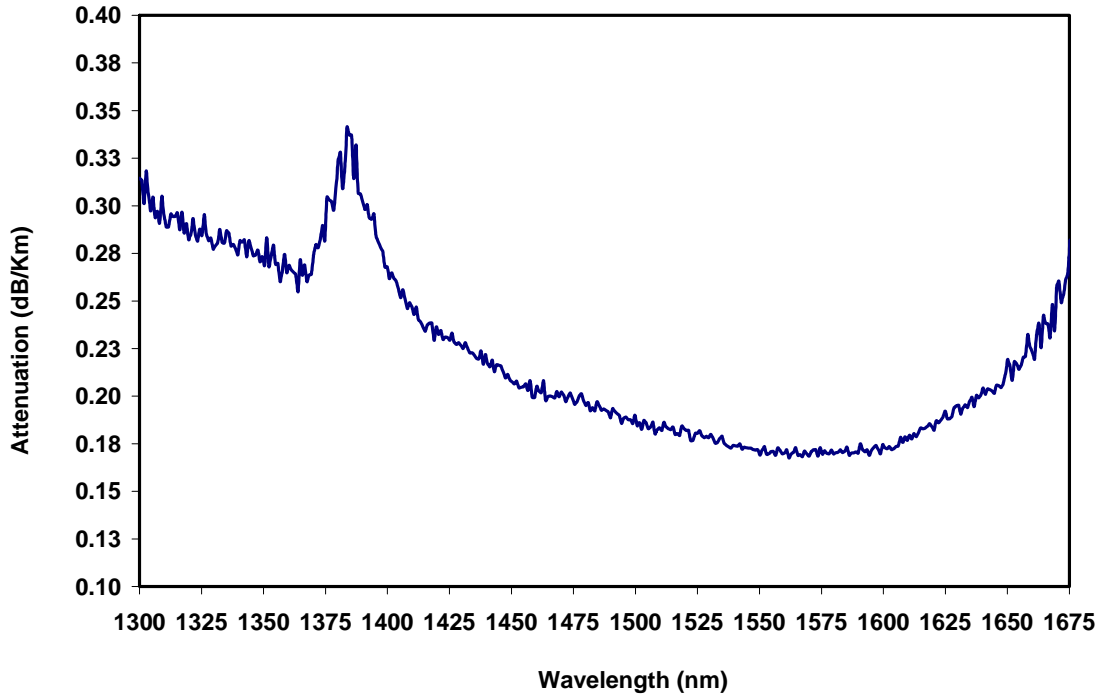


*Figure 6.15 –Attenuation Spectra of Sumitomo Z-PLUS Fiber*

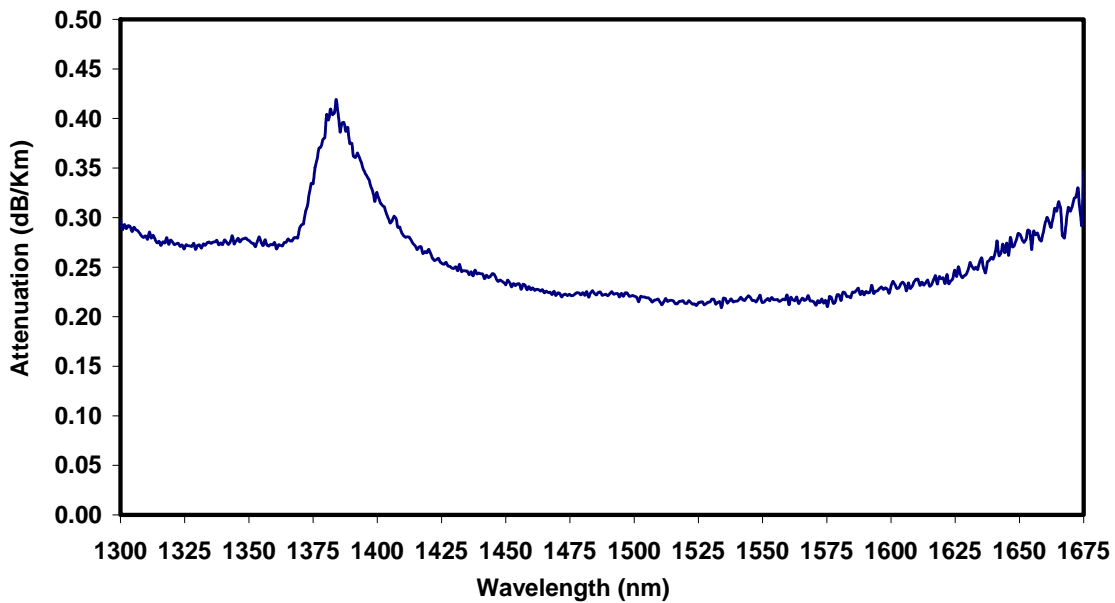


*Figure 6.16 –Attenuation Spectra of Spectran Standard Fiber*



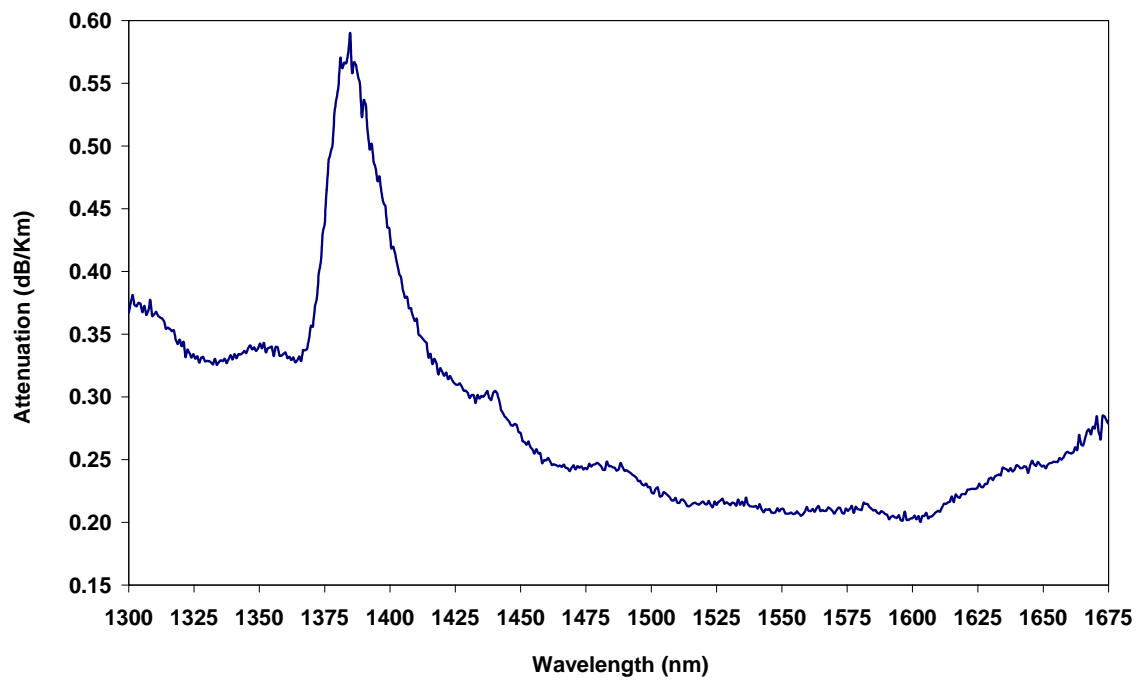


*Figure 6.17 –Attenuation Spectra of Lucent Truewave Dispersion Shifted Fiber*

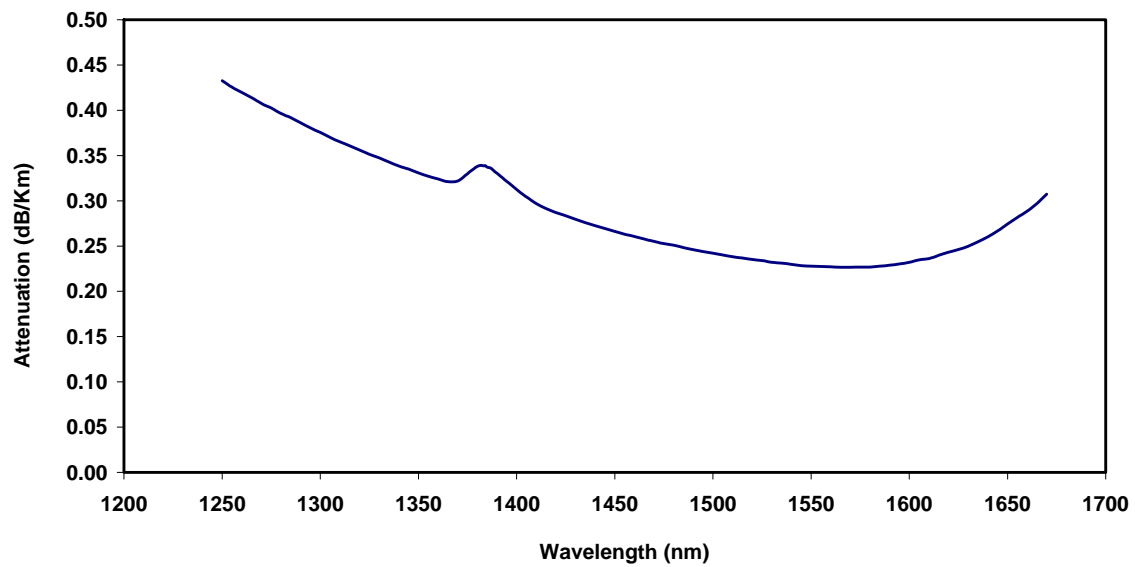


*Figure 6.18 –Attenuation Spectra of OFS Labs Dispersion Shifted Fiber*

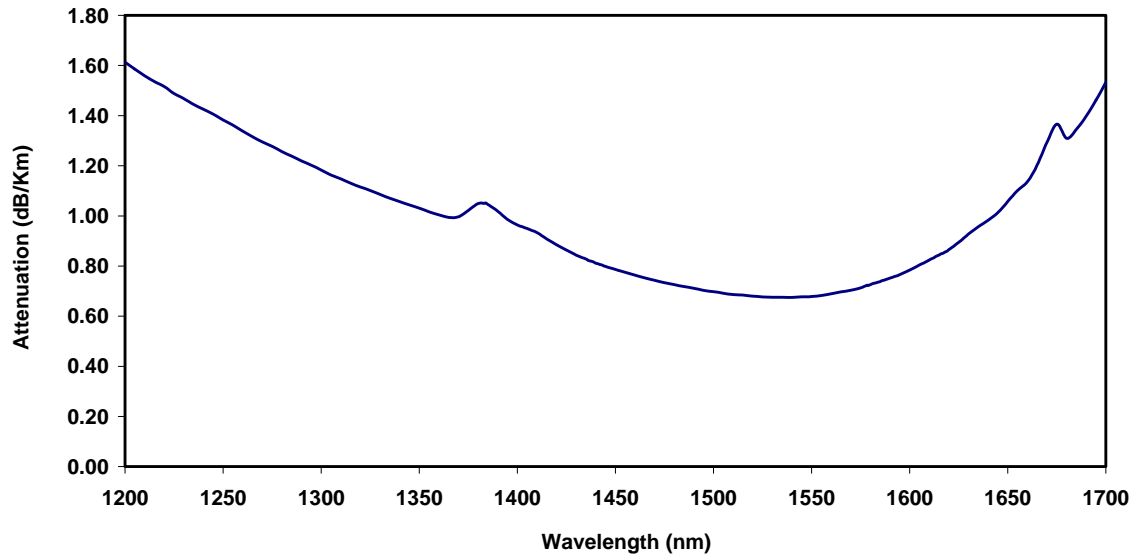


**Figure 6.19 –Attenuation Spectra of OFS Labs Dispersion Compensated Fiber**

The main reason of measuring the attenuation spectra of these fibers was to obtain the attenuation of these fibers at the pump wavelength (1450.4 nm), which will be used later to calculate the effective lengths of these fibers. The attenuation of these fibers at 1450.4 nm wavelength is tabulated in the table 6.1.

**Table 6.1- Attenuation of Different Fiber Types at 1450.4 nm**

Fiber Type	Sumitomo Z-PLUS	Spectran STF	Lucent Truewave	OFS DSF	OFS DCF
Attenuation (dB/Km)	0.210	0.261	0.276	0.266	0.889

As can be seen from the table 6.1, the attenuation of the fiber increases with GeO<sub>2</sub> concentration. Z-PLUS with no GeO<sub>2</sub> doping has the lowest attenuation while OFS Labs DCF with the highest GeO<sub>2</sub> doping has the highest attenuation. Effective lengths of the fibers can be calculated from their attenuations (at pump wavelength) and their physical lengths. Effective lengths calculated for the fibers measured are tabulated in table 6.2.

**Table 6.2- Effective Lengths for Different Fiber Types**

	Sumitomo Z-PLUS	Spectran STF	Lucent Truewave	OFS DSF	OFS DCF
Fiber Loss (dB/Km)	0.210	0.261	0.276	0.266	0.889
Fiber Loss (/Km)	0.048	0.060	0.064	0.061	0.205
Fiber Length (km)	52.000	22.114	20.070	16.445	4.735
Effective Length (km)	19.0073	12.2343	11.3404	10.3638	3.0319

## 2) Raman Gain Spectra

All the fibers, measured for their attenuation spectra were also characterized for their spontaneous Raman spectra. The schematic diagram of the experimental setup for measuring the spontaneous Raman spectra is shown in figure 6.20. This setup consists of a circulator for pumping the fiber with a pump laser and collecting the spontaneous Raman backscattered light from the fiber. The pump used in this setup was a laser diode peaked at ~1450 nm and set at a CW power of about 100 mW. The backward spontaneous scattered light was coupled to the OSA (optical spectrum analyzer) through the circulator.

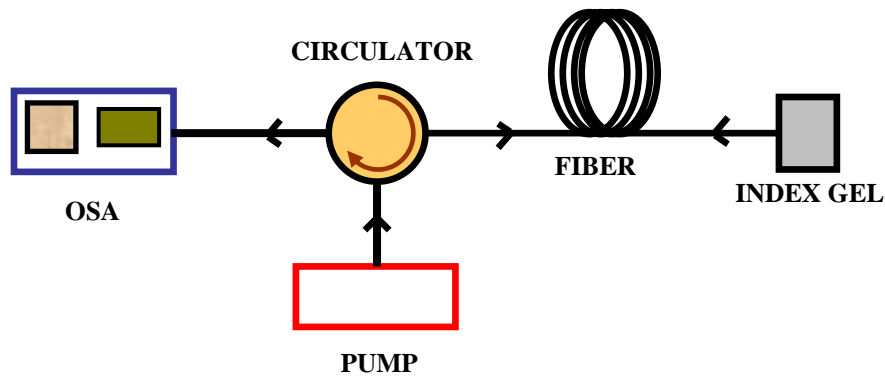


**Figure 6.20 – Schematic Diagram for Spontaneous Scattering Measurement Setup**

The spectrum of the backward spontaneous scattered light was then recorded on an OSA. The output end of the experimental fiber was terminated in an index matching fluid to avoid back reflections. The spontaneous spectrum differs from the gain spectrum by the Bose-Einstein population factor,  $n+1$ , where  $n=1/[\exp(h\nu c/k_B T)-1]$ ;  $h$  is Planck's constant,  $\nu$  is the phonon frequency in  $\text{cm}^{-1}$ ,  $k_B$  is the Boltzmann constant,  $T$  is the temperature in degrees Kelvin, and  $c$  is the vacuum velocity of light.

Thus the gain spectrum can be derived from the spontaneous spectrum by dividing it by  $n+1$ . Figure 6.21 shows the spontaneous Raman spectrum measured for the Z-PLUS fiber and the gain spectrum derived from this spontaneous Raman spectrum. This spectrum has two peaks of almost same amplitude at around  $440 \text{ cm}^{-1}$  and  $488 \text{ cm}^{-1}$ .

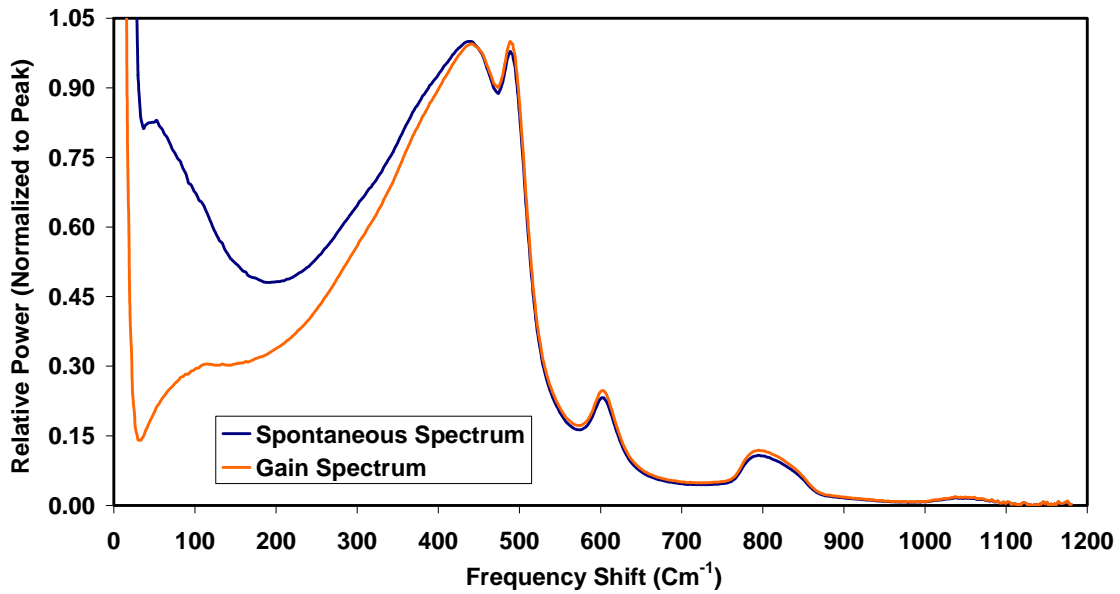


*Figure 6.21 -Spontaneous and Raman Gain Spectra of Z-Plus Fiber*

The spontaneous Raman spectra were measured for the other fibers in a similar manner. The gain spectra were then derived from the spontaneous spectra by dividing them by  $n+1$ . Raman gain spectra for the other fibers are shown in figures 6.22 through 6.25.

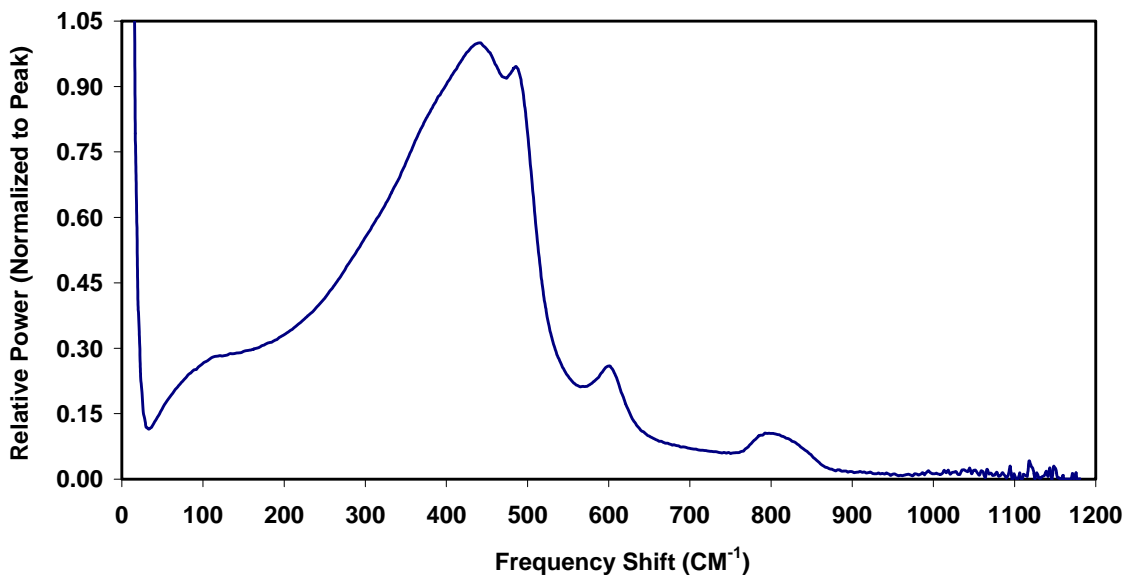


*Figure 6.22 - Raman Gain Spectrum of Spectran Standard Fiber*

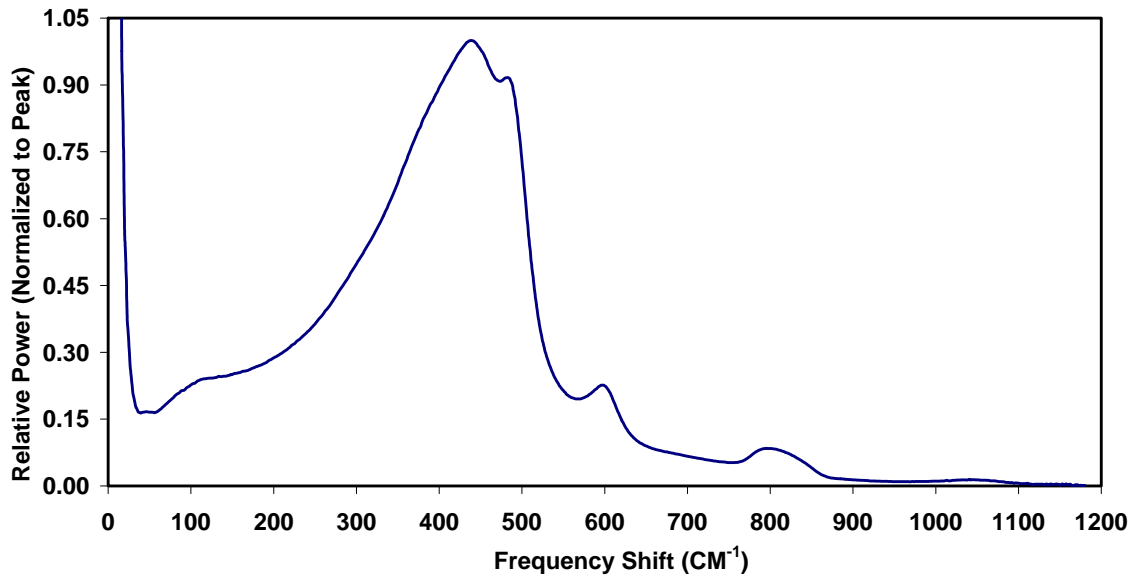


*Figure 6.23- Raman Gain Spectrum of Lucent Truwave Fiber*

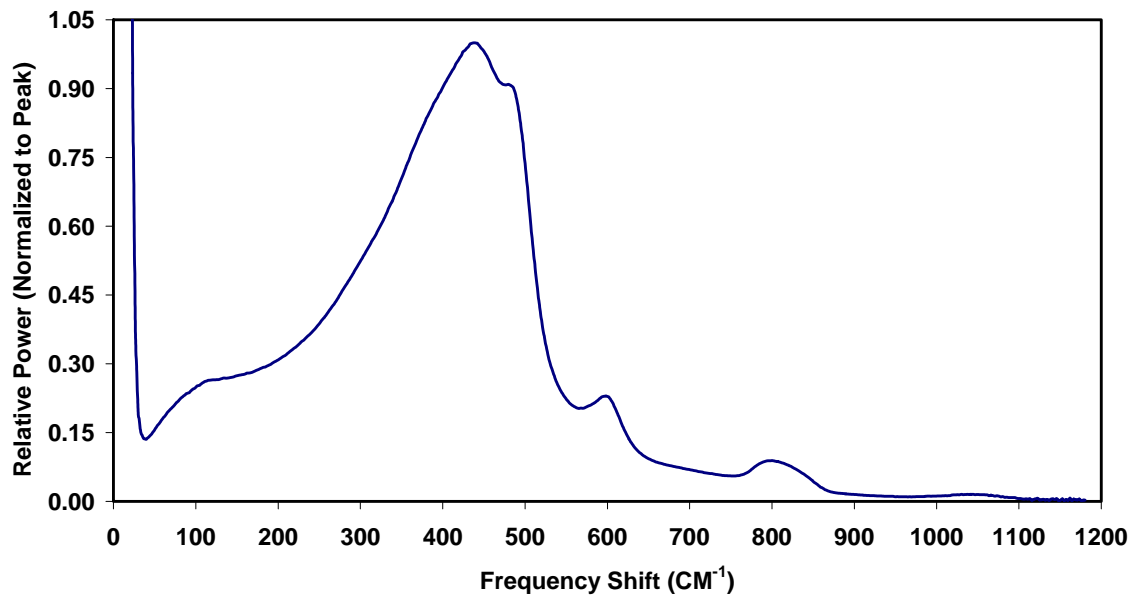


*Figure 6.24 - Raman Gain Spectrum of OFS Truwave Fiber (DSF)*

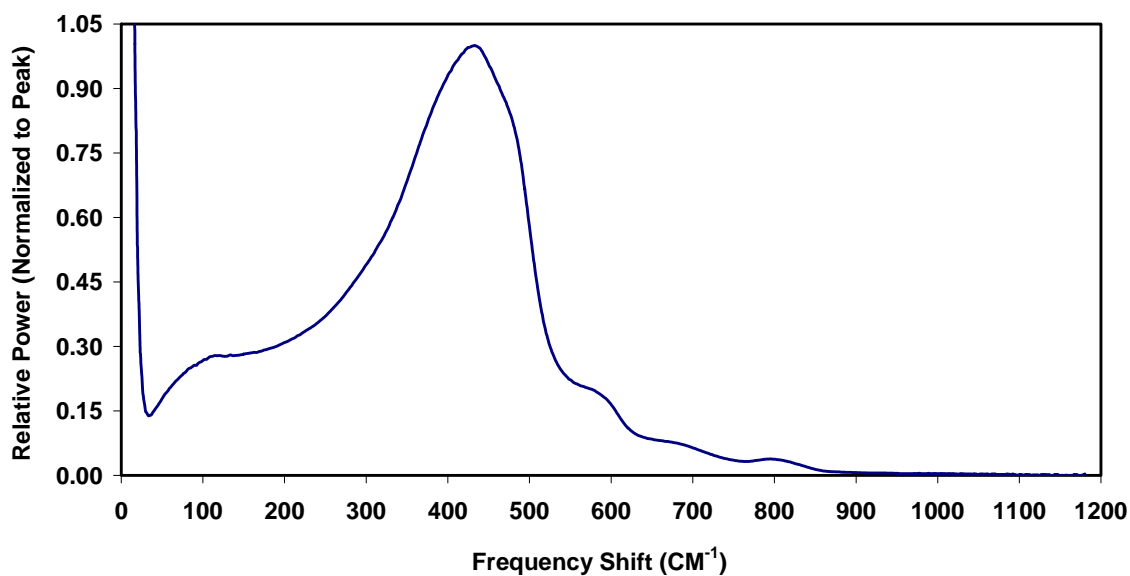


*Figure 6.25 - Raman Gain Spectrum of OFS Dispersion Compensated Fiber*

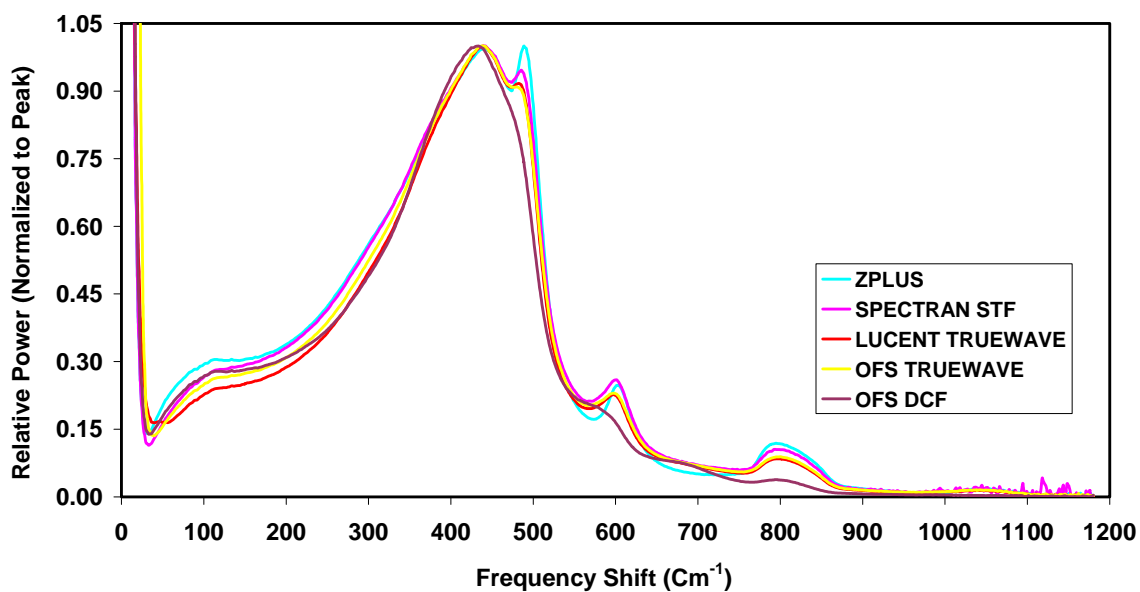


*Figure 6.26 - Raman Gain Spectra of Different Fiber Types*

Figure 6.26 compares the Raman spectra for all the fibers. It can be observed from this figure, as the GeO<sub>2</sub> doping increases the main peak of Raman gain spectra decreases in frequency.

It can be seen from the figure 6.26 that the 2<sup>nd</sup> peak at around 488 cm<sup>-1</sup> frequency shift which is more prominent for pure silica Z-PLUS fiber disappears as the GeO<sub>2</sub> doping increases. Table 6.3 summarizes the main Raman gain peaks in different fiber types.

**Table 6.3- Raman Gain Peak of Different Fiber Types (Pumped at ~1450 nm)**

Fiber Type	Sumitomo Z-PLUS	Spectran STF	Lucent Truewave	OFS DSF	OFS DCF
Fiber Length (meters)	52000	22114	20070	16445	4735
Raman Gain Peak (Cm <sup>-1</sup> )	440.75	442.20	439.29	437.83	433.45
Peak Wavelength (nm)	1549.45	1549.80	1549.10	1548.75	1547.70
Peak GeO <sub>2</sub> (Mol %)	0	3.0	5.0	NA	NA

### 6.5 Measurement of the Peak Raman Gain in different fiber types

Peak Raman gain values were measured for different fiber types characterized above. The experimental setup for the gain measurement is shown in figure 6.27.

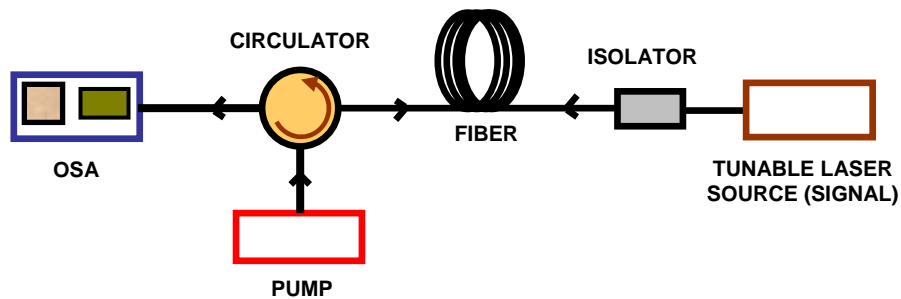


**Figure 6.27 –Schematic Diagram of the Raman Gain Measurement Setup**

This figure shows a Raman amplifier setup in backward configuration where the signal and the pump travel in opposite directions. This setup consists of a circulator for combining the pump and signal in a fiber. The pump used in this setup was a laser diode peaked at ~ 1450 nm and having a spectral width of about 0.8 nm. The pump spectrum can be seen in figure 6.28. This pump power was set at around 100 mW.

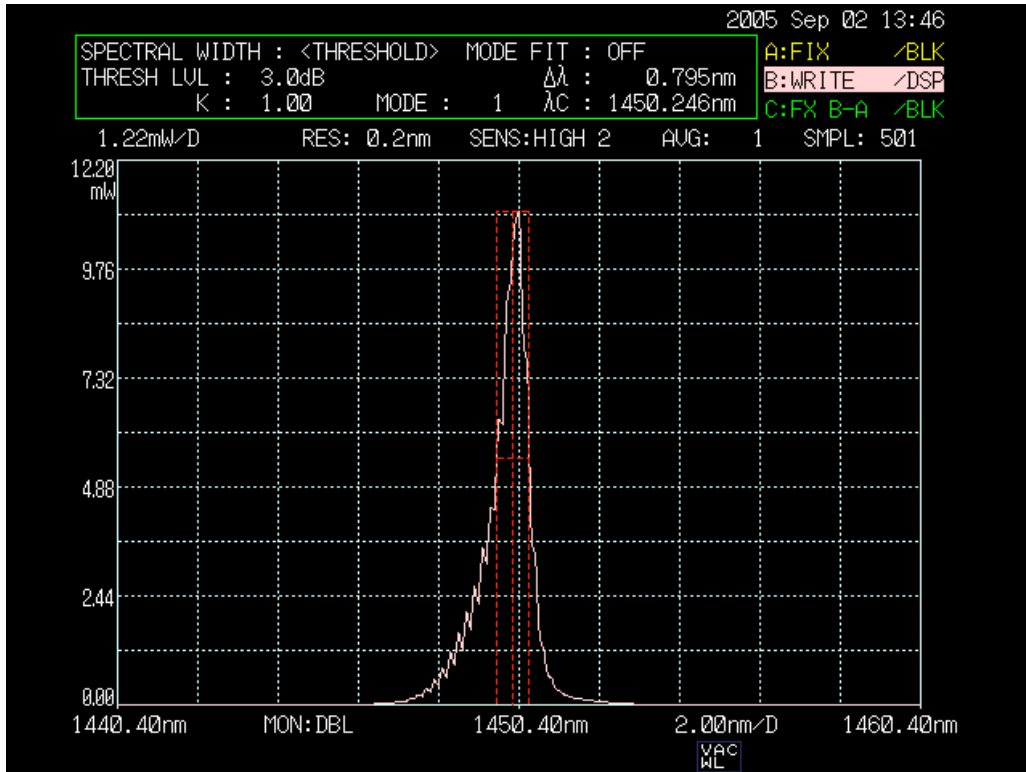


**Figure 6.28 –Spectrum of the Pump Laser used for Raman Gain Measurement**

A tunable laser source was used as the signal. For each fiber measurement the peak wavelength of the tunable laser was set to match the peak of the Raman gain spectrum for that particular fiber. The signal power was measured on the OSA (optical spectrum analyzer) through the circulator. Raman amplification was then measured by the pump “on” and “off” technique. The values of Raman amplifications measured for different fiber types are tabulated in table 6.4.

**Table 6.4- Raman Amplification values measured for Different Fiber Types**

Raman Amplification	Sumitomo Z-PLUS	Spectran STF	Lucent Truewave	OFS DSF	OFS DCF
Minimum	1.647	1.671	2.349	2.069	2.165
Maximum	1.653	1.701	2.348	2.096	2.162
Average	1.651	1.689	2.349	2.089	2.164



For each fiber type, pump power launched inside the fiber was measured by the cutback method. From the pump power, Raman amplification and effective fiber lengths, the Raman gain ( $g/A_{\text{eff}}$ ) was calculated using equation (1). Table 6.5 lists the values of all the quantities measured and the calculated Raman gain values.

**Table 6.5- Raman Gain values calculated for Different Fiber Types**

	<b>Sumitomo Z-PLUS</b>	<b>Spectran STF</b>	<b>Lucent Truewave</b>	<b>OFS DSF</b>	<b>OFS DCF</b>
<b>Fiber Loss (dB/Km)</b>	0.210	0.261	0.276	0.266	0.889
<b>Fiber Loss (/Km)</b>	0.048	0.060	0.064	0.061	0.205
<b>Fiber Length (km)</b>	52.000	22.114	20.070	16.445	4.735
<b>Effective Length (km)</b>	19.0073	12.2343	11.3404	10.3638	3.0319
<b>Pump Power (mW)</b>	100.70	105.93	92.69	98.18	101.16
<b>Amplification</b>	1.6500 $\pm$ .0030	1.6858 $\pm$ .0150	2.3485 $\pm$ .0001	2.0829 $\pm$ .0135	2.1634 $\pm$ .0012
<b>Raman Gain (g/A<sub>eff</sub>)</b>	<b>0.2620<math>\pm</math>.0010</b>	<b>0.4030<math>\pm</math>.0070</b>	<b>0.81225<math>\pm</math>.00005</b>	<b>0.7210<math>\pm</math>.0060</b>	<b>2.5160<math>\pm</math>.0020</b>

These measured values of the Raman gain were then compared with the calculated Raman gain values in the previous chapter for the same fibers. Comparison of the two Raman gain values is shown in table 6.6.

**Table 6.6- Comparison of Calculated and Measured Raman Gain**

	<b>Sumitomo Z-PLUS</b>	<b>Spectran STF</b>	<b>Lucent Truewave</b>
<b>Calculated Raman Gain (km<sup>-1</sup>W<sup>-1</sup>)</b>	0.250	0.468	0.836
<b>Measured Raman Gain (km<sup>-1</sup>W<sup>-1</sup>)</b>	0.2620 $\pm$ .0010	0.4030 $\pm$ .0070	0.81225 $\pm$ .00005

It can be seen from table 6.6 that the calculated and measured Raman gain values for the Sumitomo pure silica core Z-PLUS fiber and Lucent Truewave fiber are in good agreement within experimental error. The measured Raman gain for the Spectran standard fiber does not match well with the calculated Raman gain. The reason for this discrepancy is not understood. Fiber profiles for OFS Labs dispersion shifted and dispersion compensated fibers were not available to make the Raman gain calculations on them to compare with the measurements.

## 6.6 Measurement of the Polarization Dependence of Raman Gain

The Raman gain spectrum in optical fibers is known to be highly polarized<sup>1</sup>. The ratio of the perpendicular-to-parallel Raman gain is known as the depolarization ratio. In the small frequency shift regime of the spectrum, the depolarization ratio is much higher than for large frequency shifts. This low frequency regime is of concern for Raman interactions of channels in dense wavelength division multiplexed (DWDM) systems as the inter channel spacing is much smaller. Therefore it is necessary to understand the polarization behavior of Raman gain in this regime. Raman scattering measurements were previously done in bulk silica samples and silica based fiber<sup>2</sup> and the depolarization ratio in the small frequency regime was reported to be  $0.35 \pm 0.05$ .

In ordinary non-polarization maintaining fibers, the state of polarization varies along the fiber. For some initial distance, the pump and the signal experience the same variation in polarization state but eventually their relative polarization states are completely random because the pump and signal differ in wavelength. So to measure the polarization dependence of Raman gain, a one kilometer length of polarization maintaining fiber was used. The fiber used in this experiment was a PANDA type polarization-maintaining fiber made by Fujikura having a polarization crosstalk of  $\sim 34$  dB and a group beat length of 3.2 mm at a wavelength of 1.3  $\mu\text{m}$ . The fiber loss at 1.3  $\mu\text{m}$  was 0.27 dB/km and  $\text{GeO}_2$  concentration was estimated to be 2.4 mol%.<sup>2,4,5</sup>

The schematic diagram of the experimental setup for measurement of the polarization dependence of the Raman gain is shown in figure 6.29. First of all, a polarized pump source was created by adding a fiber polarization beam splitter (PBS) in front of a non-polarized pump. One arm of the PBS was spliced to a 1550 nm 3-dB PM fiber coupler used to couple the pump light into the PM fiber and to capture the spontaneous Raman backscattered light on the OSA. The pump used was a Raman fiber laser peaked at 1486.7 nm putting out a maximum of CW 2.0 watt CW power. The pump spectrum can be seen in figure 6.30, which has a spectral width of about 0.8 nm. The polarization extinction ratio of the PBS arm coupled to the 3-dB PMF coupler was measured to be 24 dB. Fiber splices in the setup were made using an Ericsson PM fiber splicer to align the

polarization axes of all the fibers from the coupler, the analyzer or the polarization beam splitter. Two orthogonal components of the spontaneous Raman backscattered light spectra were recorded on an OSA through an analyzer first along the analyzer axis ( $0^{\circ}$ ) and then by rotating the analyzer by  $90^{\circ}$  to the analyzer axis.

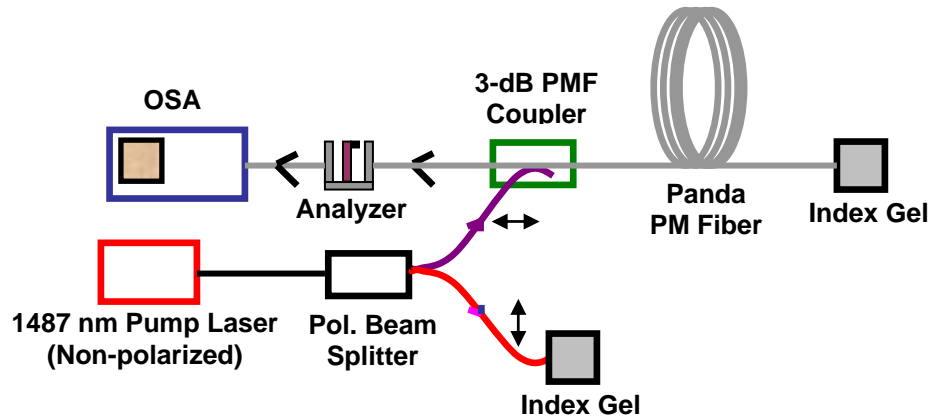


**Figure 6.29 –Schematic Diagram of the Setup for the Measurement of the Polarization Dependence of the Raman Gain**

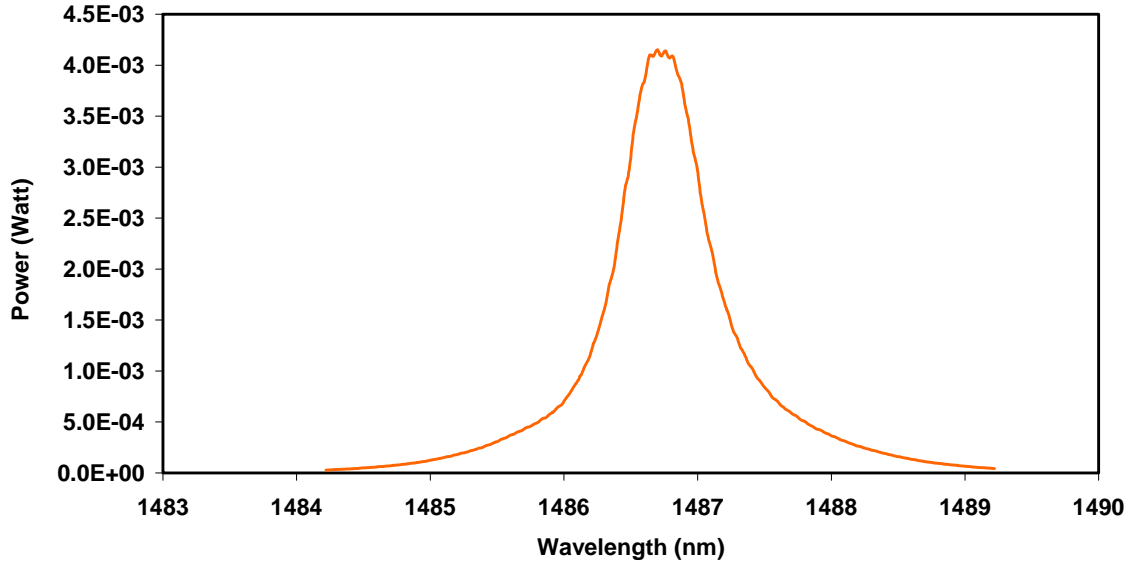


**Figure 6.30- Spectrum of the Pump**

Two orthogonal polarized components of the Raman gain are presented in figure 6.31. These components were derived from the spontaneous components by dividing them by the Bose Einstein factor ( $n+1$ ) as before.

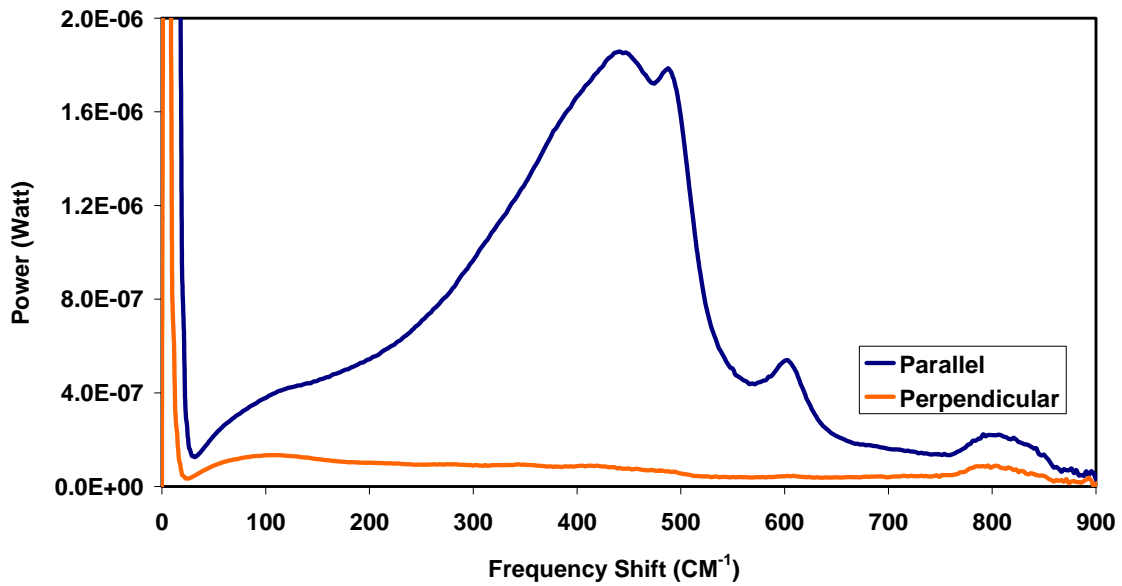


*Figure 6.31 – Polarized Components of the Raman Gain in a PM Fiber*

The depolarization ratio at lower frequency shifts is of importance for DWDM system, Figure 6.32 displays the depolarization ratio in the lower frequency shift regime.

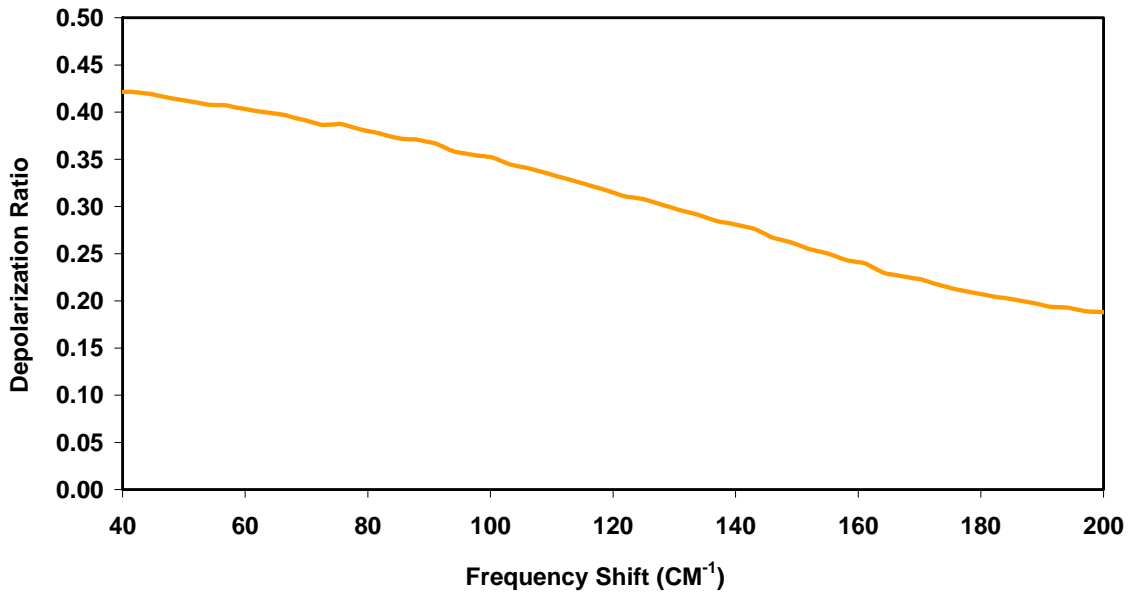


*Figure 6.32- Depolarization Ratio of Raman Scattering at Lower Frequency Shifts*

In the low frequency regime, a depolarization ratio of  $0.46 \pm 0.03$  was measured which agrees with the measurements reported by Dougherty<sup>3</sup> but disagrees with the other

reported measurements in bulk silica and fibers. The reason of this discrepancy is still not understood but it could be because of the polarization mixing along one kilometer length of the fiber because of the stresses applied by the fiber winding.

## 6.7 Summary

In this chapter, an experimental setup was made to measure the Raman gain in different fiber types. Various fiber components were characterized for their use in the Raman gain measurement setup. Some measurement issues and their solutions were addressed for accurate Raman gain measurements. Raman gain values were measured for a pure silica core Z-PLUS fiber, a low GeO<sub>2</sub> doped Spectran standard fiber, a Lucent Truwave fiber, an OFS Labs dispersion shifted fiber and an OFS Labs dispersion shifted fiber with the highest GeO<sub>2</sub> doping. The calculated and measured Raman gain values for Z-PLUS and Lucent Truwave fibers were found in good agreement. Polarized components of Raman gain were measured in one kilometer of a PM fiber. The depolarization ratio at lower frequency shifts was found to be in agreement with the measurements reported by Dougherty<sup>3</sup> but in disagreement with the other reported measurements in bulk silica and fibers.

## 6.8 References

1. R. H. Stolen, "Issues In Raman Gain Measurements," Technical Digest Symposium on Optical Fiber Measurements, 139-142, 2000.
2. I. Mandelbaum, M. Bolshtyansky, T. F. Heinz, "Polarization dependence of Raman gain in optical fibers," TuP4, Proceedings of OSA Annual Meeting 2003.
3. D. J. Dougherty, F. X. Kartner, H. A. Haus, E. P. Ippen, "Measurement of the Raman gain spectrum of optical fibers," Opt. Lett. 20, 31-33, 1995.
4. S. T. Davey, D. L. Williams, B. J. Ainslie, W. J. M. Rothwell, B. Wakefield, "Optical gain spectrum of GeO<sub>2</sub>-SiO<sub>2</sub> Raman fibre amplifiers," IEE Proceedings, Vol. 136, Pt. J, No. 6, Dec. 1989, 301-306.
5. Y. Kang, "Calculations and Measurements of Raman Gain Coefficients of Different Fiber Types," M.S. Thesis, Virginia Institute of Technology, Blacksburg, Virginia, Dec. 9, 2002.

## **VII. Conclusions and Recommendations for Future Work**

The most important outcome of this thesis is the development of a novel technique named the “Core-Suction” technique for fabricating optical fiber preforms with a non-conventional glass core in a conventional silica cladding. The developed technique is simple, inexpensive and shows great potential for fabricating preforms of highly nonlinear non-conventional multi-component glasses as the core material.

### **7.1 Conclusions Related to “Core-Suction” Technique**

- Use of the “Core-Suction” technique for manufacturing preforms with various core glasses like Schott SF6, Lead-Tellurium-Germanate, Lead-Tellurium-Germanate-Neodymium-Erbium and MM2 in silica cladding tubes was successfully demonstrated. These preforms were pulled into fibers and the fibers were characterized for their loss spectra, Raman spectra, elemental make up and index profiles.
- The measured loss values of the fibers were high but that is expected because of the purity of the starting materials. The cladding tube used in making the fiber was low grade and not the high quality fiber grade. Similarly the purity of the starting core glass was not high. The loss levels achieved by MCVD or VAD techniques can not be expected as this technique is most suitable for materials which are not suitable for MCVD or VAD.
- Electron microprobe analysis for elemental make up analysis showed diffusion of silica from the cladding into the core forming a silicate core doped with the starting core glass material. This observation was supported by a low core index value in the index profile and by the Raman spectra. No trace of tellurite was found in any of the fiber cores while the starting core glass contained tellurite. Tellurite was believed to evaporate while drawing the fibers.

- A total length of about 10 meters was drawn for each fiber but the longest sample length was about 2 meters because of the weak mechanical strength of the uncoated fiber. No steps were taken to improve fiber strength.

## **7.2 Future Work Directions in “Core-Suction” Technique**

- Electron microprobe analysis can be used to check the elemental make up of the preform. That should provide the information whether the diffusion takes place while making the preform or during drawing. Diffusion of silica into the core can be reduced using a barrier layer between the core and the cladding. V. M. Mashinsky and others at the Russian Academy of Sciences have shown that an intermediate germanosilicate cladding and  $P_2O_5$  and F-doped silica cladding matched with a silica substrate tube can provide a pure  $GeO_2$  core fiber. Similar barrier layers could be used in “Core-Suction” technique to use multi-component core glasses in silica cladding tubes to prevent the silica diffusion. First the barrier layers can be deposited in silica tubes by using the MCVD technique and this cladding tube with barrier layers then can be used to draw the non-conventional glass into this tube using the “core-suction” method.
- All the fibers fabricated in this thesis were multimode. Single mode fibers can be made by starting with a small inner diameter cladding tube. A thick walled small bore diameter tube should also help when using high thermal expansion coefficient glass material in the core. This should help in reducing the stresses on the core-cladding interface producing a high strength fiber.
- Fiber strength can be improved by starting with better fiber grade silica tubes, HF etching of the starting tubes and the preforms, and inert gas flow in the core-suction furnace. Also drawing the preforms into fibers in a dust free controlled air environment will help the strength of the fiber. Fiber loss can be improved by starting with purer starting materials. Loss can further be improved by the use of an inert controlled air atmosphere inside the furnace used for making the preform.

- This technique relies on the fact that the melting temperature of the core glass is much lower than that of the silica cladding tube. This is advantageous for making highly nonlinear fibers. Highly nonlinear glasses are usually associated with low melting temperatures and it is necessary to use them in silica cladding tubes to make them compatible with standard fibers. However serious problems can occur while drawing these preforms. The core material sometimes starts boiling much before the silica softens, leading to trapped bubbles, blow-out or evaporation. This problem might be solved by using a CO<sub>2</sub> laser heating of the preform for drawing the fiber. The temperature profile of a silica preform heated by a CO<sub>2</sub> laser beam has a lower temperature at the center and higher temperature towards the outside that makes it suitable for drawing such preforms.

### **7.3 Conclusions Related to the Application of Highly Doped Fibers for Optical Amplification**

- Using a commercial fusion splicer, fabricated fibers were easily spliced to the standard fibers showing a loss of better than 0.3 dB. Three different erbium based fibers fabricated by the “core-suction” technique were successfully used for setting up EDFAs. Fiber lengths of 30 cm, 5 cm and 1 cm were used to setup EDFAs. Gain spectra of these erbium fibers were measured.
- Distributed gain of a 30 cm erbium fiber was also measured using an OFDR technique.
- A Raman amplifier was also setup using a commercial DCF, and its gain spectrum measured. A peak gain of ~3dB was measured with ~ 100 mW pump power.

### **7.4 Future Work Directions Related to the Application of Highly Doped Fibers for Optical Amplification**

- Single mode highly doped nonlinear fibers can be fabricated and should be able to show high Raman gain in smaller lengths. These fibers can be used to setup discrete Raman amplifiers and Raman fiber lasers. Distributed gain behavior of these highly nonlinear doped fibers can be measured using the OFDR technique.



## **7.5 Conclusions Related to the Calculation and Measurement of Raman Gain in GeO<sub>2</sub> Doped Fibers**

- Effective Raman gain values were calculated for a pure silica core Z-PLUS, a low GeO<sub>2</sub> doped standard fiber and a dispersion shifted fiber with high GeO<sub>2</sub> doping. Dependence of Raman gain on GeO<sub>2</sub> doping and polarization dependence were taken into account. A Truewave fiber showed the maximum Raman gain because of its high GeO<sub>2</sub> content and lower effective area. Z-PLUS had the lowest Raman gain because of no GeO<sub>2</sub> doping.
- Raman gain values were measured for pure silica core Z-PLUS fiber, a low GeO<sub>2</sub> doped Spectran standard fiber and a Lucent Truewave fiber, OFS Labs dispersion shifted fiber and OFS Labs dispersion shifted fiber with highest GeO<sub>2</sub> doping. The calculated and measured Raman gain values for Z-PLUS fiber were found in good agreement while for Spectran standard fiber these values were in disagreement.
- Polarized components of Raman gain were measured in one kilometer of a PM fiber. Depolarization ratio at lower frequency shifts was found to be in agreement with the measurements reported by Dougherty but in disagreement with the measurements made in bulk silica and fibers.

## **7.6 Future Work Directions Related to the Calculation and Measurement of Raman Gain in GeO<sub>2</sub> Doped Fibers**

- Once the index profiles of OFS Labs dispersion shifted fiber and OFS Labs dispersion shifted fiber are measured, the Raman gain can be calculated for these fibers also. These calculated values then can be compared with the measured Raman gain values. Accuracy of polarized Raman gain components can be checked by checking the polarization stability of the PM fiber. The effect of GeO<sub>2</sub> doping on polarized components can also be measured if PM fibers with varying GeO<sub>2</sub> doping are available.

# VITA

## Nitin K. Goel

---

### EDUCATION:

**Ph.D.** in **Electrical Engineering** at **Virginia Tech, Blacksburg, VA, USA.** (Expected October, **2005**)

**M.Tech.** (Master of Technology) in **“Optoelectronics and Optical Communication”** from **Indian Institute of Technology (IIT), Delhi, India.** **1997**

**M.Sc.** (Master of Science) in **Engineering Physics** from **IIT, Roorkee, India** **1996**

**B.Sc.** (Bachelor of Science) from **C.C.S. University, Meerut, India.** **1994**

### HANDS ON EXPERIENCE:

Optical Hardware, Coupling to small core fibers, Optical Fibers (STF, MMF, DSF, DCF, HNLF, Random and Ordered Holes Fibers), WDM Couplers, Fused Fiber Couplers, Side Polished Half Block Fiber Couplers, Filters, Isolators, Fiber Bragg Gratings, Electro-Optic Modulators, Attenuators, Fiber Wave Plates, Optical Fiber Circulators, Fiber Polarizers, Optical Spectrum Analyzers, Piezo Controlled Stages.

MCVD Lathes, Drawing Towers, Fiber Index Profiler, Fiber Preform Analyzer, Fusion Splicers, Laser Diode Controllers, Tunable Lasers, Fiber Laser, Argon-Ion laser, Pump Lasers, OTDR and OFDR, EDFA, Raman Amplifier, Fiber Optic Interferometer, Optical Transmitters and Receivers, Dispersion Compensation Modules, Fabry Perot Interferometer, Collimators, Nano-Positioners, Lock-In Amplifiers, Parker Stepper Motorized Stages, DSP Processor Kit, Fiber Microbend and Modal Interference Sensors.

### CURRENT RESEARCH PROJECT:

- Fabrication and Characterization of **Highly Doped Fibers** (GeO<sub>2</sub>, TeO<sub>2</sub> and/or Erbium, Phosphate) for Optical Amplification using an innovative technique named **“Core-Suction”**.

### PROFESSIONAL EXPERIENCE:

**May 2005- August 2005:** “Graduate Research Assistant” at **Nano-Bio Materials Lab**, Department of Material Science and Engineering, Virginia Tech. Supervisor- **Dr. Gary Pickrell**

- Fabrication of Random Hole Optical Fibers
- Incorporation of Biological Agents in Random Holes Optical Fibers
- Deposition of Nano-scale materials in Random Holes Optical Fibers

**Jan. 2005- May 2005:** “**Intern**” Lambda Instruments Inc., Blacksburg, VA, USA.

- Engineering/ Scientific support on multiple on-going **Fiber Optic Sensor and Components** development projects sponsored by NASA, US Navy and US Air force.
- Worked on the development of **Fused Fiber Coupler, Fiber Bragg Gratings** and **Fiber Laser** at 2.0 micron and **Double Clad Yb doped Fiber Amplifier**.

**Jan. 2001- Dec.2004: “Graduate Research Assistant”** Department of Electrical Engineering, Virginia Tech, Blacksburg, VA, USA. Supervisor- *Dr. Roger H. Stolen*

- Investigations on “**Raman Amplification in Optical Fibers**” sponsored by **Tycom Ltd.**
- Research and development on “**Highly Nonlinear Fibers for Raman Amplification, Fabrication, Issues and Characterization**” sponsored by **NSF and NASA.**

**Jan. 2002 – May 2002: "Graduate Teaching Assistant"** Department of Electrical Engineering, Virginia Tech, Blacksburg, USA. Supervisor- *Dr. Roger H. Stolen*

- **Instructor** for the undergraduate “**Fiber Optics Laboratory**” course. Played a key role in setting up the Fiber Optics Lab and the Course structure.

**Feb., 2000 – Dec.-2000: “Project Scientist”** Fiber Optics Group, Department of Physics, **Indian Institute of Technology, Delhi**, India. Supervisor- *Dr. Arun Kumar*

- Research and Development on **Fiber Optic Components and Modal Sensors.**
- **Characterization** of different kinds of Optical Fibers using different Techniques.
- **Fabrication** and Characterization of **Side Polished Fiber Half Block Coupler** and **Modal Filter.**
- **Fabrication and Characterization** of **Fused Fiber Coupler** and **Modal Filter.**
- Developed a Fiber-Optic **Strain Sensor** based on LP<sub>01</sub>-LP<sub>02</sub> Mode Interference.
- Developed a Fiber Optic **Micro-Bend Sensor** using Few Mode Fiber for Pressure measurement.

**Aug., 1998 – Jan., 2000: Engineer- D & D** (Design & Development), **Sterlite Optical Technologies**, Aurangabad, India. Supervisor- *Dr. M.A. Saifi*

- Handled specific projects on **MCVD** (Modified Chemical Vapor Deposition), Optical Fiber **DRAWING TOWER** and Optical Fiber **Measurements.**
- Developed a prototype for **Bi-Directional OTDR** (Optical Time Domain Reflectometer) using the existing dual wavelength OTDR.

**Feb., 1998- Aug., 1998: Production Shift Engineer**, Sterlite Optical Technologies, Aurangabad, India. Supervisor- *Dr. Anand Agarwal*

- Responsible for the overall shift production including MCVD, Drawing Tower, QA & QC (Quality Assurance & Quality Control).

**Dec., 1997- Jan., 1998: Project Scientist**, Department of Electrical Engineering, IIT Delhi, India. Supervisor- *Dr. Vinod Chandra*

- Designed and developed an Optical fiber communication link between two active nodes for “**Real Time Fiber Optic Local Area Network**” sponsored by Optel Telecommunications Ltd., Bhopal, India & Indian Railways.

### **PROJECTS UNDERTAKEN:**

- Setup of EDFA (Erbium Doped Fiber Amplifier) for a test optical fiber communication link.
- Design and Implementation of an active Node with Fiber Optic Link Bypass, using TMS320C50 **DSP Processor**, for **Real Time FOLAN** (Fiber Optic Local Area Network).
- Waveguide Loss Measurement by **Fiber Probe** Method.
- Measurement of Gaussian Beam Profile of He-Ne Laser.
- Design and Implementation of a Multiplier using Fast Algorithm.

### **COMPUTER SKILLS:**

**LANGUAGES** : FORTRAN, Working Knowledge of Visual Basic, C and Lab View.

**ENVIRONMENTS** : UNIX, MS - DOS, WINDOWS

**PACKAGES** : MS-Office, MATLAB, Mathematica,

Possessing Extensive Knowledge about Computer Hardware, Spare Parts, Peripherals, Maintenance, Software Installation & Troubleshooting.

### **PATENT DISCLOSURE: VTIP Disclosure No.- 05-26, May 2005**

**Title:** “Fabrication of Optical Fiber Preforms Using “**Core Suction Technique**”

**Inventors:** Nitin K. Goel, Roger H. Stolen, Steven H. Morgon and Daniel Kominsky

### **PUBLICATIONS:**

1. **Nitin K. Goel**, Roger Stolen, Steven Morgan, Jong-Kook Kim, Dan Kominsky and Gary Pickrell, “Core-Suction Technique for the Fabrication of Optical Fiber Preforms.” Submitted to Optics Letters.
2. **Nitin K. Goel**, Roger Stolen, Mark Froggat, Jong-Kook Kim, and Gary Pickrell, “Measurements on Erbium Doped Fiber Amplifier Based on Erbium Fiber Fabricated by Core-Suction Technique” in process for submission to Optics Express.
3. **Nitin K. Goel**, Roger Stolen, Steven Morgan, Jong-Kook Kim, Dan Kominsky and Gary Pickrell, “Core-Suction Technique for Optical Fiber Preforms Fabrication.” Submitted to Optics in Southeast Conference at Atlanta, Georgia organized by OSA (Optical Society of America), October 2005.
4. **Nitin K. Goel** and Roger Stolen, ”Measurement of Raman scattering components in polarization maintaining fiber”, Submitted to Optics in Southeast Conference at Atlanta, Georgia organized by OSA (Optical Society of America), October 2005.

5. **Nitin K. Goel**, Yuhong Kang and Rogers H. Stolen," Comparison of Calculated and Measured Raman Gain in Ge-doped Silica Fibers", Optics in Southeast Conference at CREOL, UCF, Orlando, Florida, organized by OSA (Optical Society of America), Nov. 2003.
6. **Nitin K. Goel**, Yuhong Kang and Rogers H. Stolen," Estimation and Measurement of Raman Gain in Ge-doped Silica Fibers", PHOTONICS'2002, International Conference on Fiber Optics and Photonics, TIFR Mumbai, India, December 2002.
7. **Nitin K. Goel**, Yuhong Kang and Rogers H. Stolen," Measurement of the Raman gain coefficient of a Ge-doped silica fiber", Optics in Southeast Conference at Huntsville, organized by OSA (Optical Society of America), October 2002.
8. **N.K. Goel**, M. A Saifi et al., " Interpretation of SMF OTDR Signatures Using Two Way Measurement Scheme", International Conference on Fiber Optics and Photonics "PHOTONICS'98", IIT Delhi, India, December 98, VOL.-1, pp. 209 -213.
9. Jong-Kook Kim, **Nitin K. Goel**, and Rogers H. Stolen, "All-Optical Wavelength-Division Demultiplexer based on the Optical Kerr Effect using High Group-Velocity Dispersion in Highly Nonlinear Microstructure Fibers" (in process of submission).
10. Arun Kumar, **Nitin K. Goel** and R.K. Varshney, "Studies on a few-mode fiber-optic strain sensor based on LP<sub>01</sub>-LP<sub>02</sub> mode interference", IEEE Journal of Lightwave Technology, Vol.-19, No.- 3, pp. 358 –362, March 2001.
11. Arun Kumar, **Nitin K. Goel** and R.K. Varshney, "Fiber-optic strain sensor based on LP<sub>01</sub>-LP<sub>02</sub> mode interference in a few-mode fiber" SPIE Proc. on "PHOTONICS-2000" Vol.-4417, pp. 500-505, 2001.
12. Arun Kumar, **Nitin K. Goel** and R.K. Varshney, "Fiber-optic strain sensor based on LP<sub>01</sub>-LP<sub>02</sub> mode interference in a few-mode fiber" International Conference on Fiber Optics and Photonics "PHOTONICS-2000", IIT Kharagpur, Calcutta, India, December 2000.
13. Navin Manjooran, Gary Pickrell, **Nitin K. Goel**, "Incorporation of Nano-materials in Random Holes Fibers", in process for journal submission.
14. Navin Manjooran, Gary Pickrell, **Nitin K. Goel**, "Deposition of Nano-scale materials in Random Holes Optical Fibers", in process for journal submission.

15. Navin Manjooran, Gary Pickrell, **Nitin K. Goel**, “Incorporation of Biological Agents in Random Holes Optical Fibers”, in process for journal submission.
16. Gary R. Pickrell, Navin J. Manjooran, **Nitin K. Goel**, “New fabrication technique for random-hole optical fibers”, Proceedings of SPIE Volume: 5589, October 2004.
17. Gary Pickrell, Navin Manjooran, **Nitin K. Goel**, and Dan Kominsky, “Advances in Random Hole Optical Fibers”, Proc. of the Univ. Conf. on Glass Science, Penn State University, June 26-29, 2005
18. Gary Pickrell, Navin Manjooran, **Nitin K. Goel**, and Dan Kominsky, “Silicon Induced In-Situ Hole Formation in Optical Fibers”, Accepted for publication in the J. of Non-Crystalline Solids, (2005).
19. Zhiyong Wang, James R. Heflin, Rogers H. Stolen, **Nitin Goel** and Siddharth Ramachandran, “Highly sensitive wavelength tunability of optical fiber long period gratings with ionic self-assembled multilayers”, American Chemical Society’s 228th National Meeting in Philadelphia, Aug 22-26, 2004.
20. Zhiyong Wang, James R. Heflin, Rogers H. Stolen, **Nitin K. Goel** and Siddharth Ramachandran, “Sensitive optical response of long period fiber gratings to nm-thick ionic self-assembled multilayers”, Int. Conf. on Lasers and Electro-Optics (CLEO), San Francisco, CWD2, 2004.
21. Zhiyong Wang, J. R. Heflin, Rogers H. Stolen, **Nitin K. Goel**, Siddharth Ramachandran and Samir Ghalmi, "Sensitive optical response of long period fiber gratings to nm-thick ionic self-assembled multilayers," Bragg Gratings, Poling & Photosensitivity/30th Australian Conference on Optical Fibre Technology (BGPP/ACOFT) 2005, paper num. 20.00.
22. S.K. Arabasi, A. Safaai-Jazi, R.H. Stolen, G. Indebetouw, M.R. Al-Bandakji, and **N. Goel**, Coupling to Small Core Fibers using a Tapered Splice” Optics in Southeast Conf. at UNC, Charollete, November 2004.
23. S.K. Arabasi, A. Safaai-Jazi, R.H. Stolen, G. Indebetouw, M.R. Al-Bandakji, and **N. Goel**, “Characterization of tapered photonic crystal fibers”. Submitted to Optics in Southeast Conf., Atlanta, Georgia, October 2005.

## TECHNICAL PRESENTATIONS

1. Ph.D qualifying presentation on “**Noise Issues and System Aspects of Raman Amplifier**”.
2. Ph.D prelim presentation on “**Highly Nonlinear Fibers for Raman Amplification, Fabrication, Issues and Characterization**”.
3. Term paper presentation on “**Optical Network Components**” at IIT Delhi.
4. Term paper presentation on “**Architectural Considerations for Optical Network Design**” at IITD.
5. Term paper presentation on “**Optical Fiber Sensors and Applications**” at IIT Delhi.
6. Presentation on “**Fiber-Optic Strain Sensor based on LP<sub>01</sub>-LP<sub>02</sub> Mode Interference**” at IIT Delhi
7. Short course presentation on “**Polarization Mode Dispersion in optical fibers, System Impact and Measurements;**” at Sterlite Optical Technologies India.
8. Short course presentation on “**Large Effective Area Fibers**” at Sterlite Optical Technologies, India.
9. Term paper presentation on “**Fiber to the Home**” at Virginia Tech, Blacksburg USA.
10. Short course presentation on “**Optical Fiber Manufacturing**” at Virginia Tech, USA.

**AFFILIATIONS:** Student Member of IEEE and OSA (Optical Society of America)